# DEVELOPMENT OF A SUCTION-CONTROLLED RESONANT COLUMN APPARATUS WITH SELF-CONTAINED BENDER ELEMENTS

by

EDUARDO ALFONSO SUESCUN FLOREZ

Presented to the Faculty of the Graduate School of

The University of Texas at Arlington in Partial Fulfillment

of the Requirements

for the Degree of

MASTER OF SCIENCE IN CIVIL ENGINEERING

THE UNIVERSITY OF TEXAS AT ARLINGTON

May 2010

ACKNOWLEDGEMENTS

I would like to express my sincere gratitude to my advisor Dr. Laureano Hoyos, for his guidance and support during this research study. I am deeply grateful for having worked with someone who believed in me, and who gave me the opportunity to be a part of his research team. Along this period of time, I have learned additional concepts and models used nowadays in the geotechnical field: one field that I love with all of my passion.

I also thank the Department of Civil Engineering and Dr. Hoyos for providing financial support through a Graduate Research Assistant position during my stay at UTA.

Sincere thanks are also extended to other members of my thesis committee: Dr. Md Sahadat Hossain and Dr. Anand Puppala for their valuable advice and for reviewing this document. I extend my gratitude to Dr. Sireesh Saride for his valuable support. I also thank the whole civil engineering staff for their friendly help in various aspects during my course of my study at UTA.

I would like to thank Claudia, Seema, Diego, Smith, Jonathan, Getnet, Aravind, Pomme, Vijay, Jubair, Naga, Tito, Golf The Second, Kiran, Jubair, Shahed, and all other friends who supported me throughout my stay at UTA.

Finally, and most of all, I express my deepest gratitude to Johanna, my future wife, and Esperanza, my mother, who are my friends and confidants, and always supported me in all respects for successfully completing this masters program. Also, I thank my sisters Lola, Saucha, and Yeka for their affection and constant support through my life.

April 16, 2010

ABSTRACT

DEVELOPMENT OF A SUCTION-CONTROLLED RESONANT COLUMN APPARATUS WITH SELF-CONTAINED BENDER ELEMENTS

Eduardo Alfonso Suescun Florez, M.S.

The University of Texas at Arlington, 2010

Supervising Professor: Laureano R. Hoyos

Small-strain soil stiffness properties such as shear modulus, shear wave velocity, and material damping, are key subsoil parameters for an adequate analysis and design of unsaturated earth structures subject to static and non-static loading. Most conventional geotechnical testing techniques, however, are not able to capture this small-strain behavior and, hence, enormously underestimate the true soil stiffness, primarily due to inaccuracies in small-strain measurements. Around the world, a great deal of research efforts has been dedicated to field and laboratory based measurements of soil suction, assessments of soil-water retention properties, and analyses of swell-collapse behavior. However, very few efforts have been focused on small-strain response of unsaturated soils and their dynamic characterization at small strains.

The overall purpose of this research is to study the dynamic properties of soils at very small shear strain amplitudes under different controlled matric suction states via resonant

column and bender elements testing. This research work introduces a suction-controlled, proximitor-based resonant column device featuring a PCP-15U pressure control panel that allows for the implementation of the axis-translation technique via the independent control of pore-air and pore-water pressures in the specimen. The apparatus also features a full set of self-contained bender elements for simultaneous testing of small-strain dynamic properties under both techniques.

A comprehensive series of suction-controlled resonant column and bender element tests were conducted on statically compacted samples of silty sand for a range of constant suction states between 50 kPa and 400 kPa, at different net confining pressures. Results show the critical role of matric suction in the small-strain response of the tested soil, highlighting in addition the potential and reliability of the developed apparatus.

TABLE OF CONTENTS

LIST OF ILLUSTRATIONS

Figure Page

LIST OF TABLES

# CHAPTER 1

# INTRODUCTION

Civil engineers around the world continue to face problems with road and railway embankments, riverbanks, earth dams, and shallow foundation materials that remain under partially saturated conditions throughout any given year. The lack of education and training among engineering graduates and practitioners to properly deal with unsaturated soil conditions has resulted in faulty or excessively conservative designs, construction delays, and deficient long-term performance of built infrastructures. Nowadays, the unsaturated soil mechanics discipline is receiving increasing attention from researchers and practitioners worldwide, thus providing better explanations for soil behavioral patterns than the conventional saturated soil mechanics.

A great deal of research efforts has been devoted to field and laboratory based measurements of soil suction, assessments of soil-water retention properties, and analyses of swell-collapse behavior. However, few efforts have been focused on small-strain response of unsaturated soils and the dynamic characterization of these materials at small strains.

The critical role of soil stiffness at small strains in the design/analysis of geotechnical infrastructure is now widely accepted (Atkinson 2000). As most soil materials involved in these geosystems remain partially saturated, and the real strains experienced are relatively small, there is a great need for a better understanding of the small-strain behavior of soils under such conditions. The present research work is partly motivated by these research needs.

Furthermore, in the unsaturated soil mechanics practice, a thorough understanding of the critical influence that the season-dependent suction states have on small-strain soil stiffness

properties, such as shear wave velocity ($V_s$), small-strain shear modulus ($G_{max}$), and small-strain material damping ($D_{min}$), is of supreme importance. These are key sub-soil parameters for the adequate design and/or analysis of unsaturated earth structures subject to static as well as non-static loading, as depicted in Figure 1-1. To solve practical and realistic geotechnical engineering problems, rational procedures should be based on a thorough understanding of the effects of season-dependent suction states (i.e., seasonal variations that include wet-dry or freeze-thaw cycles) on small-strain soil stiffness properties. The present work is an attempt to contribute towards this goal.

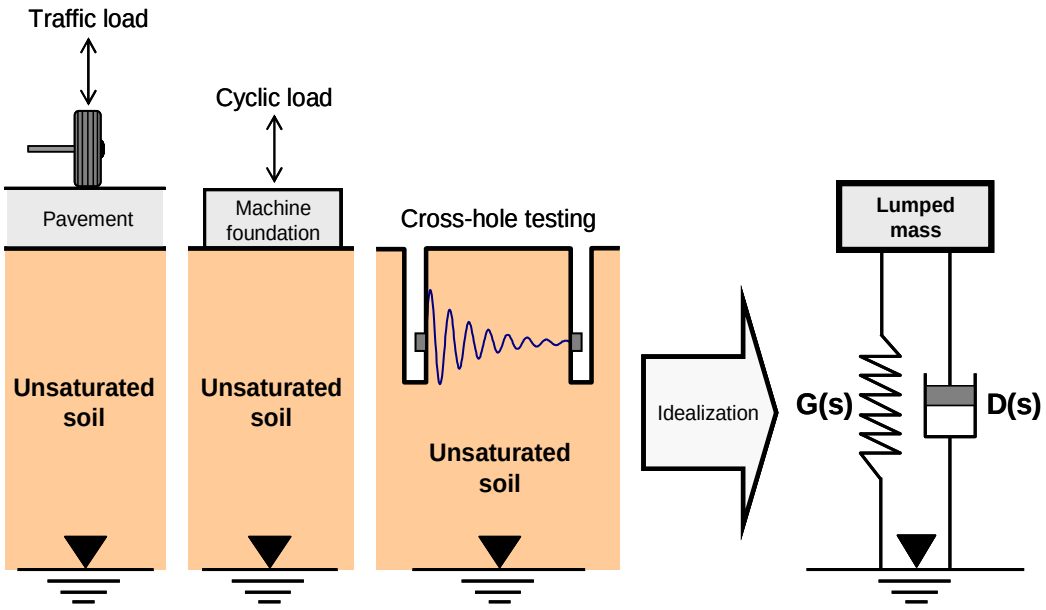


Figure 1-1 Idealization of common unsaturated geotechnical infrastructure subjected to non-static loading.

In the last four decades, the description of the stress-strain-strength behavior of unsaturated soils was closely linked with efforts to isolate the relevant effective stress fields governing unsaturated soil's mechanical response. Adopting matric suction, ($u_a$ – $u_w$), and the

excess of total stress over air pressure, $(\sigma - u_a)$, as relevant stress state variables, various features of unsaturated soil behavior have been modeled via suction-controlled oedometer, triaxial, and direct shear tests using the axis-translation technique (Fredlund and Morgenstern 1977, Alonso et al. 1987, Toll 1990, Alonso et al. 1990, Wheeler and Sivakumar 1992, Fredlund and Rahardjo 1993).

Since the static/dynamic response of unsaturated soils is known to heavily depend on suction states, the lack of consideration of these suction effects in the small-strain dynamic characterization of unsaturated soils may lead to erroneous property measurements and, ultimately, as stated earlier, faulty and/or excessively conservative designs of earth structures.

Conventional geotechnical testing techniques, however, cannot capture this small-strain behavior and, hence, vastly underestimate the true soil stiffness, mainly due to errors in small strain measurements. Despite the above, one of the most reliable and pragmatic well known test methods used for assessing dynamic properties of soils at very small strains is the resonant column (RC). This test method requires a special device where a cylindrical specimen is exited torsionally and tuned to resonance. The determination of $G_{max}$ is accomplished by obtaining the resonant frequency of the soil-driver system.

Recently, bender element based techniques have provided a viable way to investigate soil stiffness at very small strains, and they are starting to be used more widely for small-strain characterization of saturated soils. To date, however, very limited use of the bender element testing technique has been reported for unsaturated soils, and the results reported in the literature are far from conclusive.

There is, therefore, a great need for assessing the feasibility of bender element based techniques for unsaturated soils as compared to more reliable, fully standardized laboratory procedures such as resonant column and simple shear based methods.

This research work introduces a new suction-controlled, proximitor-based resonant column (RC) apparatus featuring a pressure control panel that allows for the implementation of the axis-translation technique via independent application and control of pore-air and pore-water pressures in the soil. The RC device also features a full set of self-contained bender elements for simultaneous testing of small-strain stiffness properties under both techniques.

Results from a comprehensive series of pressure plate, resonant column, and bender element tests undertaken in this research work have been used to devise empirical correlations between small-strain stiffness properties, such as shear modulus and material damping, and key environmental factors, such as matric suction state and net mean stress, for compacted sandy silty soil.

The range of the experimental variables selected in this work, as well as the scope of the experimental program, has been intended to reproduce in situ stress states at different depths within pavement or shallow foundation systems that remain under partially saturated conditions throughout any given year.

## 1.2 Research Objectives

The main objective of this research work is the development of a new proximitor-based resonant column device with both suction-controlled testing capabilities and self-contained bender elements. The secondary objective of this study is to evaluate the influence of matric suction on small-strain shear modulus and material damping response of compacted silty sand as the main key parameters for soil dynamic analysis. Specific tasks within the scope of this research work are described in the following:

- To review the literature available on dynamic properties assessed via resonant column and bender element techniques in partially saturated soils.
- To evaluate the reliability of a new proximitor-based resonant column apparatus by comparing its results with those from a conventional accelerometer-based device.

- To calibrate the new resonant column device using an aluminum-rod-based calibration set as provided by the manufacturer of the core system (GCTS, Tempe, Arizona).
- To empirically assess a fixed value for the input torque to be applied in the new RC device corresponding to a 0.25-V input signal of the conventional RC apparatus.
- To conduct resonant column tests under suction controlled states to evaluate the influence of suction in the shear modulus response of compacted silty sand at very small strains.
- To evaluate the influence of suction in the response of material damping ratio of compacted silty sand at very small strains.
- To analyze the linear and non-linear behavior of compacted silty sand from very small to small shear-strain amplitude levels.
- To perform simultaneous bender element and resonant column tests under suction-controlled conditions on compacted silty sand.
- To compare shear modulus data from resonant column and bender element tests to assess the reliability of the latter in unsaturated soils testing.

## 1.3 Thesis Organization

A brief summary of the chapters included in this thesis is presented in the following:

Chapter 2 explains the significance of dynamic properties of soils for engineering purposes. Available methods for measuring shear modulus and damping material ratio in the laboratory are described. Fundamentals of resonant column and bender element techniques, as well as basic concepts of unsaturated soils mechanics and its role in dynamic geotechnical engineering, are also included. A brief literature review is presented including recent works related to similar goals and findings.

Chapter 3 is devoted to describing the calibration process and performance of the new proximitor-based resonant column device. Physical and basic properties of the soil used in this

research program are also described in this chapter. A thorough calibration process, comparing results from accelerometer and proximitor-based resonant column devices, was accomplished to ensure and validate the reliability and accuracy of the new apparatus.

Chapter 4 describes the additional features for suction-controlled and bender element tests. Pressure control and monitoring systems for both confining pressure and pore-air pressure are described as main components of the new resonant column device.

Chapter 5 describes the experimental program and procedures followed in this research work. The sample preparation process and the basic properties of the test soil are described. A list of all experimental variables is included, as well as a description of the stress paths induced on the specimens prior to resonant column and bender element testing.

Chapter 6 presents results from suction-controlled the new resonant column tests on silty sand soil. Empirical models were devised for estimating small-strain shear modulus and damping ratio on the basis of matric suction and net isotropic confinement as stress variables.

Chapter 7 presents results from bender element tests on silty sand soil. Typical transmitting and arriving wave signals are also reported. Shear modulus values from BE tests are compared with those from RC tests on the basis of matric suction and net confinement.

Chapter 8 includes the summary and conclusions from this research study, and also provides some recommendations for future research.

# CHAPTER 2

# LITERATURE REVIEW

## 2.1 Introduction

This chapter summarizes the fundamental knowledge of small-strain stiffness characteristics of soils and their response under partially saturated conditions, as well as the techniques available for measuring these properties in the laboratory.

The first part of the chapter briefly describes the literature review regarding the meaning of shear modulus, G, and material damping ratio, D, as material properties, as well as the different ways to assess their values in the laboratory. This chapter also contains fundamental information about unsaturated soil mechanics, including basic properties of unsaturated soils and the techniques available for measuring total suction and matric suction.

This chapter also describes the fundamentals of the Resonant Column (RC) and Bender Element (BE) techniques as basic part of this research. Basic definitions and mechanism principles are presented in this work.

The Resonant Column test is the most commonly used laboratory test for measuring the dynamic soil properties at low to medium strains. The test is performed by vibrating a soils or hollow soil column in one of its nature modes. The wave propagation velocity is then determined from the resonant frequency.

Bender elements are suitable transducers of shear wave for instrumenting soil samples due to optimal soil–transducer coupling and compatible operating frequency (Lee and Santamarina, 2005). This technique has become in an excellent solution for researches and practitioners to simply achieve the dynamic properties of a given soil in the laboratory.

Finally, this chapter relates a brief review of most previous works that have assessed the suction levels influence in the variation of dynamic properties of soils. A succinct explanation of the results from some of these previous works is presented in this section, and the empirical models to predict the small-strain shear modulus and damping ratio.

## 2.2 Importance of shear modulus and material damping ratio

Two key material properties necessary to evaluate the dynamic response of soil are the shear modulus, known as G, which relates shear stresses to shear strains, and the material damping ratio, D, which is used as a measure of energy dissipation during harmonic excitation. Figure 2-1 presents the relationship between shear stresses and shear strains. At low strain levels, G is high as the curve is naturally linear.

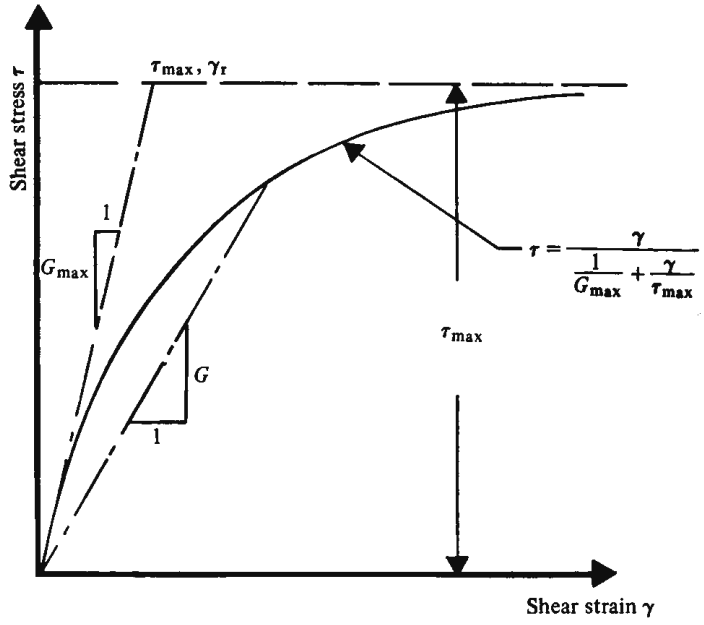


Figure 2-1 Variation of shear stress versus shear strain (Hardin and Drnevich, 1972)

This modulus is known as the low-strain shear modulus ($G_{max}$). As the strain is gradually increased, the curve becomes non-linear, and the shear modulus associated to these strains is called the secant shear modulus ($G_{sec}$). According to Viggiani and Atkinson, (1995a), the shear

modulus of soil can be merely related to the shear wave velocity; thus measurements of shear wave velocity afford a suitable method for measuring soil stiffness. The dynamic response of a soil deposit exposed to seismic excitation is the focus of much attention among engineers both in research studies and in the application of state-of-the-art technology to practical problems.

Shear modulus is necessary to evaluate various types of geotechnical engineering problems including deformations in embankments, stability of foundations for superstructures and deep foundation systems, dynamic soil structure interaction, protection of structures against earthquakes, and machine foundation design (Gazetas, 1982; Dyvik and Madshus, 1985).

On the other hand, once the seismic excitation has taken place, seismic waves appear to traveling through a soil mass. These wave amplitudes are reduced as waves propagate through an elastic medium. Such reduction is consequence of energy looses in the soil, and that is called “attenuation” (Xia et al., 2002). Seismic wave attenuation in geotechnical materials is a complex phenomenon resulting from the interaction of several mechanisms that contribute to the energy dissipation during dynamic excitation.

Several definitions have been proposed as measures of energy dissipation in geological materials. Most are dimensionless, and are assumed to be evaluated within a small range of the soil which is considered perfectly elastic, homogeneous, an isotropic. In soil dynamics and geotechnical earthquake engineering the parameter traditionally used as a measure of energy dissipation is the material Damping ratio D. which is defined as the relationship between the energy dissipated during one cycle at circular frequency, and the maximum strain energy stored during that cycle.

Values of G and D are currently required to analyze problems regarding soil dynamics fields. For many decades most of the practical geotechnical research has been focused on the area of static behavior, and assumptions based on the classical elasto-plasic theories have been adopted to easily solve constitutive models. A part of soil deformation under load is due to

elastic deformation of the soil particles. This elastic deformation often constitutes only a small part of the total deformation of the soil. Elastic deformation is often obscured by deformation resulting from slippage, rearrangement, and crushing of particles. Classical elasto-plasticity assumes the elastic and plastic deformations as separated components, which can be experimentally achieved by loading and subsequent unloading process. The recoverable strain is supposed to be elastic, and the total magnitude is the sum of elastic and plastic strain (Takkabutr, 2006). However, in soils it is not usually possible to separate the elastic strains by loading. When recovery of strain in soils is a result of stored elastic energy, the strains recovered are not always purely elastic. This strain recovery may be caused by the slippage at particle contacts.

The shear modulus of a soil varies with the cyclic shear strain amplitude. At low strain amplitudes the modulus is high, and it decreases as the strain amplitude increases. Figure 2-2 is an idealization of soil stiffness over a large range of strains, from very small to large, and roughly distinguishes strain ranges. At very small strains, which are generally less than a yield strain of 0.001%, the shear modulus is nearly constant with strain. The shear modulus value corresponding to this strain is known as the limiting value $G_0$ (or $G_{max}$). For small strains which are generally less than an arbitrary limit of around 1%, the tangent shear modulus G is a non-linear function of strain. The large strain zone exceeds 1% and the shear stiffness is very small as the soil approaches failure.

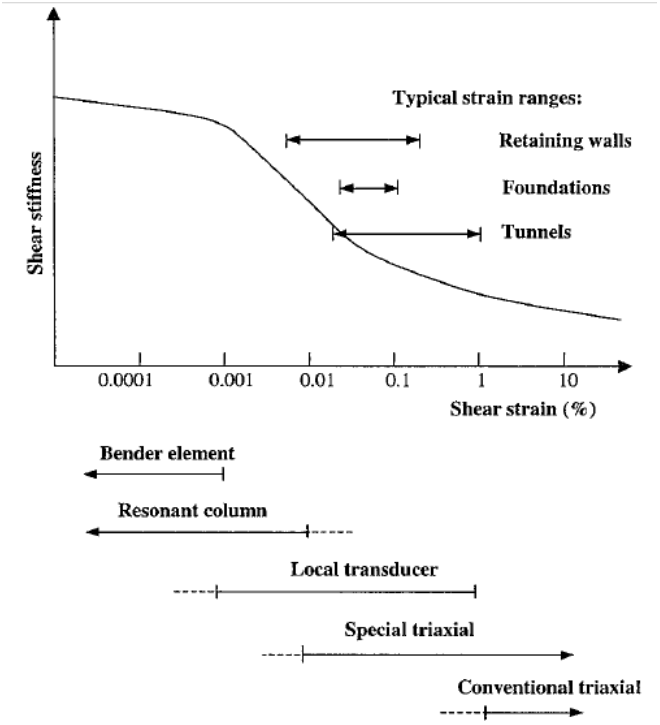


Figure 2-2 Variation of soil stiffness with shear strain
(after Atkinson and Sallfors, 1991; Mair, 1993)

At strains exceeding about 1%, the stiffness is typically an order of magnitude less than the maximum, and it continues to decrease as the state approaches failure. In the intermediate small strain range the stiffness decreases smoothly with increasing strain. The maximum shear modulus, Gmax, of a soil can be calculated from measured shear wave velocities.

## 2.3 Linear and non-linear behavior

Once shearing strains exceed about 0.001% (referred to as the linear threshold), the stress-strain behavior of soils becomes increasingly nonlinear, and there is no single way to define shear modulus and/or damping. Therefore, any approach to characterize the soil for analyses of cyclic loading of larger intensity must account for the level of cyclic strain excursions.

When ground motions consist of vertically propagating shear waves and the residual soil displacements are small, the response can often be characterized in sufficient detail by the shear modulus and the damping characteristics of the soil under cyclic loading conditions. It is usual practice to express the nonlinear stress-strain behavior of the soil in terms of the secant shear modulus and the damping associated with the energy dissipated in one cycle of deformation. With reference to the hysteresis loop shown in figure 2-3, the secant modulus is usually defined as the ratio between maximum stress and maximum strain, while the damping factor is proportional to the area ΔE enclosed by the hysteresis loop, and corresponds to the energy dissipated in one cycle of motion. It is readily apparent that each of the aforementioned properties depends on the magnitude of the strain for which the hysteresis loop is determined; thus they are functions of the maximum cyclic strain.

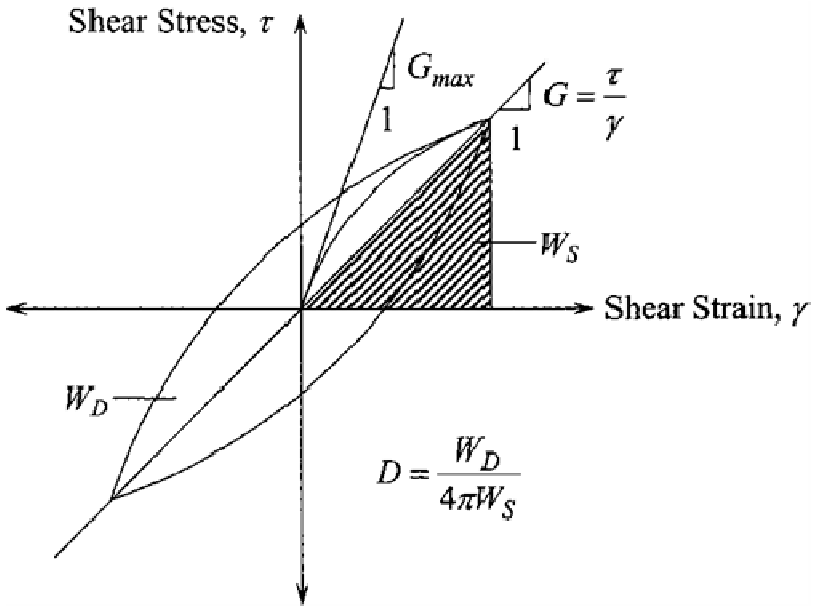


Figure 2-3 Loading-unloading at different strain amplitudes (Assimaki and Kausel, 2000)

The simplified response illustrated in figure 2-3 can be described through a backbone curve, corresponding to first loading, together with a set of rules for unloading and reloading.

Rheological models of this type can be represented by a set of elasto-plastic springs in parallel, with input parameters obtained by curve fitting the measured data. When opting for an equivalent linear analysis, the characterization of the soil consists of three parts (figure 2-4):

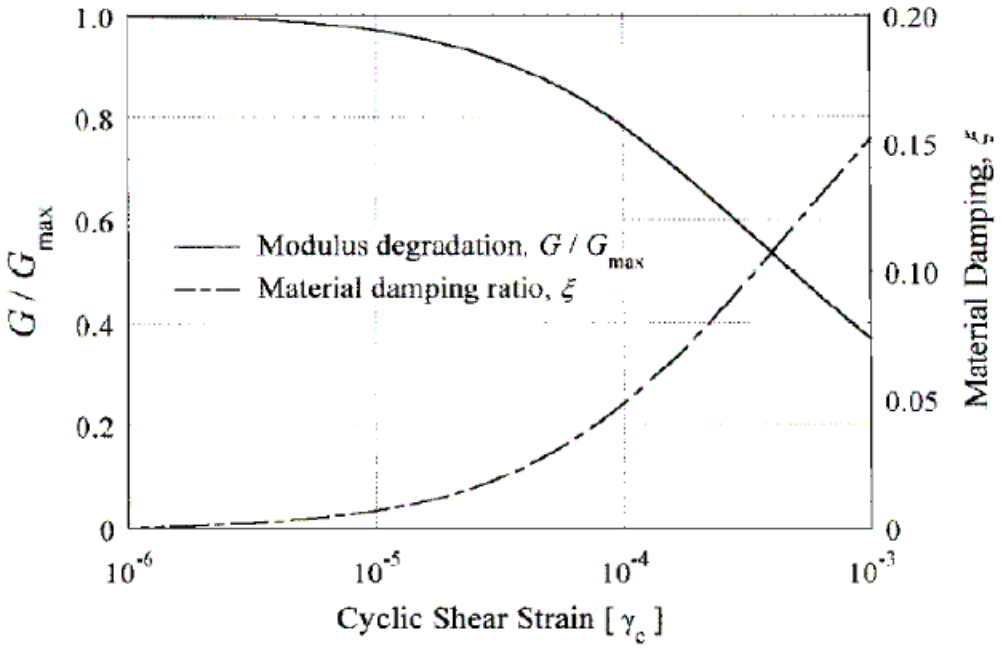


Figure 2-4 Secant modulus and material damping ratio as function of maximum strain (Assimaki and Kausel, 2000)

• The maximum shear modulus Gmax in the very small strain linear region.

• The reduction curve for G/Gmax versus maximum cyclic strain $\gamma_c$ (referred to as modulus degradation curve), with G being the secant modulus.

• The fraction of hysteretic (or material) damping D versus the maximum cyclic strain $\gamma_c$. This parameter is defined as the area ΔE of the hysteresis loop normalized by the ‘‘elastic’’ strain energy through the following expression:

$$D = \frac{\Delta E}{2\pi G \gamma_c} \qquad (2.1)$$

## 2.4 Techniques for measuring shear modulus in the laboratory

A large variety of field and laboratory techniques are nowadays used for estimating shear wave velocities, material damping, and shear modulus of soils. Some methods directly allow measuring shear modulus while others firstly evaluate shear wave velocity and then shear modulus is calculated. Field methods are in-situ techniques deployed to measure dynamic properties of soils, and develop strains within the range of $10^{-3}$-$10^{-4}$ % and less. Although field techniques are capable to develop small strain levels, laboratory methods employ a complete manipulation of the sample to achieve the desired ideal conditions.

Thus is that since the current research work is plenty experimental, the literature review, and related concepts to dynamic soils primarily focus on measuring shear modulus by using laboratory techniques, which will be described on the following pages.

### *2.4.1 Cyclic Triaxial Test*

Cyclic triaxial apparatus can be used to measure the cyclic properties of soils starting in the elastic strain range (lower than or equal to 0.001 percent) and extending into the plastic strain range (about 2 percent), provided highly specialized testing apparatus and techniques are used. The loading system should have the capability of applying cyclic sinusoidal loads and deformations varying between about 2 N (0.5 lbf) and 225 N (50 lbf) and 0.005 mm (0.0002 in.) and 2.5 mm (0.1 in.) respectively, at rates between about 0.1 Hz and 1 Hz. Such rates are typically used for wave loading and earthquake analysis, respectively. It should be noted that measured cyclic loads will be much greater than 225 N (50 lbf), frequently up to 4.5 kN (1000 lbf), and cyclic loads, not deformations, are typically applied at shear strain amplitudes less than about 0.01 percent. The basic parameters being measured and recorded during the test are changes in axial load, deformation and pore water pressures.

The maximum shear modulus is determined by applying about three or more stages of sinusoidal varying cyclic load about an ambient load, at the prescribed frequency, and with about five loading cycles being applied in each stage. In the first stage, the initial cyclic load is about ± 0.5 lbf (2 N) or a value such that the resulting cyclic shear strain amplitude will be slightly less than 1x10-3 percent. The cyclic load applied in subsequent stages is adjusted to obtain a uniform distribution of shear moduli data, G, versus shear strain amplitude, $\gamma$, up to a value of about 5x10-3 percent.

*2.4.2 Resonant Column Test*

The resonant column (RC) testing technique was first used to study dynamic properties of rock materials in the early 1930s, and has been continuously evolving since then for the dynamic characterization of a wide variety of geologic materials. During the late 1970s, Prof. Stokoe and his co-workers developed a new version of resonant column device which has been continuously refined in the last two decades. The stokoe RC testing method has been standardized by the American Society for Testing and Materials (ASTM D 4015-92), and is one of the most reliable and pragmatic test methods used for testing shear modulus (G) and material damping (D) of soils. Isenhower (1979) added a torsional shear device to the resonant column apparatus. In the torsional shear test the sample is subjected to a given number of low frequency cycles of torsional load and the soil stiffness is obtained directly from the torque-twist relationship.

The RC test essentially consists of a soil column which is in fixed-free end conditions is excited to vibrate in one of its natural modes. Once the frequency at resonance (fr) is experimentally known, the shear wave velocity ($V_S$) and, hence, the shear modulus (G) of the soil can easily be determined. Damping ratio can be determined from decaying vibrations or by hysteresis loop characteristics. The RC test is used to determine shear wave velocity, shear

modulus and damping ratio of soil under different confining pressure, void ratios, and shear strain amplitude, number of cycles and time of confinement.

*2.4.3 Bender Element Test*

The bender element method, developed by Shirley and Hampton (1977), is a simple technique to obtain small strain shear modulus of a soil, $G_{max}$, by measuring the velocity of propagation of a shear wave through a sample. Bender element systems can be set up in most laboratory apparatus like oedometer or in direct simple shear (DSS) device, but are particularly versatile when used in the triaxial test as described by Dyvik and Madshus (1985). Shear waves in soils on laboratory samples can be transmitted and received using bender elements. A pair of bender elements are embedded into the opposing ends of each sample and wired in a transmitter-receiver configuration as recommended by Dyvik and Madshus (1985) to measure Gmax, the maximum shear modulus. This is typically defined as the shear modulus measured at strain level below 0.001%.

## 2.5 Fundamentals of Resonant Column Testing

*2.5.1 Introduction*

Resonant Column (RC) devices have been used to investigate soil and rock dynamic behavior as early as 1930's. Many different implementations of the resonant column have been designed by researches throughout the world. The RC, which was introduced by Stokoe (1978) at University of Texas at Austin is a test based on the one-dimensional wave equation derived from theory of linear-elastic vibration as the solution for non-linear vibrations is extremely complex. In fact, this is one of the factors that limit the resonant column to medium and low strain amplitudes even when the apparatus is capable of measuring larger strains such as up 0.4% (Stokoe et al., 1978).

The RC is a fixed-free system suitable for testing solid or hollow specimens with a circular cylinder shape the bottom of the specimen rests on the rough, rigidly fixed pedestal; the

top cap and the torsional driven plate are securely attached on top of the sample. During RC testing the drive plate is allowed to freely rotate so that a torsional excitation is applied at the top of the specimen as depicted on figure 2-5.

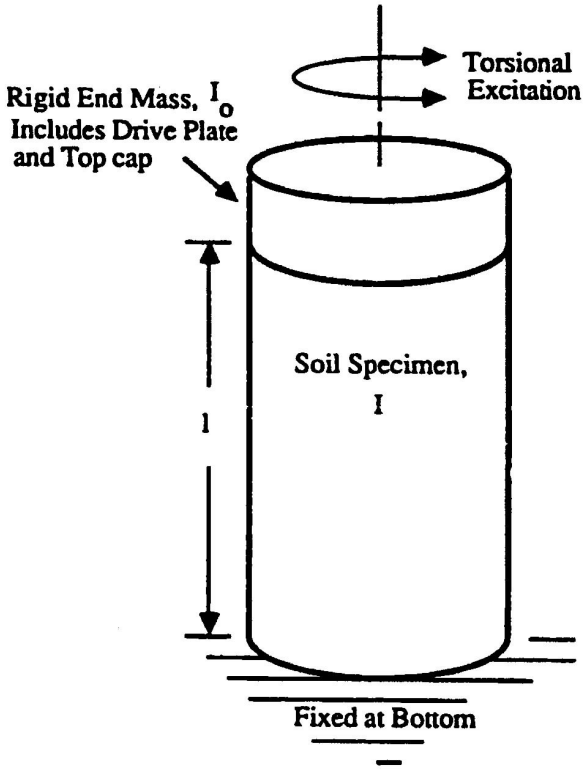


Figure 2-5 Idealization of a fixed-free RC device (from Huoo-Ni, 1987)

This testing description corresponds to a cyclic torque of constant amplitude with varying frequency that is applied to the top of the sample. During the test, the peak top displacement with frequency range is recorded to obtain the entire sweep. The peak torsional displacements are captured via an accelerometer firmly connected to the driver. From the frequency response curve or frequency sweep curve, the frequency corresponding to the peak is then obtained as is shown in figure 2-6. This value is known as resonant frequency, fr. According to Stokoe and

Huoo-Ni (1985) typical values of resonant frequency for soil samples range from 6 to 150Hz. However, results from this current research report frequencies that exceed 200 Hz under high confinements and suction levels, which will be discussed later.

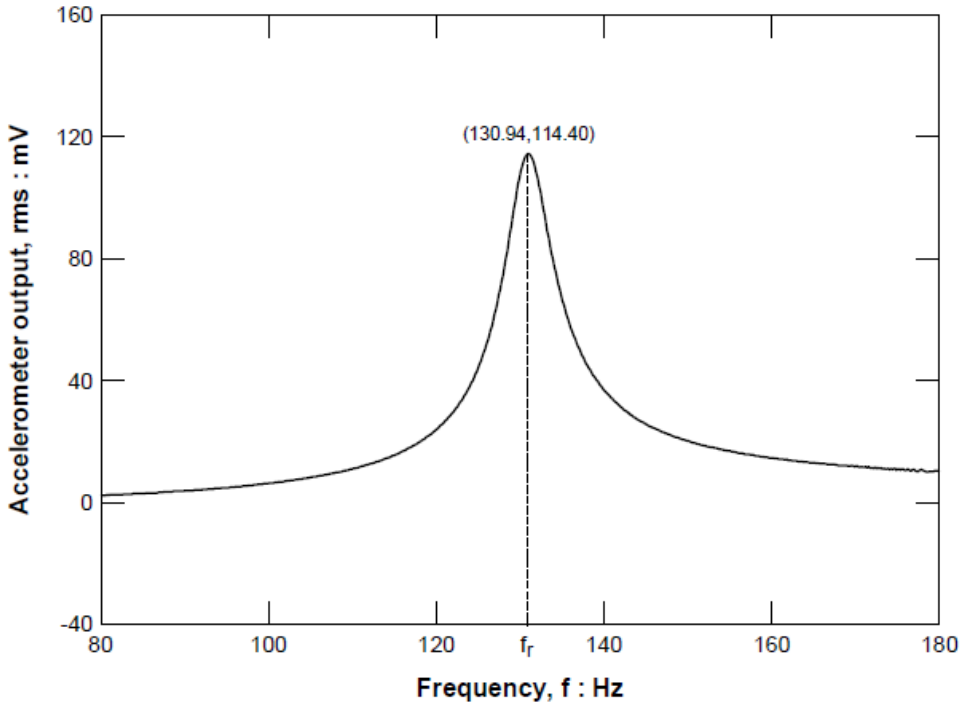


Figure 2-6 Frequency sweep curve from RC test (Takkabutr 2006)

Once the resonant frequency of the specimen is achieved, dynamic properties of the soil can easily calculate. These properties depends on the initial conditions of the soil such as moisture content, density, weathering, voids ratio, as well as external variables that influence its variation such as confinement pressure and suction levels.

*2.5.2 Determination of dynamic material properties*

As it was discussed earlier, RC test is used to determine the dynamic shear modulus, G, and material damping ratio, D. G is computed by measuring the resonant frequency o the soil

column while D is obtained either by measuring the logarithmic decay of the free-vibration-decay curve or by using he Half-power bandwith method from the frequency response curve. Following, the calculation procedure for each topic is indicated.

2.5.2.1 Shear modulus (G)

Within a linear system subjected to vibration such as resonant column testing performs, the material behaves perfectly elastic. In other words, parameters such as stiffness or viscous damping, used to describe the system, are assumed to be constant and independent of frequency and amplitude. For the case of a soil column under torsional vibration, linear vibration theory can be used as long as the peak shearing strain amplitude is less than a threshold limit. Dynamic soil properties below this threshold limit are then considered to be strain independent.

The frequency equation applied to obtain the shear wave velocity, $V_s$, of an elastic soil column is defined as,

$$\frac{\sum I}{I_o} = \frac{w_r}{V_s}\tan\left(\frac{w_r\, L}{V_s}\right) \qquad (2.2)$$

Where, $\sum I = I_s + I_m + I_w + \cdots$

$I_s$ = mass moment of inertia of soil column,

$I_m$ = mass moment of membrane,

$I_o$ = mass moment of inertia of top rigid mass (top cap + spider),

$I_w$ = mass moment of central wire (only for hollow samples)

$W_r$ = natural frequency of soil (rad/sec),

L = length of soil sample.

Although a detailed discussion made by Huoo-Ni in 1987 conclude that relationship between resonant frequency ($W_r$) and natural frequency ($W_n$) decreases as damping increases affecting the substitution $W_r$ instead of $W_n$ in the equation 2.2, material damping values in soil are less than 20%, which results in a difference of less than 4.5% between those two frequencies (Huoo-Ni, 1987).

Using the theory of elasticity, G is then obtained as following:

$$G = \rho(V_s)^2 \qquad (2.3)$$

Where, $V_s$ is the shear wave velocity, and $\rho$ is the total mass density of the soils that in nothing than unit weight divided by gravitational acceleration. Thus, $f_r$ is defined as the first mode resonant frequency, and calculations of $V_s$ are done by trial and error.

A simplified method to estimate G from resonant frequency $f_r$ and geometric characteristics o the system was proposed by Richard (1975). He states that when the system is under resonance, equation 2.2 may be rewritten as,

$$\frac{I}{I_o} = \frac{w_r L}{V_s}\tan\frac{w_r L}{V_s} = \beta\tan\beta \qquad (2.4)$$

where,

$$\beta = \frac{w_r L}{V_s} \qquad (2.5)$$

*as a result,*

$$V_s = \frac{w_r L}{\beta} = \frac{2\pi f_r L}{\beta} \qquad (2.6)$$

and by substituting eq. 2.6. into 2.3., then

$$G = \rho(2\pi L)^2\left[\frac{f_r}{\beta}\right]^2 \qquad (2.7)$$

*Now, for most of the cases,*

$$\frac{I}{I_o} \ll 1$$

then, $\beta$ = tan $\beta$ and from equation 3.3:

$$\beta^2 = \frac{I}{I_o}$$

Therefore, equation 2.7 is finally expressed as,

$$G = \rho(2\pi L)^2 \left[\frac{f_r}{\mathrm{F_r}}\right]^2 \qquad (2.8)$$

In which,

$$\mathrm{F_r} = \sqrt{\frac{I}{I_o}}$$

where, Fr is known as the dimensionless frequency factor. In the present research work, equation 2.8 was used to calculate small-strain shear modulus, G.

2.5.2.2 Material Damping Ratio (D)

In the current research work, the Half-power Bandwidth Method and the Free Vibration-Decay method were used to estimate the material damping ratio, $D_{min}$, of the soils. For the Half-power Bandwidth method, as its name says, the width of the frequency response curve near resonance is measured. Frequencies found before and after the resonant frequency ($f_1$ and $f_2$), corresponding to response amplitude ($A_{rms}$) are related to the half-power points as depicted in figure 2-7. From this curve and following this step, the material damping ratio (D) can be estimated as,

$$D\,(\%) = \frac{1}{2}\,\frac{f_2 - f_1}{f_r} \qquad (2.9)$$

where, $f_r$ is the resonant frequency of the system. Equation 3.8 was used to calculate the material damping ratio for small-strains.

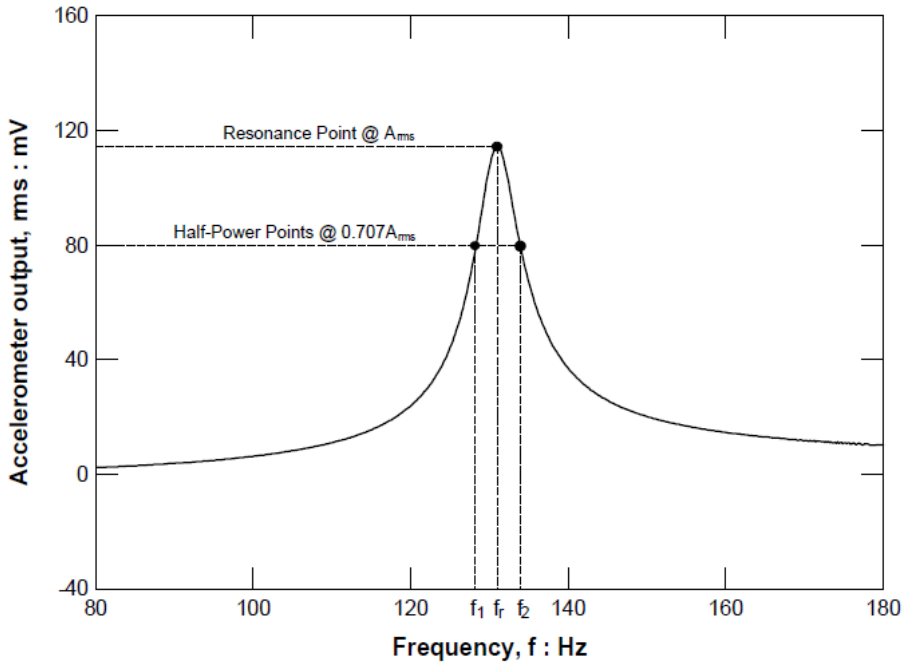


Figure 2-7 Half-power Bandwidth Method for computation of material damping ratio, D.

On the other hand, and not less important, material damping ratio may also be expressed by using the decay rate under free vibrations. This method is also well known and named as the Free Vibration-Decay method. As described in Huoo-Ni (1987) and Craig (1981), the free vibration response of soil specimens in the resonant column test normally exhibits and underdamped behavior and the general solution to this case is,

$$\theta\,(x,t) = Ce^{-Dw_n t}\sin(w_d t + \phi)\sin\left(\frac{w_n L}{V_s}\right) \qquad (2.10)$$

where,

C = constant

D = $cw_n/2G$

$w_d = w_n\sqrt{1 - D^2}$ (2.11)

$\phi$ = the phase difference between the excitation and the response of the system in radians.

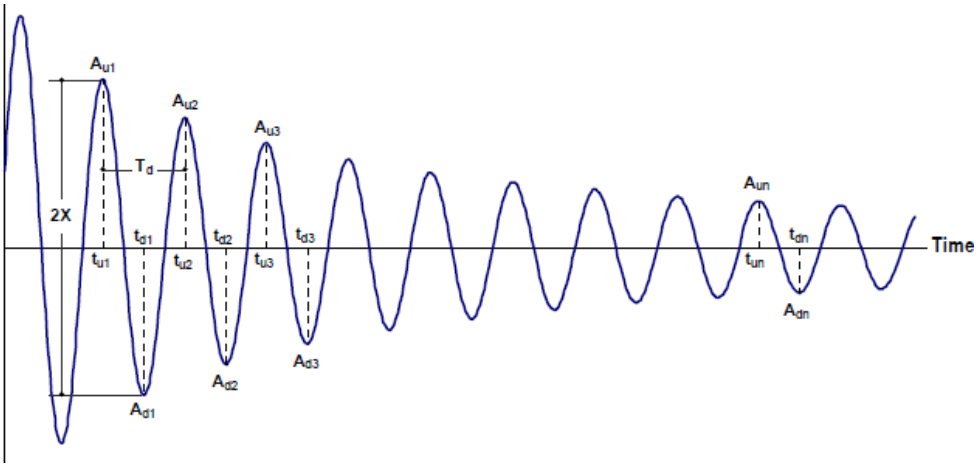


Figure 2-8 Free-vibration decay for computation of material damping ratio, D.

The ratio of any of two peaks depicted in figure 2-8 is given as:

$$\frac{x_n}{x_{n+1}} = e^{-w_n D(t_n - t_{n+1})} = e^{\frac{2\pi D}{\sqrt{1-D^2}}} \qquad (2.12)$$

where $t_{n+1} = t_n + 2\pi/w_d$, the logarithmic decrement, $\delta$, is found by taking the natural logarithm of equation 2.12.

$$\delta = \ln \frac{x_n}{x_{n+1}} = \frac{2\pi D}{\sqrt{1-D^2}} \qquad (2.13)$$

The Damping ratio is now calculated as:

$$D = \sqrt{\frac{\delta^2}{4\pi\delta^2 + \delta^2}} \qquad (2.14)$$

Equations 2.13 and 2.14 were used in this work to calculate the material damping ratio, D.

2.5.2.3 Shear strain ($\gamma$)

The shear strain in a solid cylindrical resonant column specimen loaded in torsion varies from zero at the center line of the specimen to a maximum value at its outer edge as shown in figure 2-9. The shear strain, $\gamma$is determined as following,

$$\gamma(r) = \frac{r\,\theta_{max}}{h} \qquad (2.15)$$

where, r = radial distance from the soil column axis

$\theta_{max}$ = maximum angle of twist, and

h = height of the specimen.

Because the shearing strain is not constant throughout the radial distance, an equivalent shear strain, $\gamma_{eq,}$ is required to represent the average shear strain.

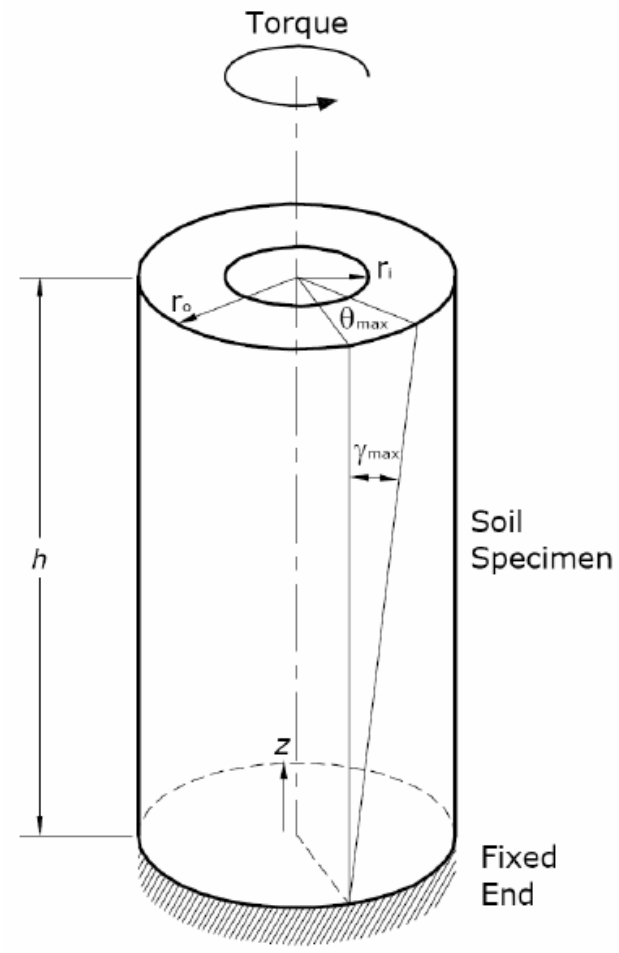


Figure 2-9 Shear strain concept in soil specimen, $\gamma$. (GCTS RC manual, 2009)

Regardless of the type of specimen, a single or unique value of shear strain amplitude associated with the measured shear modulus, G, is required. Conventionally, $r_{eq}$ is assumed as $2/3r_o$ for solid specimens. In this work, the angle of twist is measured with a proximitor mounted atop of the specimen at a radius $r_{sensor}$.

Thus, shear strain equivalent, $\gamma_{eq}$ as function of the radius may be denoted by using the following equation,

$$\gamma_{eq} = \frac{r_{eq}\,\theta_{max}}{h} \qquad (2.16)$$

where,

$$\theta_{max} = \frac{x}{r_{sensor}} \qquad (2.17)$$

Equations 2.16 and 2.17 were used in this research work to determine the equivalent shear strain for each test performed.

## 2.6 Fundamentals of Bender Elements Testing

### *2.6.1 Introduction*

Bender elements are powerful laboratory tools used worldwide to measure the shear wave velocity of the soil samples, and to further calculate the small-strain shear modulus, G. However, the continuing evolution of equipment and technique indicates that objective measurement remains a challenge, and the search for technique standard is necessary. Compared with other methods, bender element technique is relatively simple to use and is non-destructive allowing for repeated test during experiment, consequently offering a convenient method of determining shear waves velocities in laboratory samples (Leong et al., 2005).

Shirley and Hampton (1978) first suggested the concept of using piezoceramic bender elements to measure the shear wave velocity in soils. These piezoceramic plates are embedded in the bottom pedestal and the top platen of some of conventional geotechnical laboratory apparatus, such as triaxial, oedometer, and resonant column. Base pedestal and top platen can be of different sizes those specified by the ASTM. The cantilevering length is variable in the range of 3mm and 9mm. However to ensure accurate and reliable results, both transmitting and receiving cantilevering length, should maintain the same dimensions Figure 2-10.

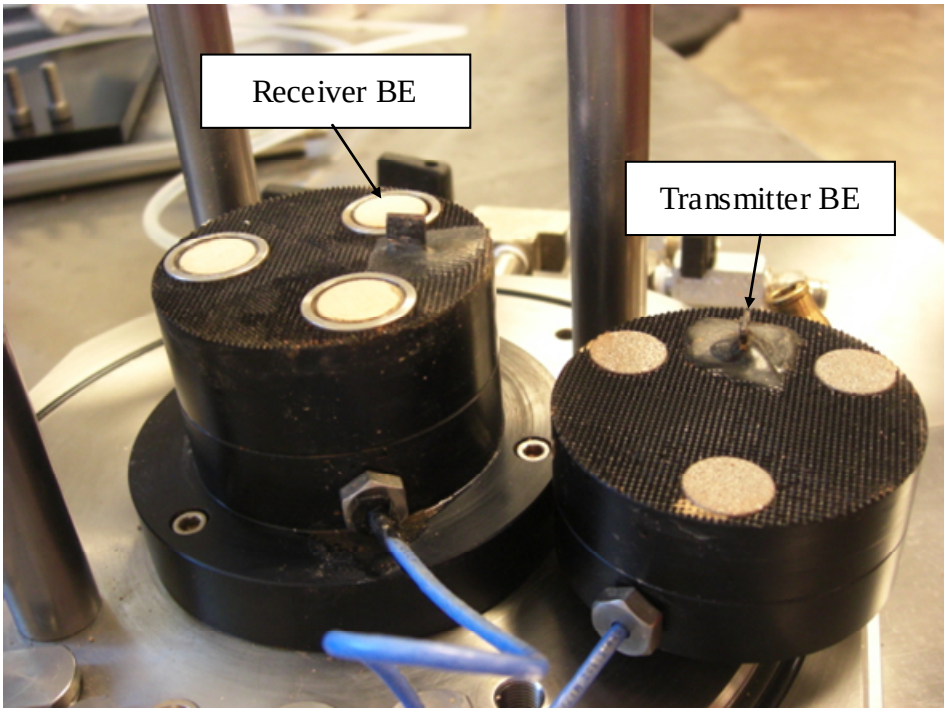


Figure 2-10 Typical set of transmitter and receiver bender elements

A pulse generator as well as a function generator feed the transmitter element with a waveform voltage of 20V, causing it to bend so that shear pulsed is sent through the sample. A small voltage between 0.1 to 5mV is generated by the motion of the receiver element caused by the arrival signal. A digital oscilloscope connected to the personal computer captures the transmitted and received waves, and G is obtained from the shear wave velocity, Vs, as it travels through the specimen.

To understand the spectrum system in the transmitter and arrival signals, Viggiani and Atkinson (1995) suggested a sine pulse as the input signal to reduce the degree of subjectivity in the interpretation, and to avoid the difficulty in interpreting the square wave response, which is typically used as transmitting wave.

*2.6.2 Working Mechanism*

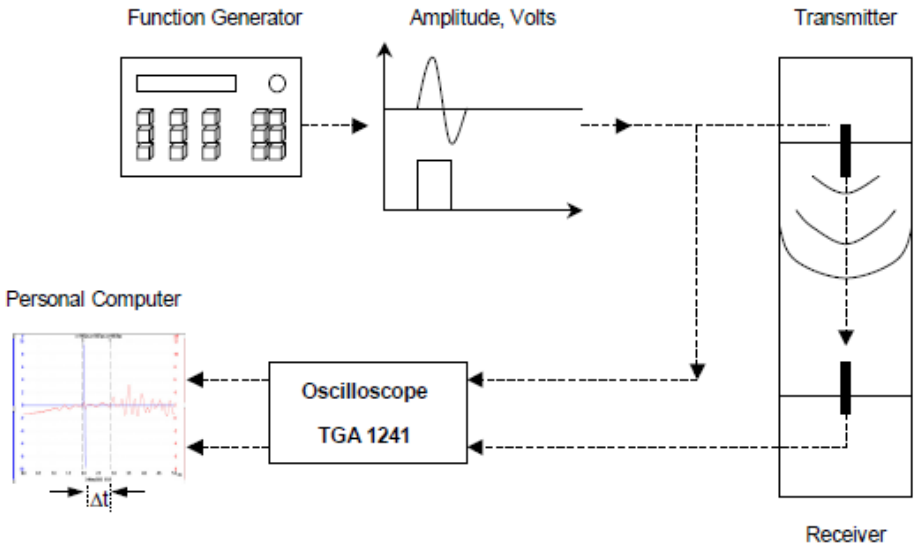


Figure 2-11 Schematic representation of bender element test layout (modified from Mohammad, 2008)

Shear waves are generated and measured by small pieces of piezoceramic called bender elements, which are mounted in the end caps of the specimens. Piezoceramics are able to convert electrical impulses to mechanical impulses and vice versa. If two piezoceramic sheets are mounted together with their respective polarities opposite to each other, an electrical impulse will cause one side to lengthen and the other side to shorten. The net result of this will be a bending of the two sheets, hence the name bender elements (Takkabur 2006).

Thus, if an electrical impulse is sent to a bender element mounted in the top cap of a specimen, the bender element will produce a small “wiggle” and generate an Oscilloscope TGA 1241 shear wave that will propagate down through the soil. When the shear wave reaches the bottom of the specimen it will cause the bender element mounted in the bottom cap to vibrate slightly, thus creating an electrical impulse. Using a parallel connection between personal computer and an oscilloscope, one can observe both the impulse that is sent to the top bender

element (transmitter) and the impulse that is generated by the bottom bender element (receiver), the time it took the wave to propagate can be measured directly, and is called arrival time.

*2.6.3 Resonant Frequency*

The resonant frequency of bender elements affects the size of the near field, travel time determination, resolution, and skin depth. Therefore, the resonant frequency is an important design parameter for bender element installations (Lee and Santamarina, 2005).

The resonant frequency of a bender element into a soil mass is affected by the soil density and stiffness. The influence zone on each side of the bender element is assumed to be the bender element width *b*. Hence the spring constant of the soil $k_s$ can be estimated as

$$k_s = \frac{F}{\delta} = \frac{(bL_b)\sigma}{\frac{\sigma}{E_s}\cdot b} = E_s L_b \qquad (2.18)$$

The elastic modulus of the soil $E_s$ can be calculated using the shear wave velocity $V_S$, Poisson's ratio $\upsilon$ and the mass density of soil $\rho_s$. Then, the equivalent spring constant of the soil mass becomes

$$k_s = 2V_S^2 \rho_s (1+\upsilon) L_b \qquad (2.19)$$

The effective soil mass $m_s$ is related to the $b^2 L_b$ volume,

$$m_s = (\rho_s b^2 L_b)\beta \qquad (2.20)$$

where $\beta$ is an experimental value. Finally, the resonant frequency of a bender element in soil is herein estimated by combining the mass and stiffness of the bender element and the affected soil, resulting in an equivalent spring constant $k_{eq}=k_b+k_s$ and an equivalent mass $m_{eq}=m_b+m_s$. Then, the resonant frequency of a bender element buried in a soil mass becomes (refer to Equation 3),

$$f_r = \frac{1}{2\pi}\left[\frac{1.875^4 \frac{E_b I}{(\alpha L_b)^3} + 2V_S^2 \rho_s (1+\upsilon) L_b}{\rho_b bt(\alpha L_b) + (\rho_s b^2 L_b)\beta}\right]^{\frac{1}{2}} \qquad (2.21)$$

## 2.7 Basic of Unsaturated Soil Mechanics

For long time, traditional soil mechanics primarily focus on soils under saturated conditions, which commonly employ effective stress as a key element for estimating effective shear strength behavior for being used in different applied cases. This classical theory estimates positive pore water pressures for those materials beneath water table and fully dry conditions for those soils above water. However, in unsaturated soils, both soil suction and stresses contribute to the variations in strength and volume change properties of soils. The majority of expansive, compacted and stabilized soils in the field are under partial saturation soil conditions. In this section, parameters of importance in unsaturated soil mechanics, suction properties, and soil water characteristic curves are detailed.

Saturated soil mechanics has experienced significant changes in the past few decades. Some of these changes are related to increased attention given to the unsaturated soil zone (vadose zone), which is above the ground water table (Fredlund and Rahardjo, 1993). However, the development of unsaturated soil mechanics has been relatively slow in comparison to saturated soil mechanics. It is interesting to note that the earlier form of the literature in 1936 had started focusing on unsaturated soil behavior (Fredlund and Rahardjo, 1993).

Subsequently, the concepts for understanding unsaturated soil behavior, are slowly established (Bishop, 1959). In the 1950's, most of the attention given to unsaturated soils was related to capillary flow (Black and Croney, 1957; Williams, 1957; Bishop et al., 1960; and Atchison, 1967). This research resulted in the proposal of several effective stress equations for unsaturated soils. In 1977, Fredlund and Morgenstern described the stress state for unsaturated soil by using two independent normal stress variables, which are net normal stress ($\sigma_{net} = \sigma - u_a$) and matric suction ($\psi = u_a - u_w$).

Basically, the water content in unsaturated soil is a function of the suction present in the soil. The relationship between the water content in soil and the suction can be expressed in a plot of volumetric water content versus suction curve that is well-known as the soil-water characteristic curve (SWCC). Both suction and SWCC profiles can be used to understand changes in void and saturation levels in unsaturated expansive soils that are subjected to soaking. Hence, an understanding of these principles will provide a better explanation of the mechanisms that lead to soil swelling and shrinking. Sections 2.7.2, 2.7.3, and 2.7.4 describe various properties of unsaturated soils, suction measurement techniques, and fundamentals of soil-water characteristic curve, respectively.

*2.7.1 Partially saturated soil profile*

The unsaturated zone can be divided into three subzones, the capillary, intermediate (or vadose), and soil water zones as shown in Figure 2-12. In coarse materials, the saturated zone is located below the ground water table. In fine-grained materials, the saturated zone can reach higher levels than the ground water table because of capillary forces (Bear, 1979). The extension of this so-called capillary zone depends on the soil stratigraphy, the grain size distribution, and the soil density. The unsaturated zone is located above the saturated part of the capillary zone (Bear, 1979).

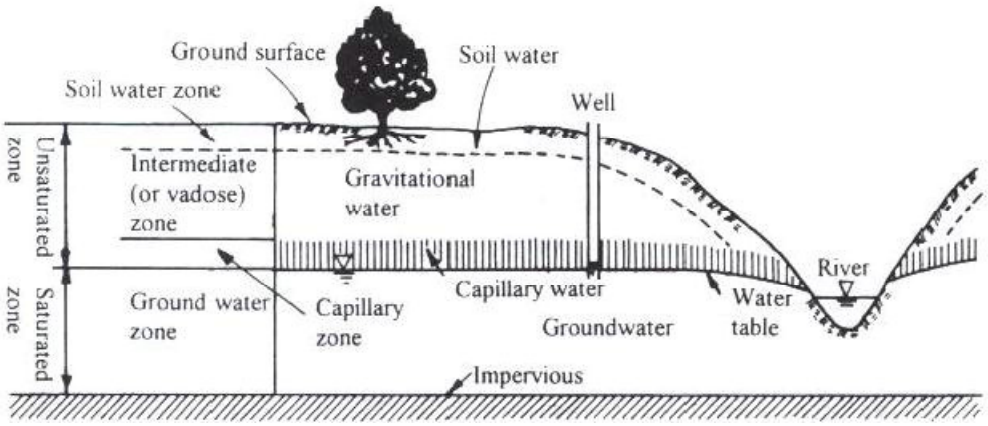


Figure 2-12 Unsaturated soil profile (Bear, 1979)

The zone situated closest to the ground surface is called the soil water zone. The water content in this zone depends heavily on climatic conditions. During periods with high precipitation, the pores may be filled with water and fully saturated, while during dry periods the pores may be almost completely filled with air. Evaporation and transpiration as well as the root system of vegetation play an important role for how much of the precipitation that will infiltrate down to the ground water table.

Finally, the zone situated between the soil water zone and the capillary zone is called the intermediate zone. The water content in this zone depends on the percolation from the upper layer. The water is transported by gravitational forces down to the ground water.

*2.7.2 Soil suction*

Soil suction is commonly referred to as the free energy state of soil water (Edlefsen and Anderson, 1943). The free energy of the soil water can be measured in terms of the partial vapor pressure of the soil water (Richards, 1965). According to Fredlund and Rahardjo (1988), the soil suction in terms of relative humidity is normally called total suction. Total suction of a soil is made up of components, namely, matric and osmotic suctions. The total suction is then described as

$$\psi = (u_a - u_w) + \pi \qquad (2.22)$$

where: ψ is total suction, ($u_a$-$u_w$) is matric suction, $u_a$ is the pore-air pressure, $u_w$ is pore-water pressure, and π is defined as osmotic suction. While matric suction varies with time due to weather changes, osmotic suction is associated more with the presence of salt content in the pore-water phase, where its role is therefore applicable to both saturated and unsaturated soils.

2.7.2.1 Osmotic suction

According to The Department f the Army USA (1983), the osmotic suction, also known as π, is caused by the concentration of salts into the water, and it is pressure-independent. It is result from the difference between the pure water and the partial pressure of water vapor in equilibrium so that it can be in equilibrium with the groundwater. Nonetheless salts in the pore water may be found in both saturated and unsaturated soils, even if the osmotic effect is being associated more with unsaturated soils.

The osmotic pressure has an effect on the mechanical behavior of the soil in both the saturated and unsaturated zones, but is normally neglected. Fredlund (1989, 1991) and Fredlund and Rahardjo (1993) discussed reasons for this practice. In most geotechnical problems, the change in osmotic suction can be neglected and the change in total suction is equal to the change in matric suction, as shown in Figure 2-13. Consequently, if the pore air pressure is equal to the atmospheric pressure, the total pressure becomes equal to the negative pore pressure. However, if salts are present in soils, then the osmotic component of suction must be taken into account.

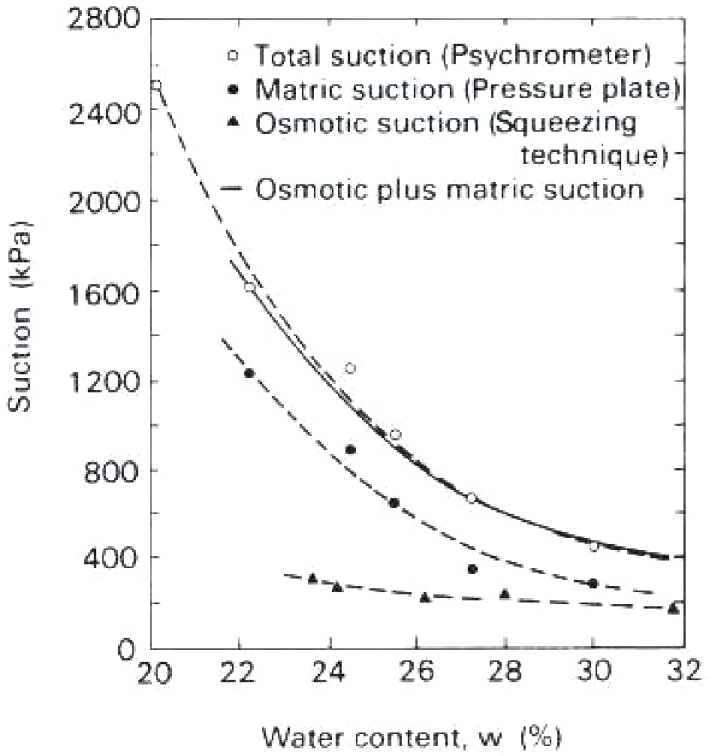


Figure 2-13 Total, matric, and osmotic suction measurements on compacted Regina clay (from Fredlund and Rahardjo, 1993)

2.7.2.2 Matric suction

The matric suction is defined as the difference between the pore-air pressure, known as $u_a$, and the pore-water pressure, $u_w$ (Fredlund and Rahardjo, 1993). This suction, identified as $(u_a-u_w)$ is associated to capillary tension in the pore water, and water sorption forces of the soil particles, both of them linked to the geometrical configuration of the soil (Department of the Army USA, 1983; Lu and Likos, 2004). Matric suction may fluctuate with time due to weather and surrounding environmental changes. For this reason, dry and wet seasons create variation in the suction profile, mainly close to the surface (Fredlund and Rahardjo, 1993. In addition, field factors such as ground surface conditions, environmental conditions, vegetation, water table, and permeability of soil play an important role on the suction variation into the soil profile.

**Ground surface condition**: The matric suction below an uncovered ground surface is affected by environmental changes. Dry and wet seasons cause variations in the suction, particularly near the ground surface. In real field conditions, suction beneath a covered ground surface is more constant with time than beneath an uncovered surface (Fredlund and Rahardjo, 1993).

**Environmental conditions**: The matric suction in the soil increases during dry seasons and decreases during wet seasons. Maximum changes in soil suctions occur near the ground surface (Fredlund and Rahardjo, 1993).

**Vegetation**: The presence of vegetation on the ground surface has the ability to apply a tension to the pore-water of up to 1-2 MPa through the evapotranspiration process. Evapotranspiration results in the removal of water from the soil and an increase in the matric suction. However, the evapotranspiration rate is the function of climate, the type of vegetation, and the depth of the root zone (Fredlund and Rahardjo, 1993).

**Water table**: The depth of the water table influences the magnitude of the matric suction. The deeper the water table, the higher the possible matric suction (Fredlund and Rahardjo, 1993).

**Permeability of the soil profile**: The permeability of soil represents its ability to transmit and drain water. This indicates the ability of the soil to change matric suction as the environment changes (Fredlund and Rahardjo, 1993).

*2.7.3 Soil Water Characteristic Curve, SWCC*

The soil water characteristic curve, SWCC, plays a key role in applying unsaturated soil mechanics in engineering practice. The suction versus volumetric water content, gravimetric water content or degree of saturation is referred to as the soil-water characteristic curve (SWCC) or the water retention curve.

The soil-water characteristic curve can be obtained by performing tests using pressure plate device in the laboratory by following the axis-translation technique (Hilf, 1956). In the late 1950's, soil-water characteristic curve was commonly used to predict the coefficient of permeability at specific water content in terms of matric suction (Mashall, 1958, Millington and Quirk, 1961). This soil-water characteristic curve is also required in the determination of water volume changes in the soil respect to matric suction change. The coefficient of water volume change with respect to matric suction is given by the slope of the soil-water characteristic curve.

Table 2-1 Devices for estimating soil water characterisic curve (Fredlund and Rahardjo, 1993)

| Name of device | Suction component measured | Range (kPa) | Comments |
|---|---|---|---|
| Psychrometers | Total | 100-~8000 | Constant temperature environment required |
| Filter paper | Total | (Entire range) | May measure matric suction when in good contact with moist soil |
| Tensiometers | Negative pore-water pressures or matric suction when pore-air pressure is atmospheric | 0 – 90 | Difficulties with cavitation and air diffusion through ceramic cup |
| pressure plates (axis translation) | Matric | 0 – 1500 | Range of measurement is a function of the air entry value of the ceramic disk |
| Thermal conductivity sensors | Matric | 0-~ 400+ | Indirect measurement using a variable pore size ceramic sensor |
| Pore fluid squeezer | Osmotic | (Entire range) | Used in conjunction with a psychrometer or electrical conductivity measurement |

Experimental techniques for measuring the SWCC vary widely in terms of costs, complexity, and measurement range. It is possible to use different equipments to test the soil depending on whether the material is sand, silt, or clay. The Tempe pressure cell and other pressure plate apparatuses (Soil moisture Equipment Corporation), thermal conductivity

sensors (Phene et al., 1971; Fredlund and Wong 1989), thermocouple psychrometers (Spanner 1951; Richards and Ogata 1958), chilled-mirror hygrometers (Gee et al., 1992), and filter paper methods (Gardner 1937) can be used for the determination of the suction-water content relationship. Used techniques and measurement ranges of the above given equipments are summarized in Table 2.1.

The Pressure plate apparatuses use the axis-translation technique (Hilf 1956) and have a measuring range between 0 and 1500 kPa depending on the ceramic disk placed in the device. These types of cells are often used to investigate porous material. For testing sand samples Eching and Hopmans (1993), Wildenschild et al. (1997), Wildenschild et al. (2001), and Chen et al. (2007) either used pressure cells or modified pressure cells. Pressure plate was used in this research work to build a plot the SWCC of the tested soil. Figure 2-14 depicts a typical SWCC of several samples from different soil deposits.

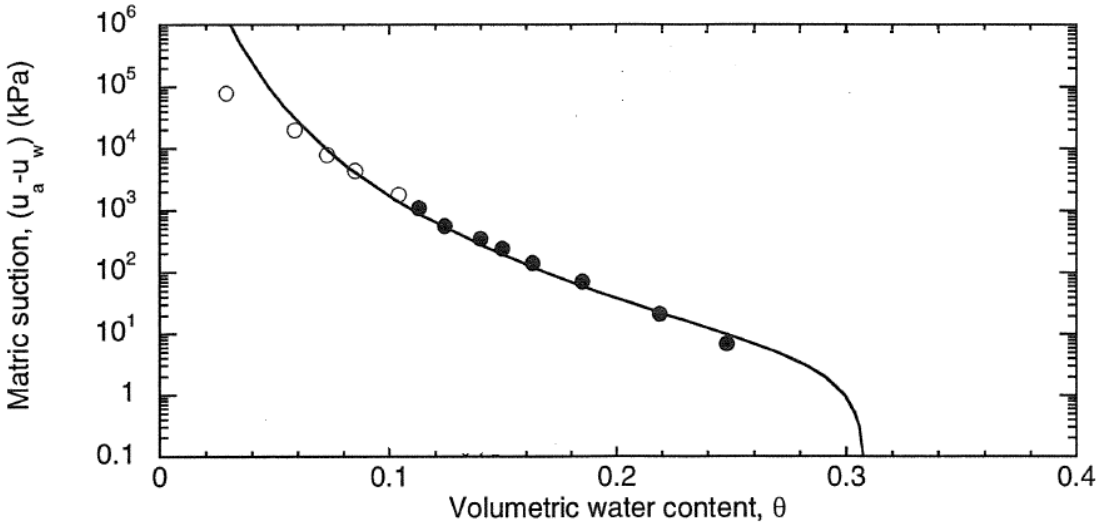


Figure 2-14 Typical soil water characteristic curve (Sawangsuriya et al., 2006)

According to Bear (1979), three different stages of saturation can be distinguished in a soil profile as shown early in Figure 2-12. The water phase is discontinuous except for the very thin film of water around the solids at low degrees of saturation the water phase. This stage is called “pendicular” stage. As saturation is high, both water and air phases are continuous and water flow is expected to occur. This stage is termed as ‘”Funicular” stage. As the degree of saturation increases more, the air in the water turns into small bubbles and the air phase becomes discontinuous.

Likewise, as the soil is drained, the total or matric suction will increase, and suction will reduce when soil is refilled with water again. By comparing the amount of drained water with the increase in suction, a relationship between the degree of saturation (or volumetric water content) and the matric suction of the soil can be established. This relationship is called the soil water characteristic curve of a soil as may be seen in figure 2-14.

*2.7.4 Measurement of suction*

Total suction or the free energy of the soil water can be determined by measuring the vapor pressure of the soil water or the relative humidity in the soil. The direct measurement of relative humidity in soil can be conducted using a device called a Psychrometer. The relative humidity in soil can be indirectly measured by using filter paper as a measuring sensor.

2.7.4.1 Direct measurement – Psychrometer

The thermocouple psychrometers can be used to measure the total suction of soil by measuring the relative humidity in the air phase of the soil pores or the region near the soil. Nowadays, the most commonly used instrument is the Wescor Dew Point Microvoltmeter.

2.7.4.2 Indirect measurement – Filter paper

Filter paper method is classified as an “indirect method” of measuring soil suction. It is based on the assumption that filter paper will come into equilibrium with the soil having a specific suction. Equilibrium can be reached by either liquid or vapor moisture exchange

between the soil and the filter paper. After the filter paper reaches equilibrium, the water content of the filter paper was measured. There are two types of filter papers used in practice, which are contact and non-contact filter papers. The water content of contact paper corresponds to the matric suction, and the water content of non-contact filter paper corresponds the total suction of the soil.

*2.7.5 Measurement of Matric Suction*

Matric suction can be measured either in a direct or indirect manner. Tensiometer, piezometer, and the axis-translation apparatus are commonly used as a direct measurement. Indirect measurement of soil matric suction can be made using a standard porous block as the measuring sensor. This particular work briefly describes some of direct measurement methods to achieve matric suction in a soil specimen. From all devices described below, pressure plate extractor was chosen for the purposes of this research.

2.7.5.1Tensiometers

Tensiometer measures matric suctions in the field (Richards and Gardner, 1936, Fredlund and Rahardjo, 1993). The tensiometer consists of a high air entry porous cup connected to a measuring device through a narrow, very stiff plastic tube. The negative pressure measured in the tensiometer is equal to the matric suction (if $u_a = u_{atm}$) in the soil. The negative pressure in the tensiometer can be measured by the use of a mercury manometer, electrical pressure transducer, or vacuum gauge. The suction range of the tensiometer is limited due to cavitation in the system when the pressure approaches the vacuum. The upper limit is about 90 kPa. Problems with diffusion of air through the porous cup into the tensiometer constitute another limitation (Fredlund, 1989). Removal of the diffused air and the refilling of water on a regular basis is a method of reduce the problem (Fredlund and Rahardjo, 1993).

#### 2.7.5.2 Piezometers

The piezometer, named as the BAT-piezometer, consists of a chamber closed at the top by a double rubber membrane and surrounded by a porous filter. A special ceramic high-air-entry filter is used in the measurements of the matric suction. The piezometer can be used to measure either a negative or positive pressure relative to the atmospheric pressure depending on whether the ground water table rises above the filter tip or not. This means that the transducer used must be calibrated for both positive and negative pressure ranges (Tremblay, 1995).

#### 2.7.5.3 Pressure Plate Drying Test

The pressure plate utilizes the axis translation technique (Hilf, 1956) to measure matric suction in soil specimens over a wide pressure range in the laboratory. As shown in figure 2-15, different soil specimens may be placed on a saturated high air- entry porous disc, and the air-tight chamber is pressurized to desired matric suction. Matric suction is measured versus various different degrees of saturation states, gravimetric or volumetric water content of soil samples. This device can induce suction levels up to 15bars.

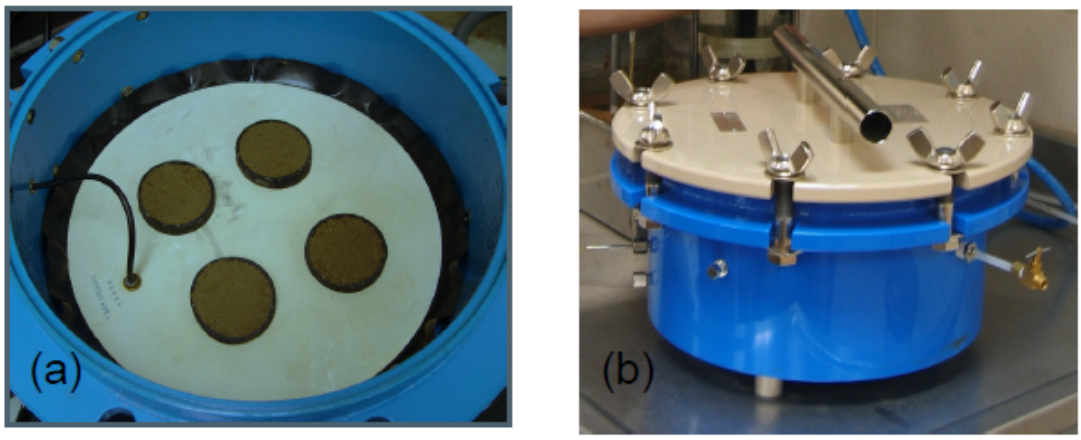


Figure 2-15 Pressure plate device: (a) sample placing arrangement, and (b) sealed vessel

## 2.8 Previous Works

Many studies have been performed to describe the factors that affect *G*/*G*max and material damping ratio, D, of soils (e.g., Richart et al. 1970; Seed and Idriss 1970; Hardin and Drnevich 1972b; Iwasaki et al. 1978; Lee and Finn 1978; Zen et al. 1978; Kokusho et al. 1982; Seed et al.1986; Ni 1987; Sun et al. 1988; Vucetic and Dobry 1991; Ishibashiand Zhang 1993; Rollins et al. 1998; Vucetic et al. 1998; Stokoe et al. 1999; Darendeli 2001; Roblee and Chiou 2004; Stokoe et al. 2004). All above research coincided that the most important factors affecting *G*/*G*max include shear strain magnitude $\gamma$, mean effective confining stress ($\sigma'$), soil type and plasticity index (PI). Other factors that affect *G*/*G*max, but appear to be less important, include: frequency of loading, number of loading cycles, overconsolidation ratio, void ratio, degree of saturation, and grain characteristics (Darendeli 2001).

In terms of degree of saturation, which is nothing than presence of water content within the sample, a large branch of geotechnical engineering have emerged to establish that stiffness properties highly depend on degree of saturation. In the last three decades significant attempts regarding dynamic properties of the soils have been performed by using resonant column

testing, bender elements and axis translation technique to measuring the variation of shear modulus and damping ratio at very small strain under partially saturated conditions. First, Brull (1980) and Wu et al. (1985) reported linear relationships between initial shear modulus $G_o$ and soil suction for silty and sandy soils in the 0-80 kPa suction range. In both cases, the degree of saturation $S_r$ of the soil was evaluated after measuring soil stiffness via resonant column testing. The testing procedure consisted in applying a confining pressure on the unsaturated specimen, under drained conditions, and then measuring $G_o$ after 1,000 minutes. The $G_o$ vs. $S_r$ functions show a distinct peak for initial shear modulus $G_o$ corresponding to $S_r$ values between 10%-20%, for any given confining stress.

The effect of capillarity on small-strain shear modulus of partially saturated sands was studied by Qian et al. (1991) by using a Hall-type resonant column apparatus. They concluded that the increment on shear modulus depends on the capillary stress levels. Void ratio, confining pressure, degree of saturation, grain shape and size distribution were identified as the major factors affecting the soil's shear modulus.

In the 90's decade bender element testing became a feasible, simple and suitable technique for measuring shear modulus of soils. Marinho et al. (1995) performed bender element tests on London clay samples assessing soil suction via filter paper technique. Picornell and Nazarian (1998) also reported some results obtained from reconstituted samples of silt and clay using bender elements inside a suction plate. They concluded in both cases that the small-strain modulus tends to be a constant value as the soil moistures moves towards residual water content.

Bender element testing was also adapted by Cabarkapa et al. (1998) to a cylindrical triaxial cell to test silty specimens, in this case, under controlled suction states via axis-translation technique. They stated that, for normally-consolidated quartz silt, the unsaturated $G_o$

values can be readily assessed by multiplying the saturated $G_{sat}$ values corresponding to the same net pressure, $(p - u_a)$, by a factor that depends only on matric suction, $s = (u_a - u_w)$.

Recently, an experiment based on unsaturated particulate material with emphasis on pendular menisci stage was performed by Cho and Santamarina (2001). They performed a series of bender element and small-strain stiffness was continuously measured on soil specimens subject to drying while changes in stiffness were related to changes in interparticle forces. Soils included glass beads (spherical particle), a mixture of glass beads and kaolinite (flat particles – clay), granite powder (angular particles – silt), and sandboil sand. They concluded that while capillary forces affect small-strain stiffness (shear-wave velocity), they may not contribute to the large-strain stiffness or strength.

As seen on the previous review, considerable efforts have been shown in the last thirty years to investigate the influence of both capillarity and degree of saturation on the small-strain stiffness under unsaturated conditions by using either resonant column or bender element based testing technique.

Despite all of these efforts have made important contributions in this area, practically none have directly dealt with neither resonant column testing non bender elements mounted within resonant column under suction-controlled techniques. Nonetheless, it was not until this decade when Mancuso et al. (2002) and Vasallo et al. (2007) performed a series of suction-controlled resonant column/torsional shear tests on unsaturated silty soil using an RC/TS, which was originally developed at the University of Napoli, Italy. Matric suction, $s = (u_a - u_w)$, was induced via the axis-translation technique, while the torsional torque was progressively increased to study soil stiffness response at small, mid, and high-shear strain amplitude levels. Results within the small-strain range were similar to those reported by Cabarkapa et al. (1998) using bender element based technique, and no attempt was made to study the effects of suction state on material damping D of the tested unsaturated silty sand.

# CHAPTER 3

# CALIBRATION AND PERFORMANCE OF RESONANT COLUMN DEVICE

## 3.1 Introduction

This chapter presents results from calibration and reliability tests performed on a new proximitor-based resonant column device. The calibration process was performed through a comparative analysis of results from this apparatus and those from an accelerometer based-resonant column.

At the beginning of this chapter, a complete process of device calibration by using stainless aluminum bars and discs was achieved. Resonant column tests for this exercise were conducted to figure out the polar moment of inertia of the driver system, which is a needed requirement for running actual tests in soil samples.

A family of physical and basic soil mechanic tests was conducted on the same soil mass. Their results are shown to characterize the soil type used in this research work. The soil mass was defined as yellow compacted silty sand.

A detailed description of the proximitor based-resonant column is included. All main components such as main cell, driver system, measurement digital sensors, and software capabilities are presented.

This chapter also describes the comparative analysis between both resonant column devices (accelerometer-based and proximitor-based). Linear and non-linear behavior of compacted silty sand from both devices are presented and compared through frequency sweeps induced to the samples. Also, shear modulus and material damping ratio were evaluated for each device and later compared.

## 3.2 Calibration of Resonant Column

The calibration of the proximitor-based RC is performed using an aluminum rod instead of a real soil specimen. The rod is assumed to have zero, or close to zero, damping and a constant torsional stiffness, k. Then, from Newton's second law, the mass moment of inertia is related to the natural resonant frequency, $\omega$, as following:

$$I = \frac{k}{\omega^2} \qquad (3.1)$$

Even though the torsional stiffness, k, of the aluminum rod can be found by applying a constant torque and measuring the angular rotation, this is not normally done. Without knowing the torsional stiffness, k, the mass moment of inertia, I, in equation 3.1 cannot be solved. The recommended procedure to find the mass moment of inertia of the system, $I_o$, is to perform two resonant column tests with metal calibration specimens, one by itself and the other with added mass. Perform a frequency sweep with constant force amplitude to find the resonant frequency of each configuration. The force amplitude is selected to excite the calibration specimen within the limits of the installed sensors (proximitor) but still provide a large enough signal to measure the response accurately. The solution of equation 3.1 for the first calibration run without the added mass becomes:

$$I_o + I_{cal} = \frac{k}{{\omega_1}^2} \qquad (3.2)$$

where, $I_o$ = mass moment of inertia of the drive system and any other fixture that will be used during the test.

$I_{cal}$ = mass moment of inertia of the calibration specimen, and

$\omega_1$ = resonant frequency of calibration specimen without the added mass.

The second equation for the second calibration run attaching the added mass is:

$$I_o + I_{cal} + I_{mass} = \frac{k}{{\omega_2}^2} \qquad (3.3)$$

where, $I_{mass}$ = mass moment of inertia of the added mass, and

$\omega_2$ = resonant frequency of calibration specimen with the added mass.

Now, to find the mass moment of inertia of the whole driving system that will be used for solving the mass moment of inertia of the system including the top cap, $I_o$, equations 3.2 and 3.3 are combined to get:

$$I_o = \frac{(I_{cal} + I_{mass}){\omega_2}^2 - I_{cal}{\omega_1}^2}{{\omega_1}^2 - {\omega_2}^2} \qquad (3.4)$$

It should be noted that for this calibration procedure, the specimen top cap is not used. Hence, its mass moment of inertia has to be added to the result of equation 3.4 to calculate the actual $I_o$ value that is entered into the RC software. The mass moment of inertia of the top cap is calculated from its geometry and mass. The calibration specimen and added mass geometries are shown in Figure 3-1 and Figure 3-2 respectively

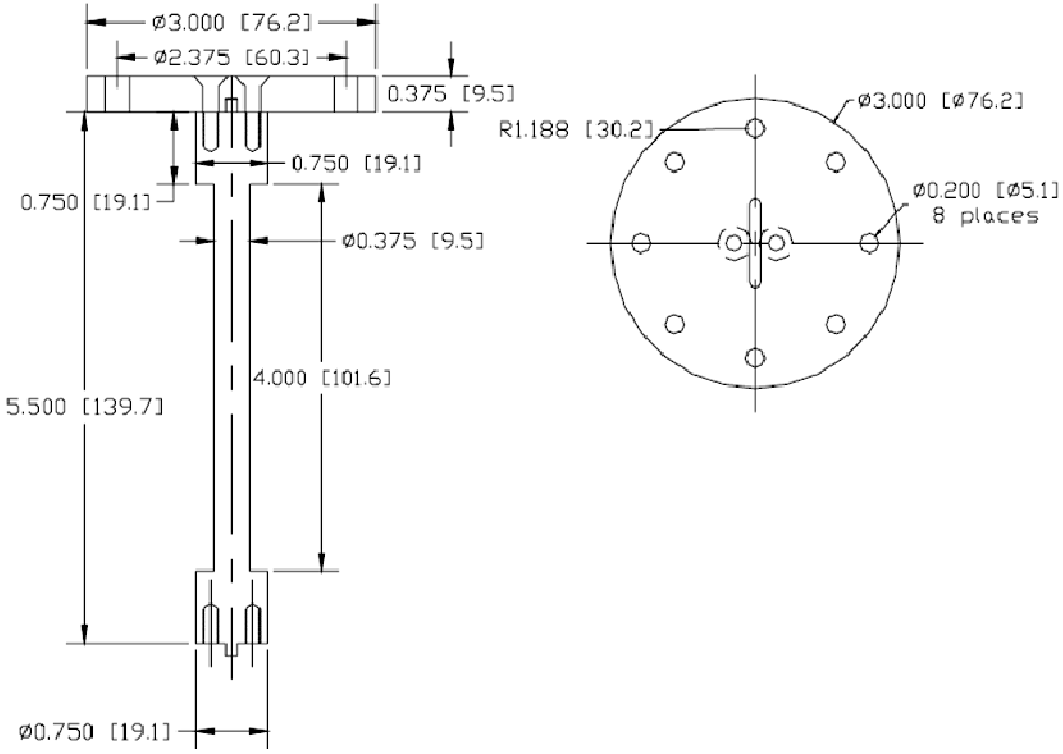


Figure 3-1 Calibration specimen geometry. Units in inches (milimeters)

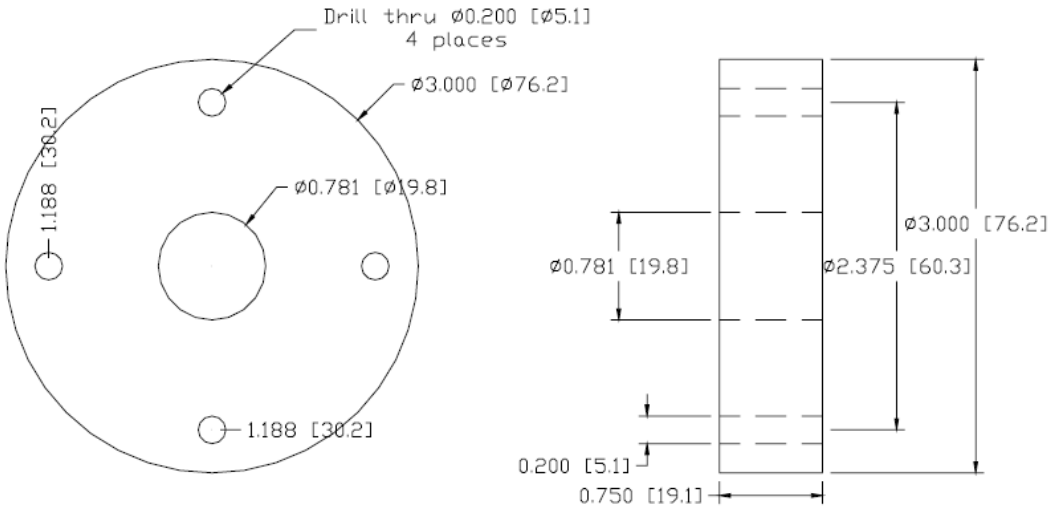


Figure 3-2 Added mass geometry. Units in inches (milimeters)

First, the moment of inertia of calibration specimen is calculated. The calibration specimen is made of 6061-T6 aluminum with a mass density of 2.7 g/cm$^3$. This calculation is done in three parts using the principle of superposition. Then $I_{cal}$ is calculated as:

$$I_{cal} = I_{cal-plate} + I_{cal-rod-end} + I_{cal-rod} - I_{cal-holes} \qquad (3.5)$$

and

$$I_{cal-plate} = \frac{1}{2}mR^2 = \frac{1}{2} * 0.117kg * (38.1mm^2) = 84.9\ kg * mm^2$$

$$I_{cal-rod-end} = \frac{1}{2}mR^2 = \frac{1}{2} * 0.015kg * (9.5mm^2) = 0.7kg * mm^2$$

$$I_{cal-rod} = \frac{1}{2}mR^2 = \frac{1}{2} * 0.019kg * (4.7mm^2) = 0.2kg * mm^2$$

$$I_{cal-holes} = 8 * [I_{hole} + md^2]$$

$$= 8 * \left[\tfrac{1}{2} * 0.01kg * (2.5mm)^2 + 0.001kg * (30.2mm)^2\right] = 3.8\ kg * mm^2$$

thus,

$$I_{cal} = 84.9 + 0.7 + 0.2 - 3.8 = 82.0\ kg * mm^2$$

The threated holes used to attach the top plate to the bar of the calibration specimen are included in the calculation. The voids will be filled with the screws and even though they have a larger density than the aluminum, the error is negligible.

The added-mass is made of 303 stainless steel with a mass density of 7.7 g/cm$^3$. The moment of inertia of the added mass is obtained as:

$$I_{mass} = I_{mass-plate} + I_{mass-holes} \quad (3.6)$$

and,

$$I_{mass-plate} = \frac{1}{2} m\left({R_i}^2 + {R_o}^2\right) = \frac{1}{2} * 0.624kg * (9.9^2 + 38.1^2)mm$$

$$= 483.5\ kg * mm^2$$

$$I_{mass-holes} = 4 * [I_{hole} + md^2]$$

$$= 4 * \left[\frac{1}{2} * 0.003kg * (2.5mm)^2 + 0.003kg * (30.2mm)^2\right]$$

$$= 11.0\ kg * mm^2$$

then,

$$I_{mass} = 483.5 - 11.0 = 472.5\ kg * mm^2$$

Figure 3.3 shows the metal calibration set and its mounting into the Resonant Column apparatus during the calibration process.

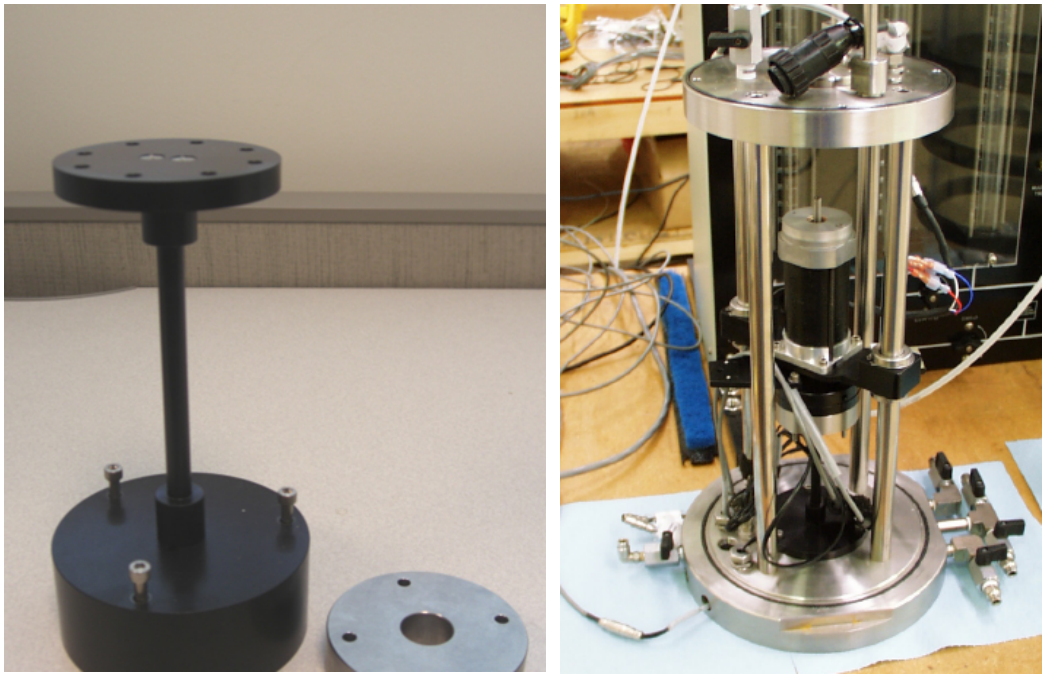

Figure 3-3. Calibration test setup

By performing resonant column tests on the calibration specimen, first without the added-mass and then with the added-mass, the following resonant frequencies are obtained:

$\omega_{\text{no added mass}} = \omega_1 = 84.2$ Hz, and $\omega_{\text{added mass}} = \omega_2 = 66.4$ Hz,

Then from equation 3.4 it is obtained,

---

Because the top specimen cap is not used during this calibration procedure, the mass moment of inertia of the top cap should be added to the above value.

Figure 3-4 shows the two frequency peaks that correspond to each analysis calibration test condition (no mass and mass added). Since the added-mass has lower stiffness than the aluminum bar, the addition of this mass produces a decrement on its stiffness properties. These values are computed to obtain the shear modulus, G.

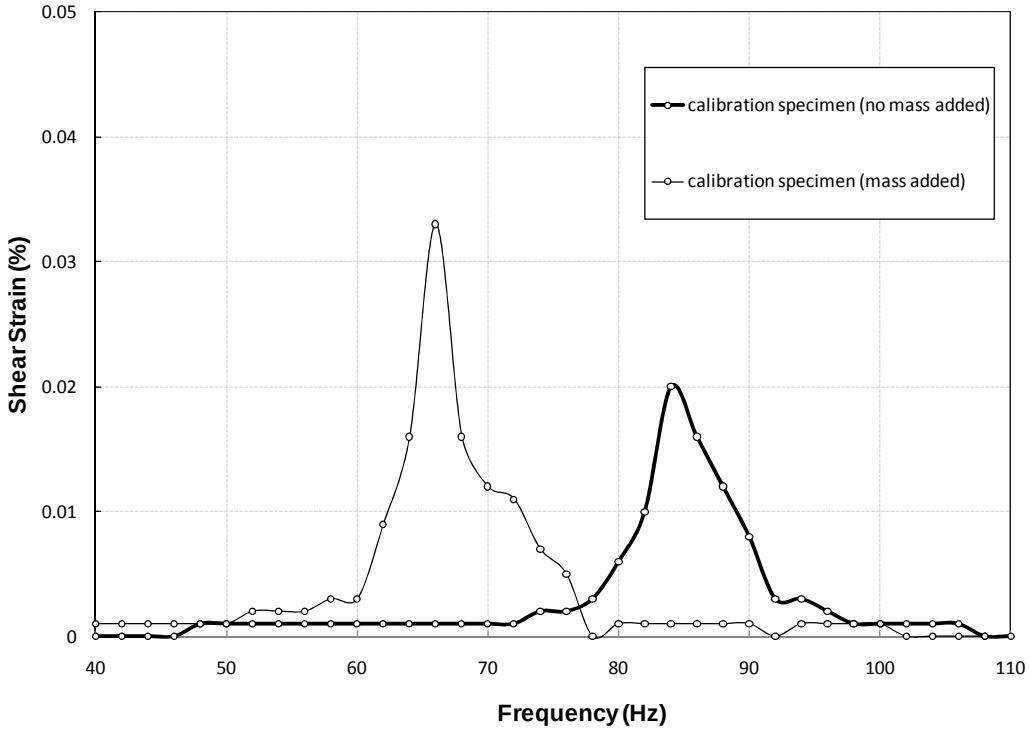


Figure 3-4 Frequency response curves from calibration specimens

To complete the calibration exercise, the shear modulus of the aluminum rod from resonant column tests ought to be compared with those reported in the literature, as shown in table 3.1.

Table 3-1 Comparison of shear modulus values from current RC testing and literature.

| Source | Shear Modulus (GPa) |
|---|---|
| ASTM B308 / B308M - 02 | 26.00 |
| Resonant Column testing, no added mass | 26.04 |

It can be noted that both stiffness values match very close, which means that the new resonant column apparatus yields reliable and accurate stiffness results.

## 3.3 Properties of Testing Soil

### *3.3.1 Basic engineering properties*

The test soil used in this work is a fine grained silty sand rusty dark yellow in color. The soil classifies as A-2-4 and SM according to the AASHTO and USCS, respectively.

In general, from the sieve analysis, particle sizes vary between 11mm and 0.08mm, which means that this soil mainly behaves as a granular soil. Fine percentages ranges between 25 and 35%, while the percentage of sand varies from 65 to 75%. The natural water content ranges between 24% and 29%, with an average value of 26.5%, liquid limit (LL) of 26.4%, plastic index (PI) of 6.2%. For this condition, the total unit weight is 16.7 $kN/m^3$ and the dry unit weight is 13.0 $KN/m^3$. In this material, the specific gravity was estimated between 2.71 and 2.72, and the void ratio was estimated within a range of 1.0 to 1.10.

Basic engineering properties of the testing soil are summarized in table 3.2, and results from sieve analyses are plotted in figure 3.5 to show the granulometric distribution of the soil particles.

Table 3-2 General properties of test soil.

| Property | Value / Result |
|---|---|
| Color | yellow |
| Moisture content (%) | 26.50 |
| Passing No.200 sieve (%) | 30 |
| Specific gravity (Gs) | 2.71 |
| Liquid limit, LL (%) | 26.40 |
| Plastic Index, PI (%) | 6.20 |
| Total unit weight, $\gamma$ (kN/m$^3$) | 16.70 |
| Void ratio | 1.05 |
| AASHTO classification | A-2-4 |
| USCS classification | SM |

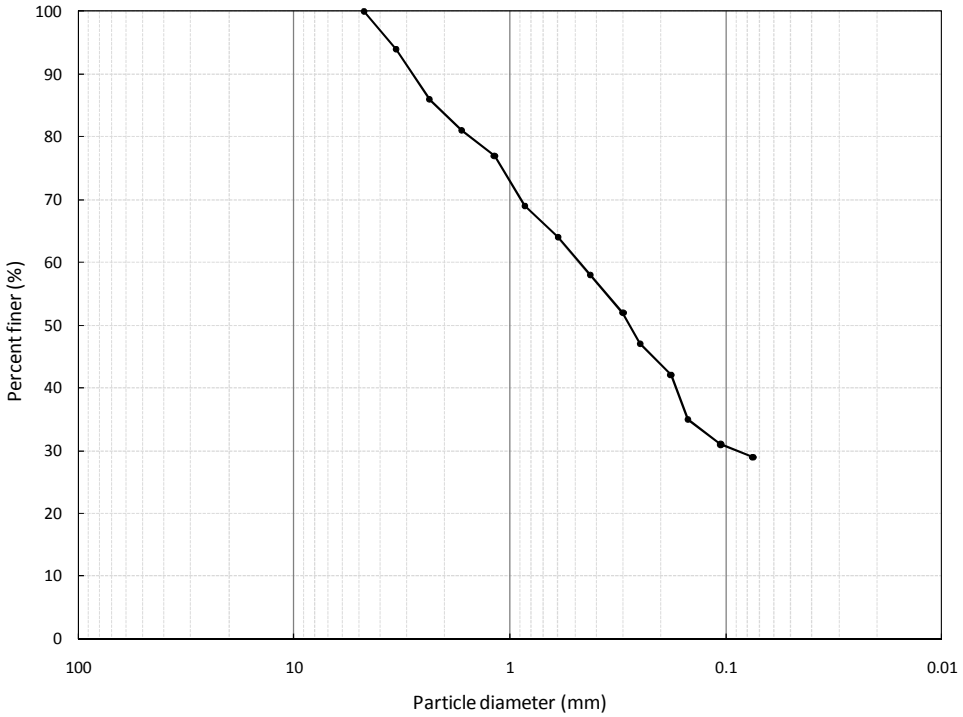


Figure 3-5 Particle-size distribution curve for SM soil

*3.3.2 Soil water characteristic curve*

As mentioned in chapter 2, the soil water characteristic curve of a soil relates the moisture content to the applied matric suction in the soil (Fredlund and Rahardjo, 1993). In order to plot the SWCC for the tested soil, matric suction was induced via a pressure plate extractor by applying axis translation technique. Nine samples of identical dimensions and weights were placed inside the pressure plate vessel and over the ceramic plate. To obtain the experimental points of the SWCC curve, nine different suction levels were induced. These values of matric suction varied between 0 and 800 kPa, as shown in figure 3-6.

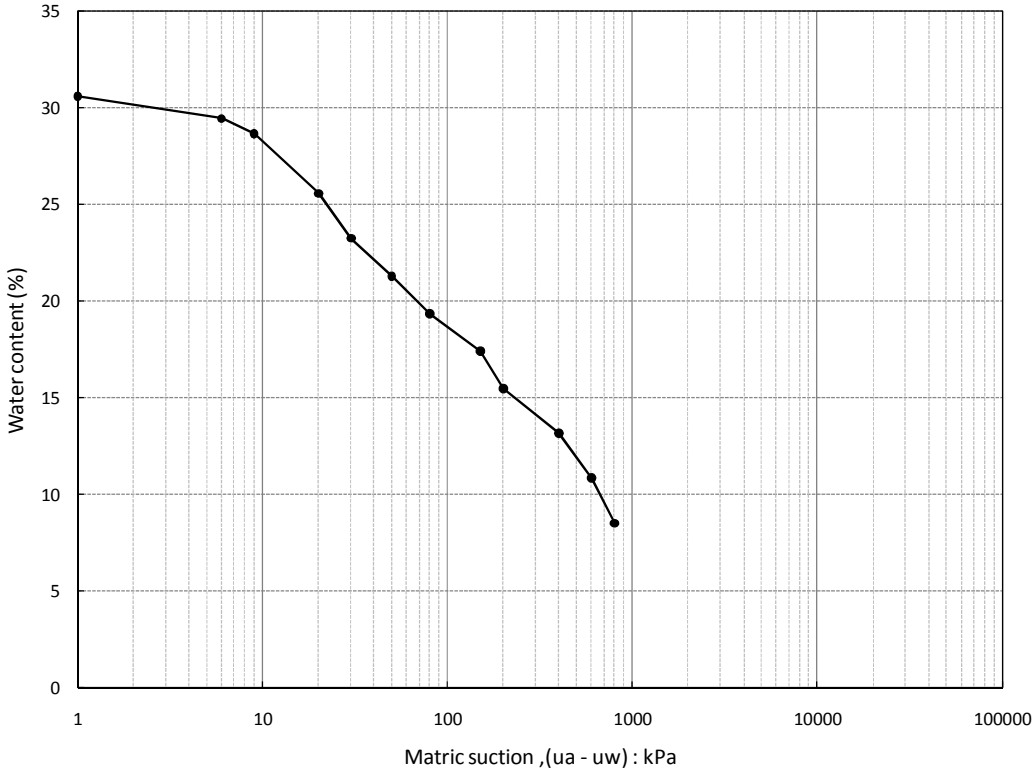


Figure 3-6 SWCC of silty sand

Since the air-entry value is close to 15 kPa, and the residual volumetric water content corresponds to a suction value close to 6000 kPa, the selected range of matric suction states used for testing SM soil is from 50 kPa to 400 kPa.

### 3.4 Basic components of Proximitor-Based Resonant Column device

The proximitor-based resonant column apparatus, which was used throughout this research work, has been developed into a fully automated system to perform suction-controlled through the use of modern sensors and computerized electronics that performs these tests automatically.

In the proximitor-based RC, a harmonic torsional excitation is applied to the top of the specimen by an electromagnetic loading system or motor. A torsional harmonic load with constant amplitude is applied over a range of frequencies and the response curve (strain amplitude) is measured. The shear wave velocity is assessed by measuring the first-mode resonant frequency. The shear modulus hence is obtained from this shear wave velocity and the soil density. Material damping may also be obtained from either the free vibration decay curve after the force vibration is removed or from the Half-power bandwidth method assuming viscous damping.

The proximitor-based RC device developed in this work combines both resonant column and torsional shear effects into one system so that the effects of soil parameters can be evaluated. This system is also capable to measure shear modulus from very low to high strains. Figure 3-7 shows the general layout of the proximitor based-RC used in this research. The RC testing system features five major components: (a) the main cell, (b) servo controller and acquisition system, (c) deformation sensor, (d) resonant column software, and (e) computer unit.


Figure 3-7 General layout of the proximitor-based RC device

*3.4.1Resonant Column main cell*

The resonant column main cell (see figure 3.8) is assembled using four column stainless steel, two of which are used as displacement channel for the driver system and displacement sensor. The cell wall is represented with an external reinforced transparent acrylic plastic. A maximum of 1,000 kPa as isotropic confining pressure capacity is allowed into the system at the time of the test. Also, some feed connectors for internal angular displacement/velocity, torque, and axial deformation transducers are attached to the main top cap of the cell, which make a bridge between the specimen and electronic components. In addition, a drainage system at top and bottom of specimen, which will be discussed in the chapter four, was arranged to control the flow out of the water, and the entering of the air pressure directly upon the sample,


Figure 3-8 Proximitor-based RC Main cell

*3.4.2 Electrical Servo motor driver*

An electrical servo motor actuator is used for the application of torsional loads with a +/- 2.33 kN-m (peak) capacity and 300-Hz frequency. Mounted on an internal floating frame to allow for large vertical specimen deformations, the actuator includes a servo amplifier for closed-loop control of torsional load or angular deformations, as shown in Figure 3-9.

Figure 3-9 Close-up view of proximitor mounting (internal angular displacement transducer)

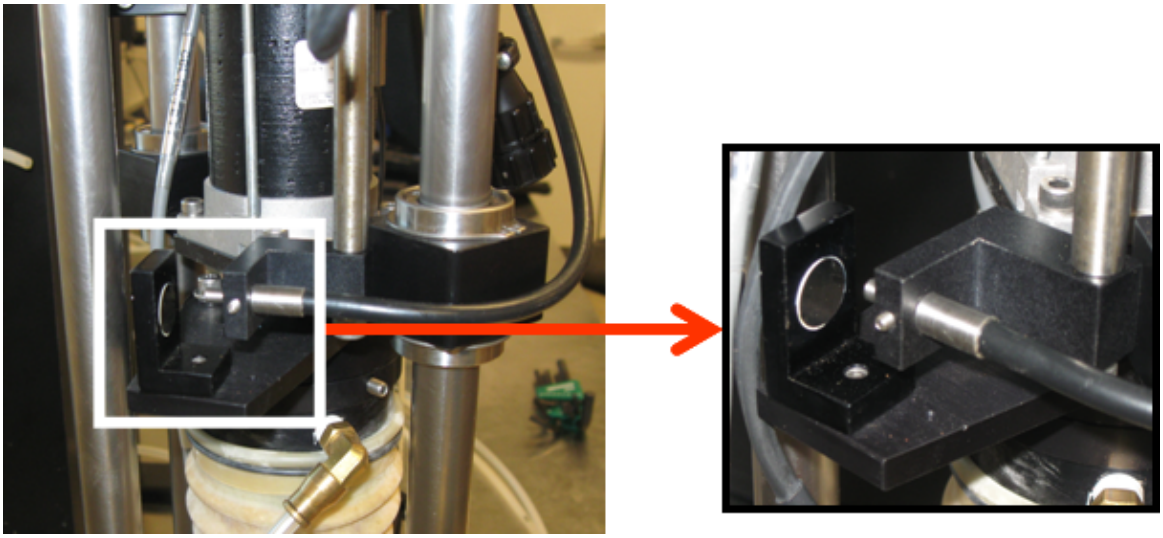

*3.4.3 Digital servo controller and acquisition system*

The digital servo-controlled and acquisition system, which is called by the manufacturer as GCTS SCON-1500 Digital System Controller features digital electronics. Configuration settings are directly operated by software control. This electronic system is capable to activate, control, and storage, vertical and angular displacement, as well as all other variables presented during the at the testing time.

The SCON-1500 model DA/PC system consists of a microprocessor based digital servo controller, function generator, data acquisition, and digital I/O unit. It includes software for performance and data reduction of resonant column tests with automatic calculation of shear modulus, shear strain, and damping ratio at strain levels ranging from 10% to $10^{-4}$%. The signal conditioning mother board accepts up to eight universal signal conditioning module slots (Fig. 3-7).

*3.4.4 Displacement sensor*

Displacement sensors are the vital components of the system as they provide information on the status of the parameters. The novel resonant column test mode requires electrical

sensors to measure the shear strain, in this particular case a proximitor was selected. To guarantee a proper functioning and reliable results, the distance between proximitor and the center of the resonant column should be determined as one of the major variables of the device configuration. The proximitor is a SR-DF-FO-250 fiber optics deformation sensor with dual range output +/- 0.1 mm low range and +/-6.0 mm high range with 0-15 kHz flat frequency response.

*3.4.5 Resonant column software*

The proximitor-base RC software, called as CATS-RC, is compatible with most resonant column systems. This software has de ability to graphically determine resonant frequency and damping from free vibration data. In this particular case, proximitor was used to measure static and dynamic shear strain.

The following results are measured by using CATS-RC.

a) Resonant frequency (Hz)
b) Maximum shear strain (fraction)
c) Shear velocity (m/s)
d) Shear modulus (MPa)
e) Damping ratio-Free vibration decay (%)
f) Damping ratio-Half power bandwidth (%)
g) Predominant frequency from Free vibration data FFT Analysis
h) Natural frequency –from resonant frequency and phase shift (Hz)
i) Natural frequency –from resonant frequency and free vibration decay (Hz)
j) Natural frequency –from FFT frequency and free vibration decay (Hz)

Figure 3-10 shows some of the windows and software environment. When values such as frequency step, starting frequency, stop frequency, and few other parameters are defined as input data, the software conducts the test automatically without user intervention. At the end of

the test, CATS-RC calculates the specimen results and the user may see the frequency sweep on how resonant frequency is determined.

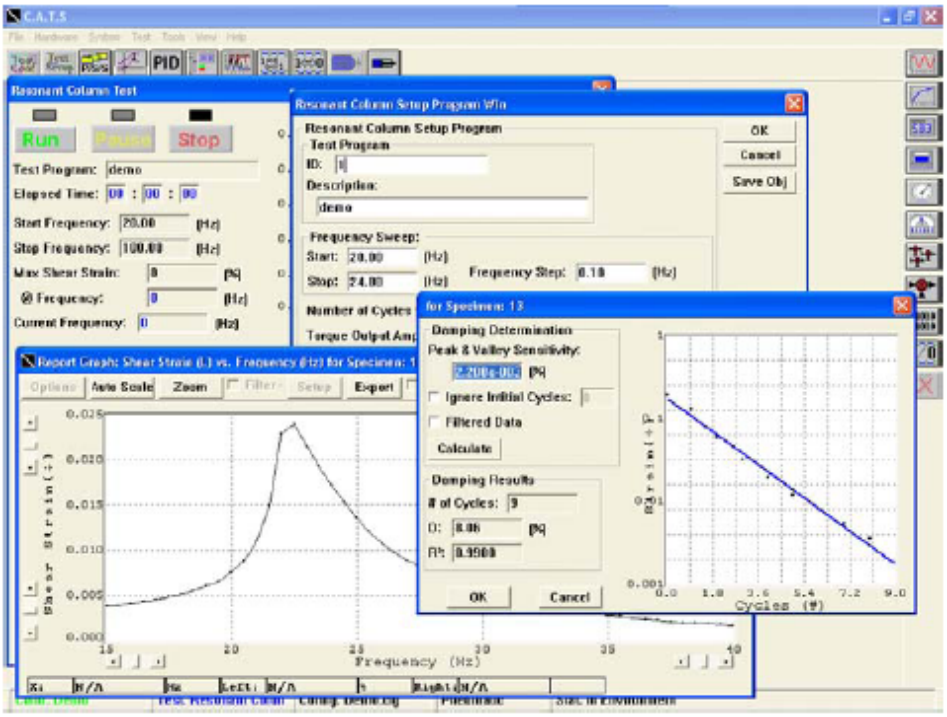


Figure 3-10 RC sofware display

It can also see the forced vibration data of the specimen, as well as the free vibration data, from which one of the damping is determined.

## 3.5 Comparative Performance of Conventional and Proximitor-based RC Devices

The proximitor-based RC device introduces several advantages over previous ones. Having the driving system completely automated not only simplifies its operation but also reduces the total number of cycles applied at each frequency while finding the peak response and thus avoiding early specimen degradation. However, to ensure the reliability of this RC device, the following exercise attempts to compare the response from two resonant column systems: the conventional one, which is based on accelerometer response, and the proximitor-based system used in this work.

Several tests on identically prepared specimens of SM soil were performed in both systems. Physical properties of soil are the same as shown in table 3.2. All samples were statically compacted as explained in chapter 5. Same confining pressures were applied at constant time intervals. Also, identical ranges of frequencies were evaluated for each test in both devices.

The following present the frequency sweep results and the linear and non-linear analyses from both resonant column systems.

*3.5.1 Frequency response under sinusoidal excitation*

During resonant column testing, the sample is subjected to a constant sinusoidal force excitation with varying frequencies. The frequencies are swept so that resonance frequency may be identified. Two samples were tested in both resonant columns devices. Confinement stresses varying from 0 to 40 psi were applied to each specimen, and the corresponding resonant frequencies were measured. Figure 3-11 shows the frequency sweeps performed on SM soil in the accelerometer-based RC or conventional one, while figure 3-12 shows the frequency sweeps performed in the proximitor-based RC.

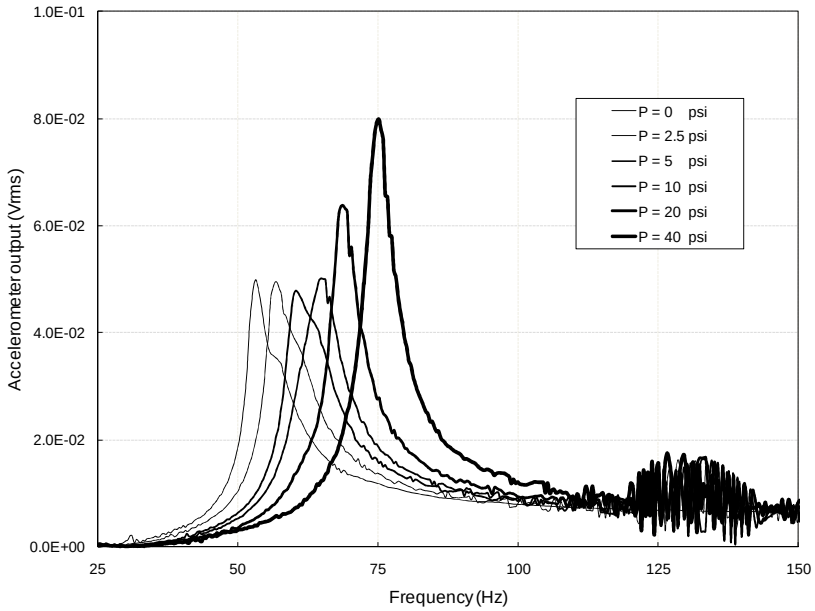


Figure 3-11 Frequency response curves of compacted silty sand performed in accelerometer- based RC with 0.25V input signal

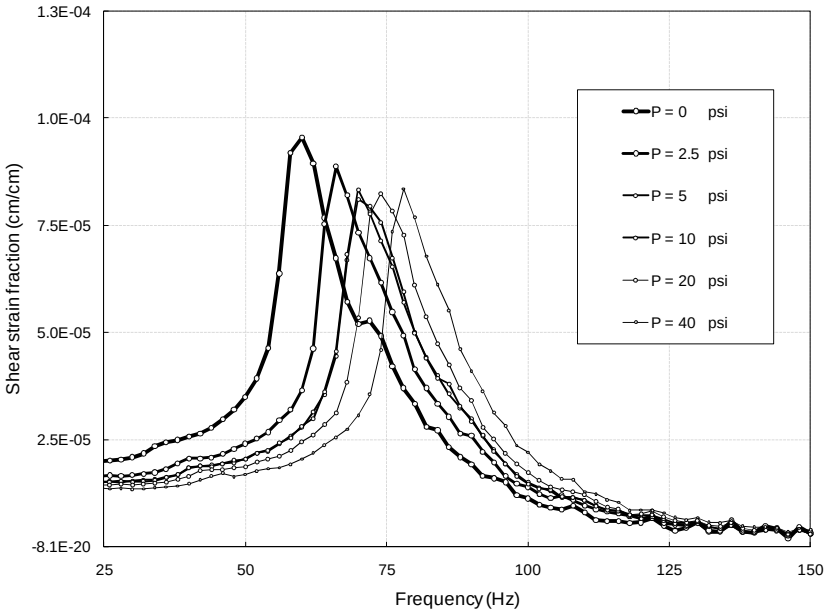


Figure 3-12 Frequency response curves of compacted silty sand perfomed in proximitor-based RC with 1-pfs input torque

From figures 3-11 and 3-12, it can be noticed that regardless of the strain level of the output values, the range of frequencies varies from 55 to 75 Hz for the conventional apparatus, while for the proximitor-based RC these results fluctuate between 60 and 80 Hz. Although accelerometer and proximitor-based resonant column devices work under different input variables, the frequency response seems to be very similar. These values are also reflected on the shear modulus and damping results, as well as in the non-linear behavior, which will be discussed later in this section.

In addition, each frequency sweep has one decay curve, and these curves are shown in figure 3-13. Six confining pressures were applied (0, 2.5, 5, 10, 20, and 40 psi), therefore six logarithmic decay curves are presented. The upper curve corresponds to the unconfined test, while the lower one corresponds to the 40psi confinement. It should be noted that as the confinement increases, the initial output amplitude decreases, which confirms that confining pressures have an important influence on free-vibration response of SM soil.

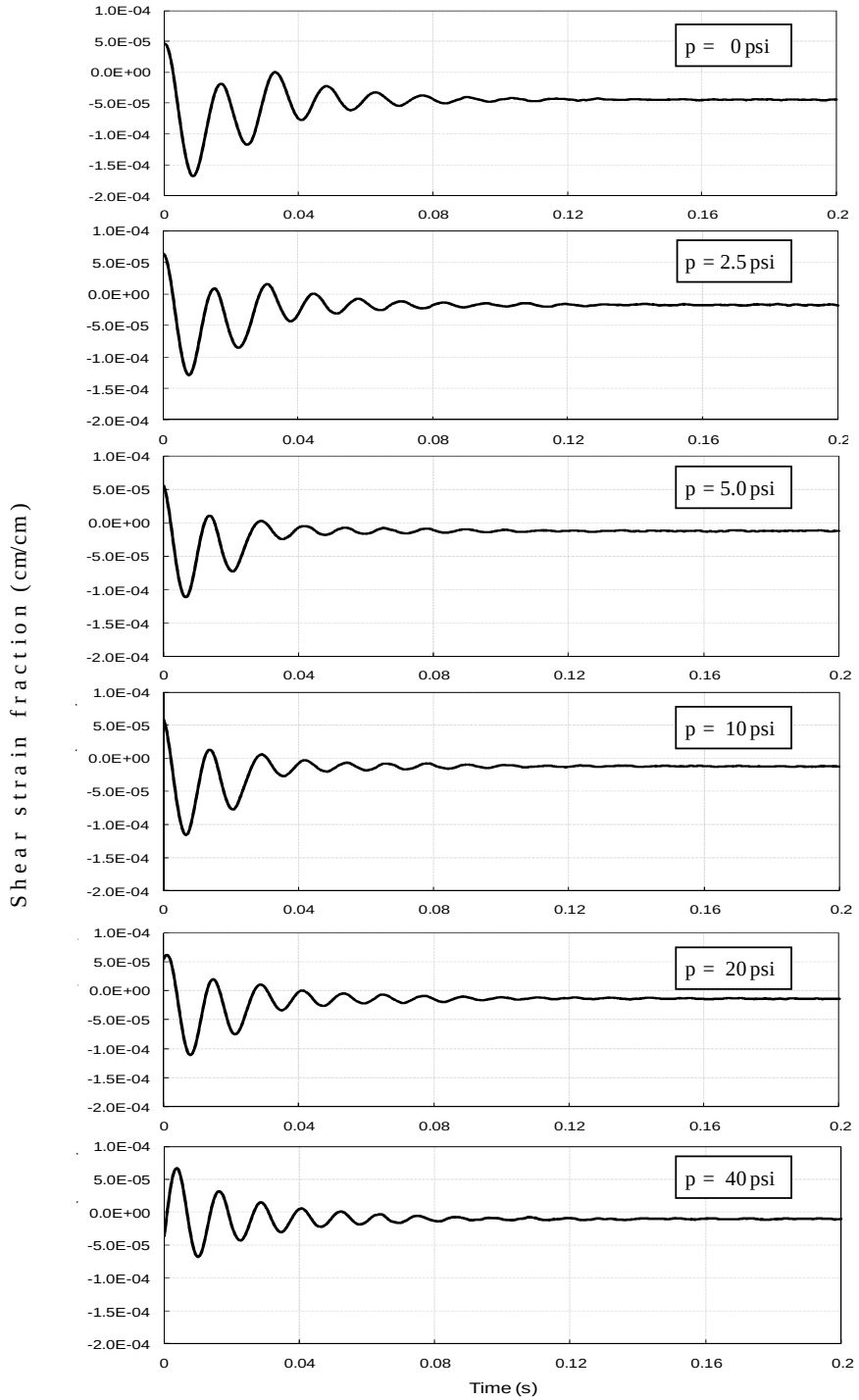


Figure 3-13 Logaritmic decay curves from proximitor-based RC device at different confining pressures

*3.5.2 Nonlinear response*

During high-amplitude testing, cyclic shearing strains induced in the specimen, may go significantly beyond a threshold strain, at which the soil exhibits strain-dependent behavior. To assess the similarity in response between both RC devices, at higher confinement level of 40 psi, a full set of frequency response curves were obtained for different amplitude voltages and torque input values in the accelerometer-based and proximitor-based RC devices, respectively.

It should be noted that while the input values for amplitude in the accelerometer-based RC device are given in voltage units, values for proximitor-based RC device are presented in terms of pfs (percent of full scale) as the main torque input data. The maximum pfs allowed by system is 100 pfs, and the normal pfs to achieve very small strain levels oscillate between 1 and 10. Figures 3-14 and 3-15 show the frequency backbone curves from both devices.

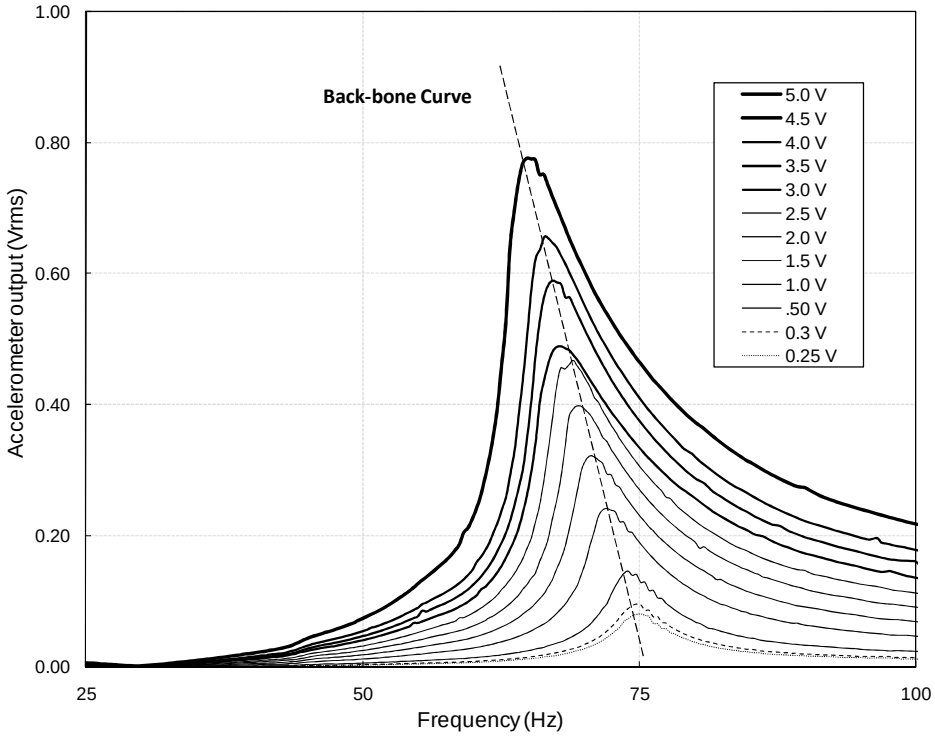


Figure 3-14 Frequency response curves of SM soil performed in accelerometer-based RC device

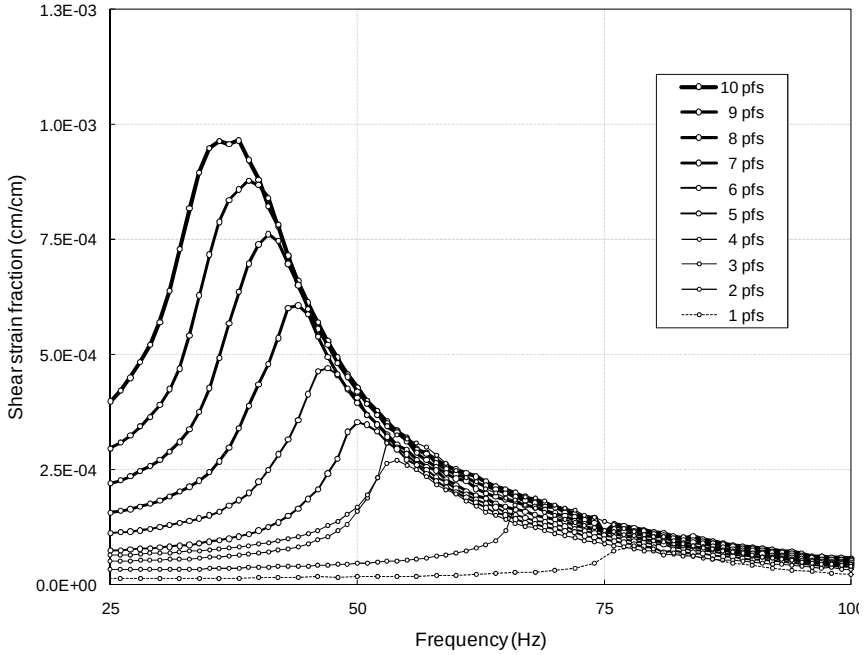


Figure 3-15 Frequency response curves of SM soil performed in proximitor-based RC device

Although the shapes and trends of the backbone curves from both devices are somewhat similar, the resonant frequencies vary within a broad range, from 40 to 75 Hz. This variation could be attributed to the differences in the operation mechanisms and assembly of each apparatus. It should also be noticed that the output strain amplitude values are given in different units. The accelerometer-based resonant column works with volts while the proximitor-based resonant column presents output values in strain fraction.

The following two figures (3-16 and 3-17) show the increase in the initial shear strain under free-vibration with increasing input torque under constant confining pressure (40 psi). Ten curves are presented, the first corresponding to the lowest harmonic torque induced (in this case 1pfs), and the last to the highest torque value (in this case 10 pfs).

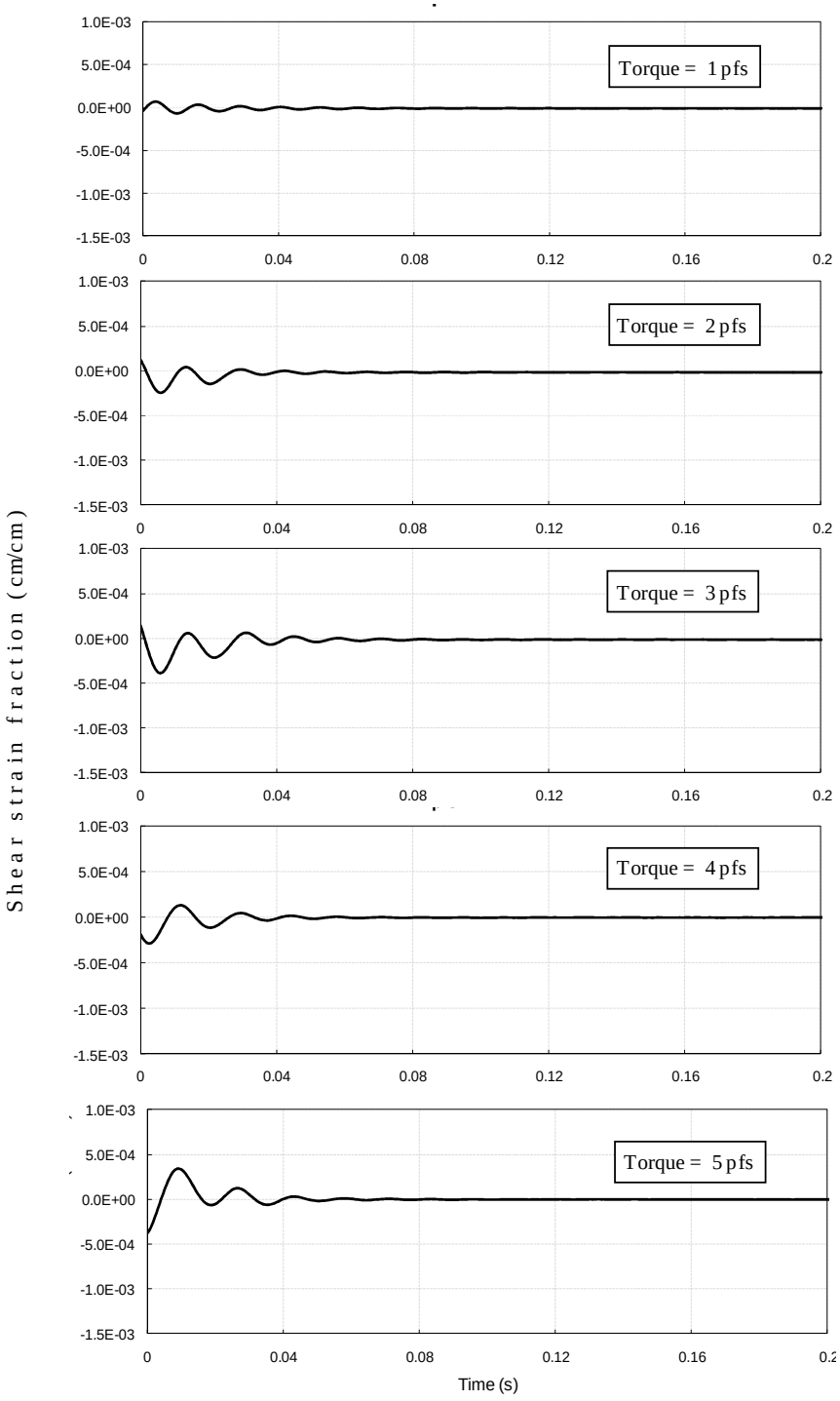


Figure 3-16 Logaritmic decay curves from proximitor-based RC device at different torque input values

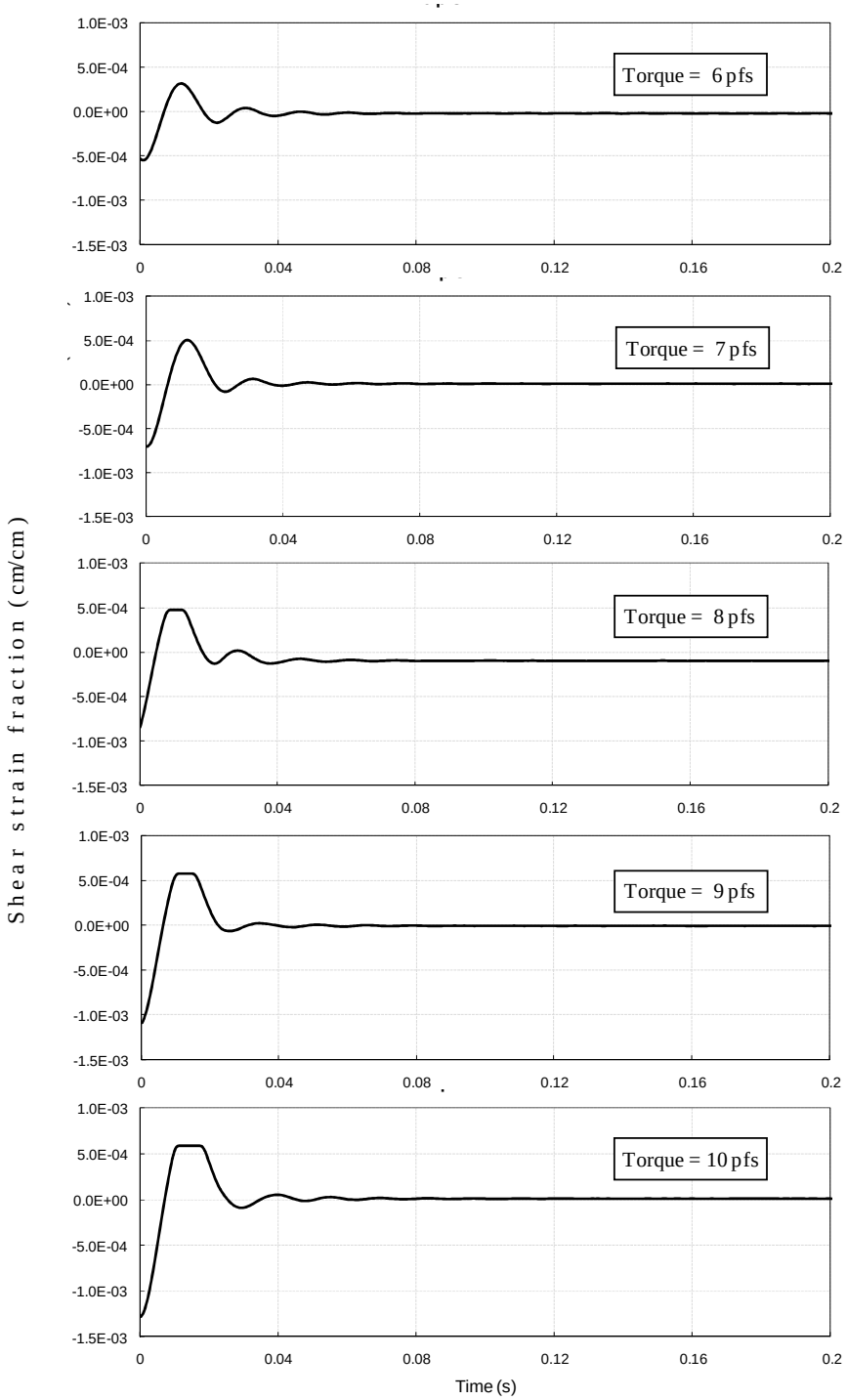


Figure 3-17 Logaritmic decay curves from proximitor-based RC device at different torque input values

*3.5.3 Variation in shear modulus, G, and material damping ratio, D, with confinement stress, p*

To assess the correspondence between input signal values of accelerometer and proximitor-based resonant columns, the shear modulus values were calculated for different confining pressures in both devices. While a constant 0.25-Volt signal was used for the conventional apparatus, the input torque in the proximitor-based RC device was changed from 1 to 10 pfs.

Figure 3-18 shows the increase in shear modulus, G, as confining stress increases, as well as the variation in G when the input torque is increased. As the values of pfs increases, the soil stiffness decreases. The dashed line represents the analysis from accelerometer base-resonant column while the continuous lines come from the new device. It is possible to conclude that 0.25-Volt of input amplitude can create similar responses to 1 or 2 pfs performed in the novel device. Additional points on the figure were plotted by increasing the pfs values for 40 psi of confinement. This further exercise had the objective of showing the reduction of G as pfs values increase.

Once it is established that a 1pfs torque induces a similar shear modulus response to that induced by a 0.25-Volt input signal, values of material damping ratio can also be computed.

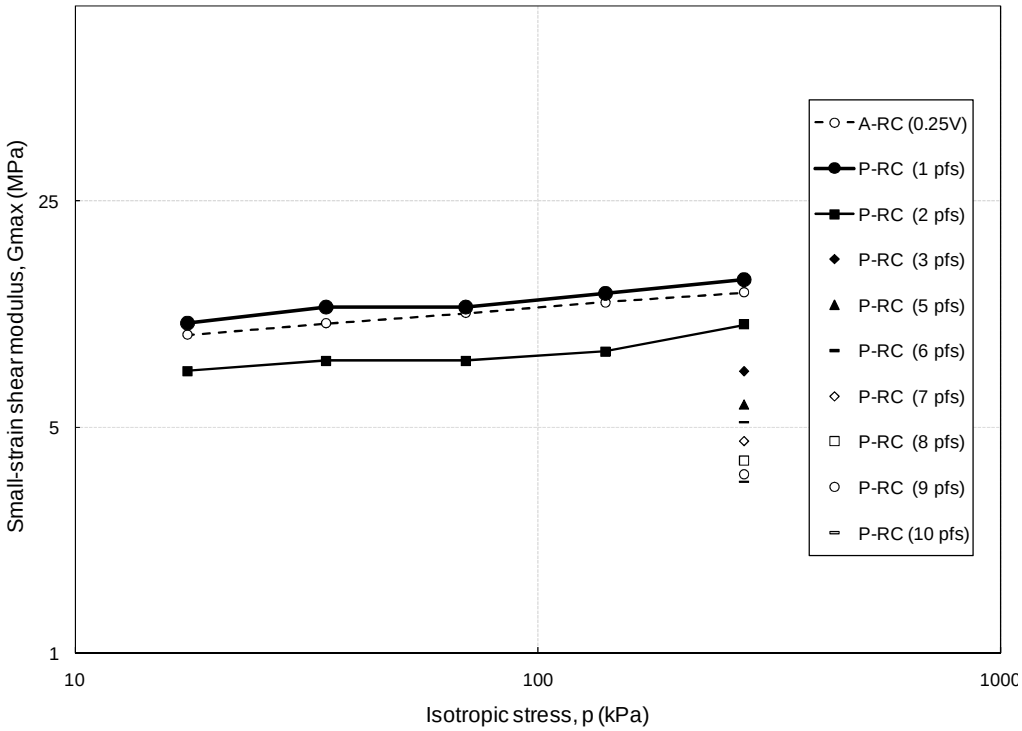


Figure 3-18 Comparative analysis of variation of small-strain shear modulus with isotropic stress

Figure 3-19 shows three curves that come from analysis of variation of damping with confining pressure. The black line is the only one performed in the conventional resonant column, and is built by following the half-power bandwidth method, and the others two were made from proximitor based-resonant column, using the same method and the free decay curve method. Although there is a similar trend, which results in a reduction of the damping with the increase in confinement, half-power bandwidth method from novel device underestimate damping reply. However, other two responses tend to match, letting it to conclude that for this particular exercise, free vibration decay curve from proximitor-based RC and half-power bandwidth from accelerometer-based RC provide matching and accurate results

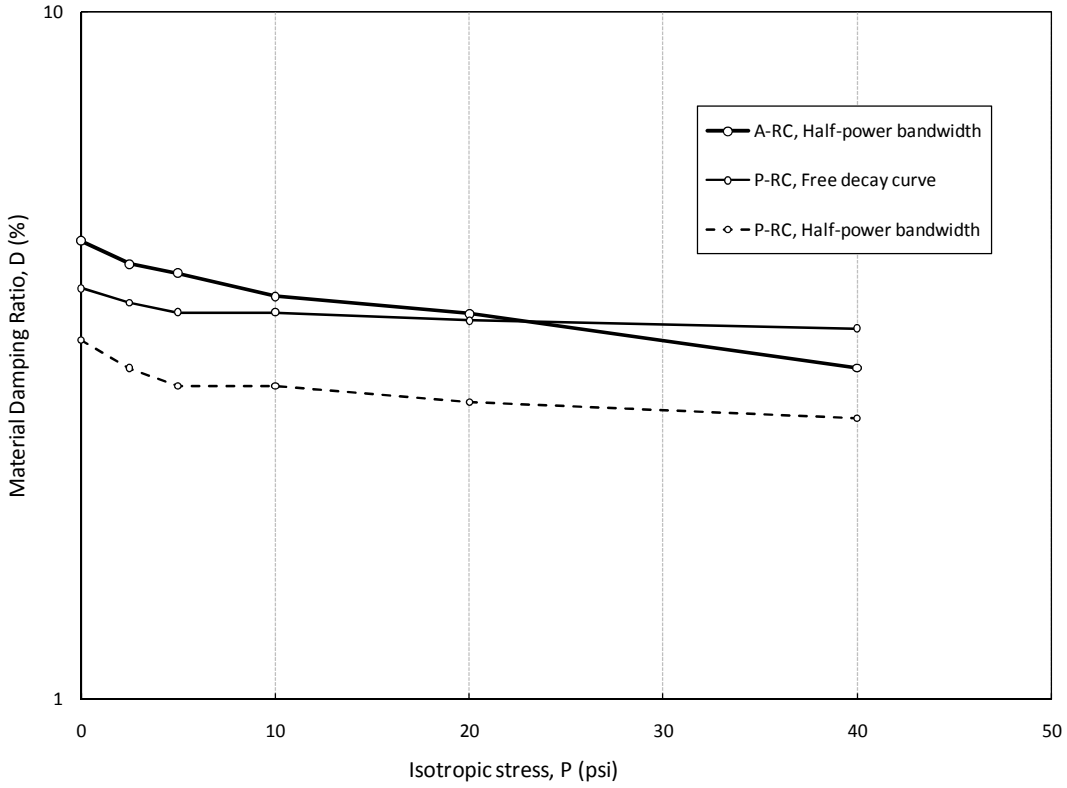


Figure 3-19 Comparative analysis of variation of material damping ratio with isotropic stress

*3.5.4 Variation in shear modulus, G, and material damping ratio, D, with shear strain, $\gamma$*

Combining the shear moduli determined from accelerometer-based resonant column, A-RC, and proximitor-based resonant column, P-RC, the shear stiffness at very small strain levels were obtained by plotting the normalized shear modulus and its shear strains.

Figure 3-20 shows the shear modulus, G, as function of the shear strain for 40 psi of confinement level. Each curve contains a change in shape, and a drop in their slopes between 0.01% and 0.05% of strain.

For each stress level, the low-amplitude modulus remains constant, $G_{max}$, prior to overcoming the apparent threshold strain. Beyond this limit, the high amplitude shear modulus

decreases due to the softening and degradation of the soil material under mid to high amplitude torsional vibrations.

For this comparative analysis, it is important to note that the slopes of the both curves in the linear and non-linear zone are comparable; the similarity of values observed for the strains levels and their corresponding shear modulus, ratify the earlier statement.

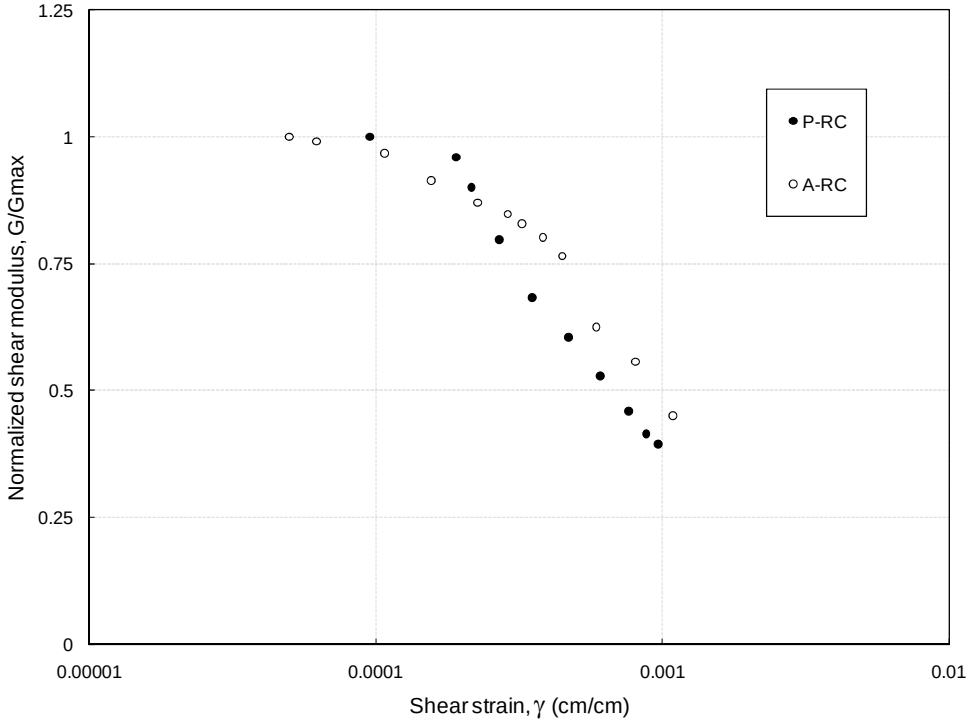


Figure 3-20 Comparative analysis of variation in normalized shear modulus with shear strain

Both, the half-power and the free decay curve methods were used to determine the material damping ratio for low to mid amplitude tests. Damping ratios for half-power method were calculated using both devices, and their value come from figures 3-14 and 3-15. Damping ratios for free decay method were calculated from proximitor-based RC, and their values were obtained from decay curves captured using computerized means in each curve of figures 3-16 and 3-17.

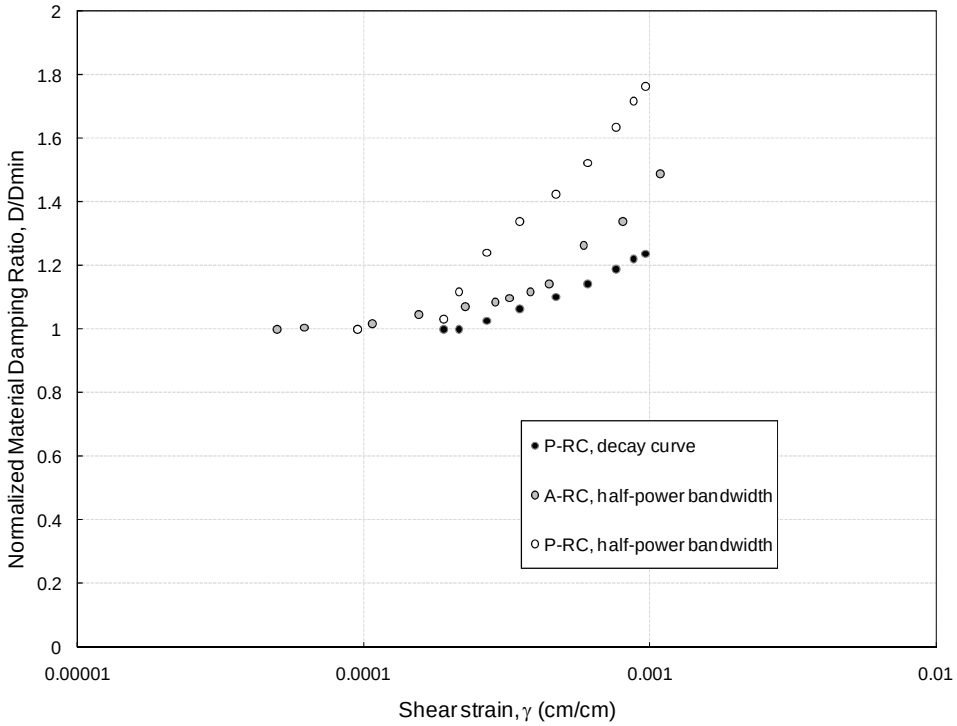


Figure 3-21 Comparative analysis of variation in material damping ratio with shear strain

As previously mentioned, the half-power bandwidth method determined from proximitor-based RC underestimates the damping response. However, the other two responses tend to match, showing a correlation between the free vibration decay curve from proximitor-based RC and the half-power bandwidth from accelerometer-based RC as illustrated in Figure 3-21.

# CHAPTER 4

# SUCTION-CONTROLLED RC APPARATUS WITH BENDER ELEMENTS

## 4.1 Introduction

This chapter is devoted to describe the additional components assembled into the proximitor-based RC device with which this research was performed. This study introduces a novel suction-controlled, proximitor-based RC device featuring a PCP-15U pressure control panel that allows for the implementation of the axis-translation technique via the independent control of pore-air and pore-water pressures in the specimen. Similarly, the novel apparatus also features a full set of self-contained bender elements for simultaneous testing under both techniques.

## 4.2 Pressure control monitoring system

### *4.2.1 Pore-air pressure control*

This arrangement contains two pressure panels: The PCP-15U and the HM-414. A PCP-15U model pressure control system ( see Fig. 4-1) is used for direct control of pore-air pressure $u_a$ at the top of the soil specimen with dual pressure regulators and gauges for precise measurement and control of matric suction, $s = u_a$ ($u_w = 0$). The panel also features a flushing mechanism for removal of diffused air beneath the HAE ceramics during constant-suction RC testing.

On the other hand, a HM-414 model pressure panel is used for application of external confining pressure (Fig.4-2). Air pressure is supplied by this panel via the inlet air-pressure port located at the cover plate of the main cell, which was designed to withstand a maximum air pressure of 1000 kPa.

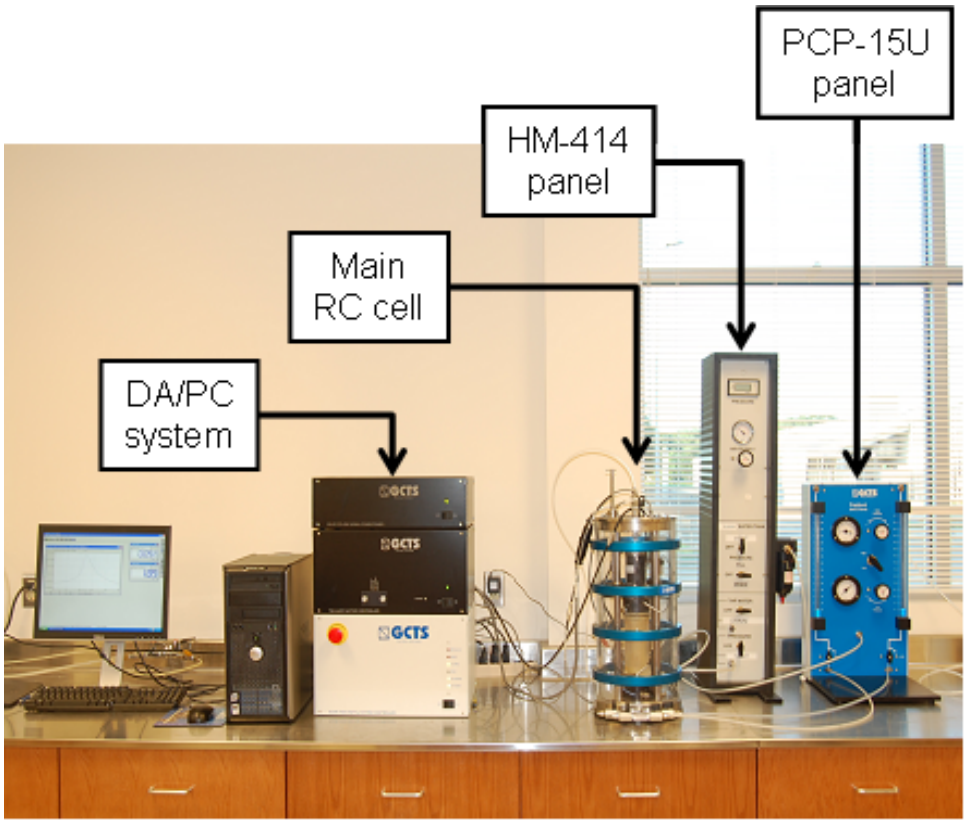


Figure 4-1 Panoramic view of entire suction-controlled resonant column test layout


Figure 4-2 Pressure control panels

*4.2.2 Pore-water monitoring system*

Three ceramic disks mounted at the bottom, and three coarse porous stones located on the top cap were used to impose and measuring matric suction in the unsaturated soil specimen via axis translation technique (see figure 4-3.). The selection of the HAE (High-Air-Entry) ceramic disk for testing unsaturated soils should be primarily based upon the maximum possible matric suction that is applied during the test. In this research work, a maximum value of 400 kPa was imposed to the cylindrical solid sample. Hence, the 16.95 mm(0.667in) diameter, 7.65mm, (0.301 in) height, 5 bars (505 kPa) manufactured by GCTS was selected for testing procedure. As a result, with readings from PCP-15U pressure panel, the system is able to monitoring the drying path of the sample until the water content equilibrium in the internal menisci has been reached.

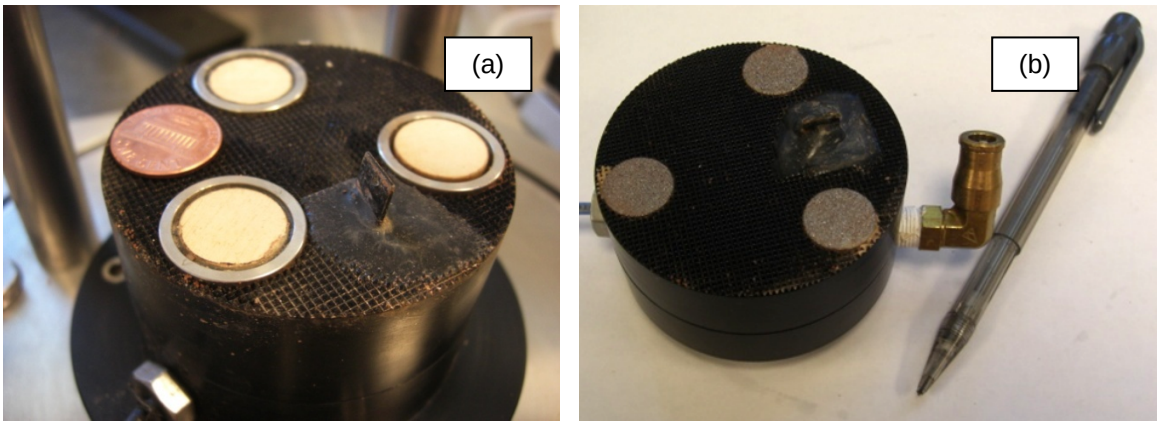


Figure 4-3 Bottom pedestal and top cap: (a) HAE ceramic disk at bottom pedestal, and (b) porous stones and tubing conector at top cap.

## 4.3 Self-contained Bender Elements features

Since the critical role of small-strain soil stiffness in the design of geosystems is now widely accepted, in recent years, significant progress has been made on suction-controlled testing using conventional geotechnical devices with self-containing bender elements. In order to achieve accurate BE testing process, some major components in the testing setup need to be assembled. Basically, there are five important components in the BE configuration, which are: (a) the oscilloscope, (b) receiving signal converter, (c) piezo-ceramic bender elements, (d) resonant column main cell, and (e) personal computer. The bender element setup in this research (shown in figure 4-4) was provided by GCTS within the complete set of the resonant column parts and components. As RC main cell was already discussed on chapter 3, the descriptions of the other components are described in the following.

### *4.3.1 Oscilloscope*

The oscilloscope used in this work is known as the Arbitrary Waveform Generator Model TGA 1241 as depicted in Figure 4-4. This oscilloscope can generate any waveform signal at different frequencies vary from 1 to 40 MHz. However, the frequencies used in this research,

range from 1 to 5Hz, and the amplitude was applied at 20 Volts peak-to-peak which is the maximum amplitude available for this oscilloscope in order to the received signal can be observed readily and clearly on the computer by not using the amplifier. The main function of this oscilloscope was not only performing a waveform signal but also sending the waveform to the receiver signal converter.

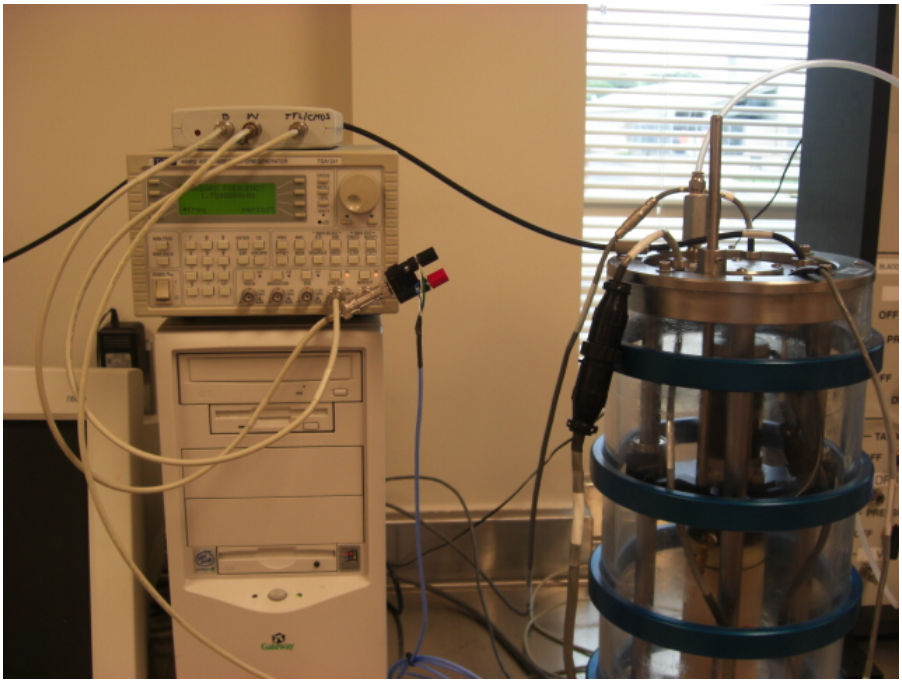

Figure 4-4 Arbitrary wave generator and receiving signal converter mounted into the RC.

*4.3.2 Receiving signal converter*

Figure 4-4 also shows the receiving signal converter placed on the top of the oscilloscope. The major role of the signal converter is to convert the voltage signals from both top and bottom bender elements into digital signals. These digital signals are sent to the personal computer that has been installed the Picowave program to view the waveform generated from oscilloscope.

*4.3.3 Bender element set*

Bender element setup shown in Figure 4-5 is used to perform the horizontal vibration through the soil specimen from top to bottom as described in previous section. In other words, the top bender element vibrates when received the signal from the oscilloscope, and then the vibration expands through the soil specimen so that the bottom bender element receives the vibration. Consequently, the elapsed time between the transmitted signal and received signal is measured and calculated.

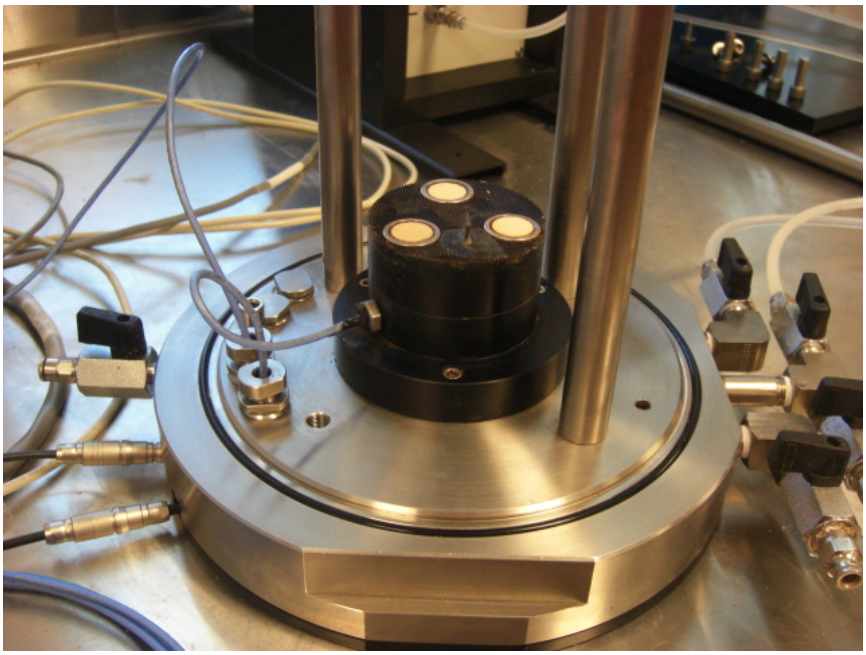

Figure 4-5 Bender Element receiver on the RC base pedestal.

# CHAPTER 5

# EXPERIMENTAL VARIABLES AND TEST PROCEDURES

## 5.1 Introduction

The experimental program accomplished in this work was designed to assess the influence of key in-situ factors on small-strain stiffness properties of unsaturated soils using bender element and resonant column testing techniques. A series of constant-suction Resonant column and Bender element tests has been accomplished on four identically prepared samples of SM soil, which was described in chapter 3, using the static compaction process summarized below. Each sample was tested for a different value of net confining pressure, $(p - u_a) = 50$, 100, 200, or 400 kPa. RC and BE tests were then performed on the same sample under a constant net confining pressure $(p - u_a)$ and for four different suction states induced by axis-translation, that is, $s = (u_a - u_w) = 50$, 100, 200, and 400 kPa.

The following sections provide a detailed description of all the experimental variables and specimen preparation procedures.

## 5.2 Experimental Variables

Table 5.1 summarizes the experimental variables used in this research work for Resonant Column (RC) featuring self-container Bender Elements.

Table 5-1 Experimental variables used for RC and BE Testing

| Variable description | Number of variables |
|---|---|
| Soil type | 1. Silty Sand (SM) |
| Confining pressure, p | 1. 100 kPa<br>2. 150 kPa<br>3. 200 kPa<br>4. 250 kPa<br>5. 300 kPa<br>6. 400 kPa<br>7. 450 KPa<br>8. 500 kPa<br>9. 600 kPa<br>10. 800 kPa |
| Net mean stress, $(p-u_a)$ | 1. 50 kPa<br>2. 100 kPa<br>3. 200 kPa<br>4. 400 KPa |
| Matric suction $(u_a-u_w)$ | 1. 50 kPa<br>2. 100 kPa<br>3. 200 kPa<br>4. 400 KPa |

## 5.3 Sample preparation and Test Procedure

### *5.3.1 Sample preparation*

Samples were compacted into a 70-mm diameter, 130-mm height, compaction split mold using static compaction. During compaction, a monotonic force is applied using a triaxial loading

frame. Samples are prepared in three lifts under a constant compaction displacement rate of 1.0 mm/min (Venkatarama and Jagadih 1995).

The sample was prepared by using a cylindrical stainless steel mold shown in figure 5-1. The mold was filled with 904 g of silty sand SM, and sited on the triaxial load frame. Once the loose soil is in the mold under the frame, the axial load is then applied as shown in figure 5-1.

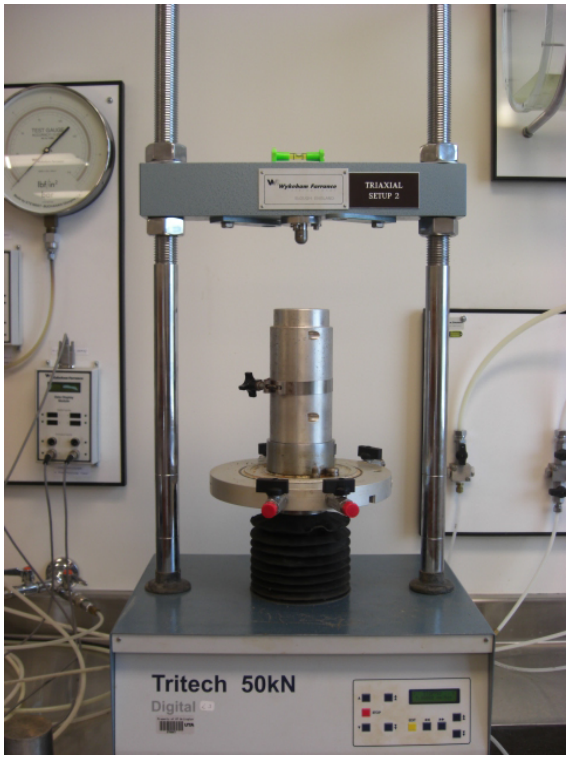


Figure 5-1 Cilindrical mold and traxial loading frame used for static compaction

Once the sample is compacted, it was extruded from the stainless steel mold and delivered into the resonant column main cell to be tested.

*5.3.2 Test procedure and stress paths prior to RC and BE testing*

After full assembly of the RC apparatus, a confining pressure is applied to the sample via the HM-414 panel in order to induce a confinement that is 50 kPa greater than the first desired value of suction. The sample is then allowed to consolidate under this confinement for at least 2 hours. Pore-air pressure $u_a$ is then increased via the PCP-15U panel until achieving the desired suction state. The external confinement was adjusted accordingly to keep a constant net confining pressure, $(p - u_a) = 50$ kPa.

After complete equalization of pore fluids under a constant pore-air pressure, which may take up to seven days, a RC test is conducted by inducing a torsional vibration at the top of the soil specimen via the servo motor actuator (0.2 kN-m torque). The frequency of the vibration is changed by sweeping the entire input frequency scale until obtaining a frequency response curve, normally between 60 Hz and 240 Hz. Frequency response curves are presented in terms of shear strain fraction (cm/cm) versus frequency (Hz).

The steady torsional vibration is then completely cut off in order to obtain the logarithmic decay curve for the assessment of material damping. Logarithmic decay curves are presented in terms of shear strain fraction (cm/cm) versus decay time (sec).

Immediately, Bender elements testing are performed maintaining the same confining pressures as well as pore-air pressure. The travel time of the shear wave is then captured and measured.

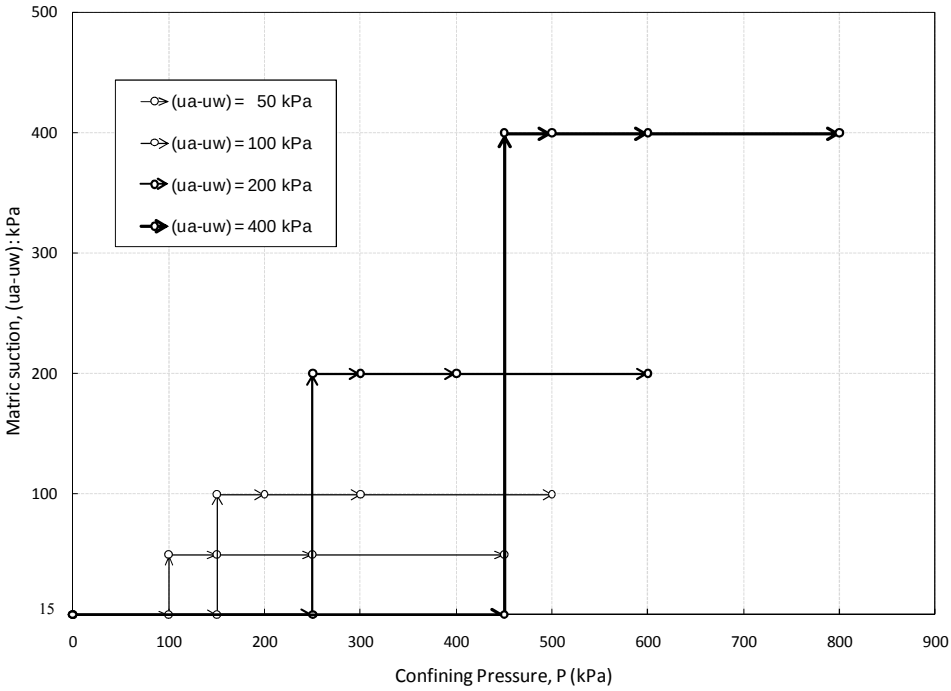


Figure 5-2 Stress paths induced on silty sand samples in p:s plane prior to RC and BE tests.

Pore-air pressure $u_a$ is then further increased until achieving the next desired matric suction state. After complete equalization of the pore fluids, a new RC and BE test, as described above, is conducted. The same test procedure is repeated for suction states, $s = (u_a - u_w) = 50$, 100, 200, and 400 kPa, on the same sample at constant net confining pressure, $(p - u_a)$. This identical procedure was followed in testing SM soil samples at constant net confining pressures, $(p - u_a) = 100$, 200, and 400 kPa.

# CHAPTER 6

# RESONANT COLUMN TEST RESULTS AND ANALYSIS

## 6.1 Introduction

In this chapter the results from suction-controlled resonant column tests are discussed in detail. A comprehensive series of 16 tests at different confining pressures and matric suctions was conducted on identically prepared SM soil samples. The influence of these variables on the frequency response, free vibration behavior, shear modulus, and damping material ratio are analyzed. In addition, empirical models for shear modulus and material damping ratio of compacted silty sand are proposed on the basis of suction and confining pressure.

## 6.2 Frequency response curves

### *6.2.1 Influence of net mean stress (p-$u_a$) under constant suction*

Full set of frequency response curves from suction-controlled RC tests conducted on four identically prepared SM soil samples at net confining pressures, ($p - u_a$) = 50, 100, 200, and 400 kPa, respectively, and under four constant matric suctions of s = 50, 100, 200, and 400 kPa, is shown in Figures 6-1, 6-2, 6-3, and 6-4.

The magnitudes of the induced shear strain amplitude range from 0.017% to 0.0025% for all combinations of pressure-suction conditions. In all tests, the percentage of reduction of shear strain amplitude is in the range of 40 and 70%. It can be observed that an increment of net pressure makes the peak strain levels to decrease.

On the other hand, from each individual figure, it can be noticed that the confining pressure significantly influences the resonant frequency response of SM soil. Resonant frequencies fluctuate between 110 and 180 Hz for s = 50 kPa (see figure 6-1), 120 and 185 Hz

for s = 100 kPa (see figure 6-2), 130 and 205 Hz for s = 200 kPa (see figure 6-3), and 140 and 225 Hz for s = 400 kPa (see figure 6-4).

In addition, matric suction levels have an even more pronounced effect on resonant frequency response. As matric suction varies from 50 to 400kPa, the resonant frequency response curves progressively move toward right side of the horizontal axes, which means a significant increase of soil stiffness properties.

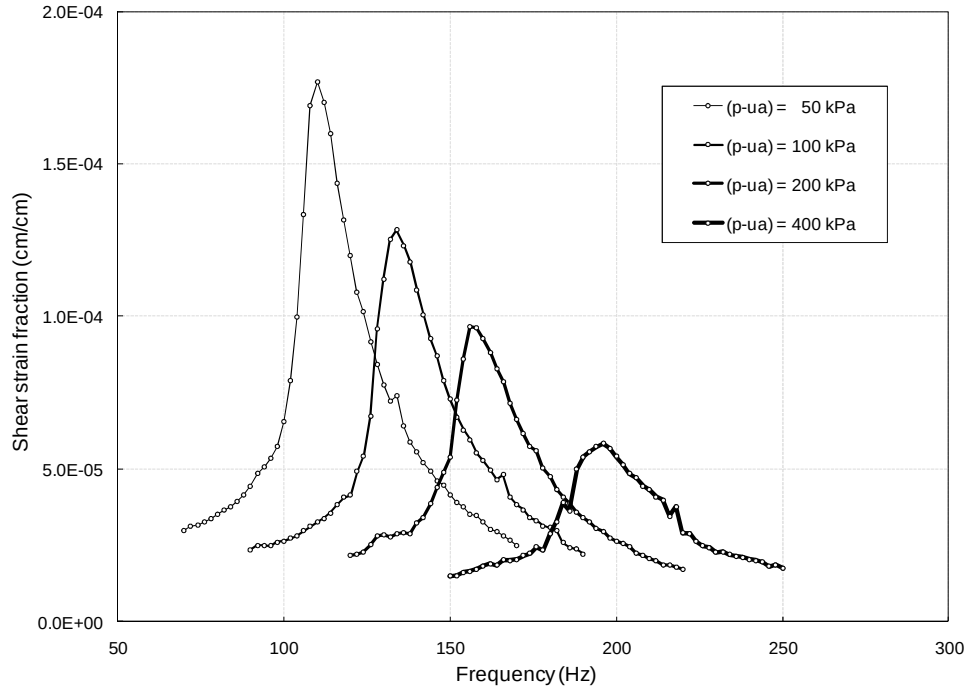


Figure 6-1 Frequency response curves from suction-controlled RC tests at s = 50 kPa

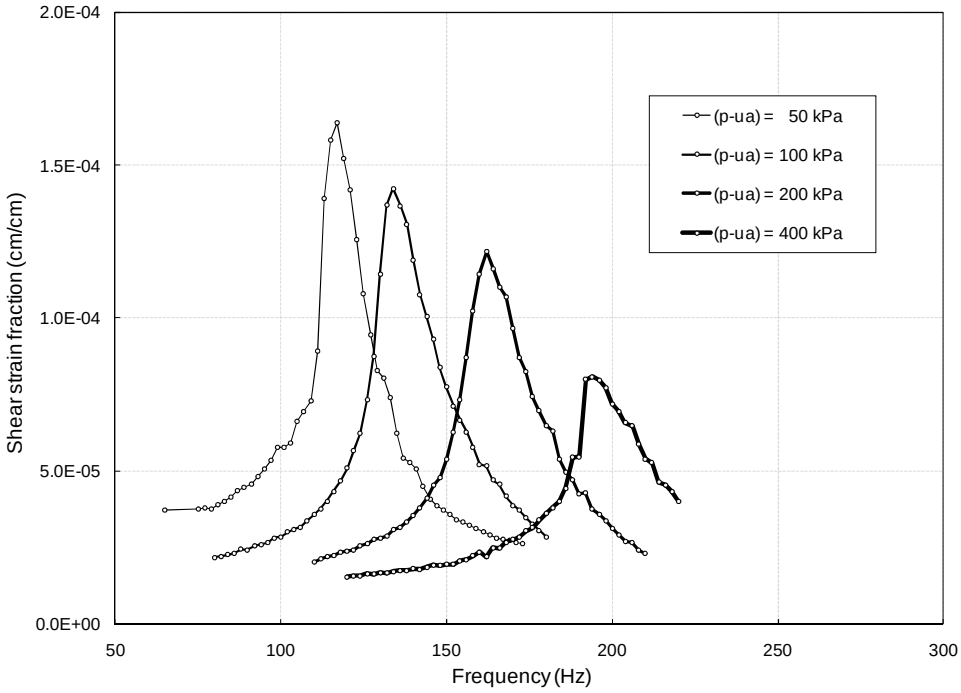


Figure 6-2 Frequency response curves from suction-controlled RC tests at s = 100 kPa

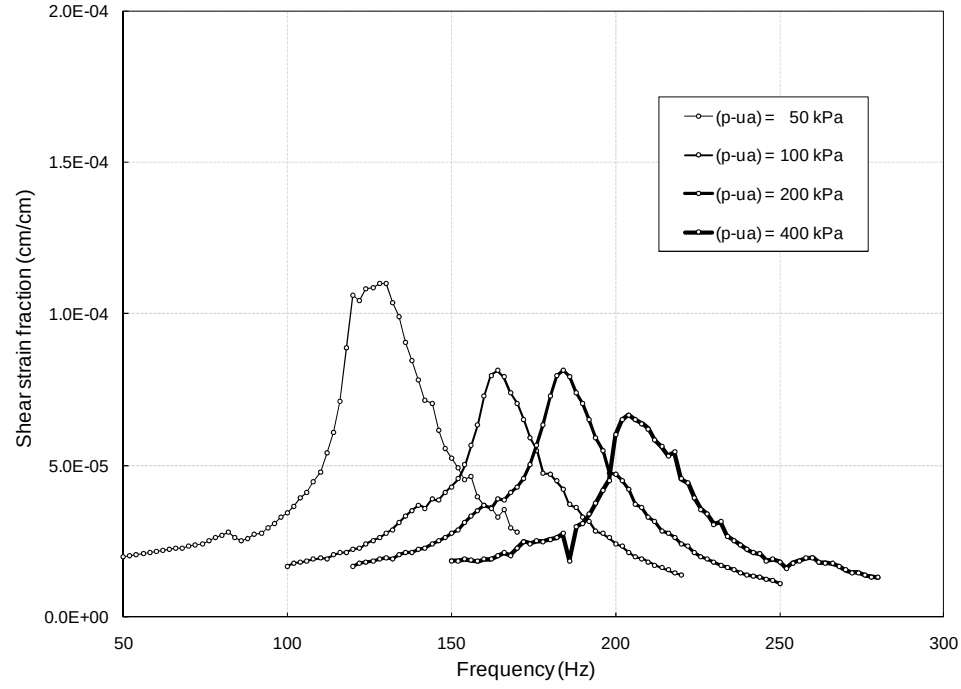


Figure 6-3 Frequency response curves from suction-controlled RC tests at s = 200 kPa

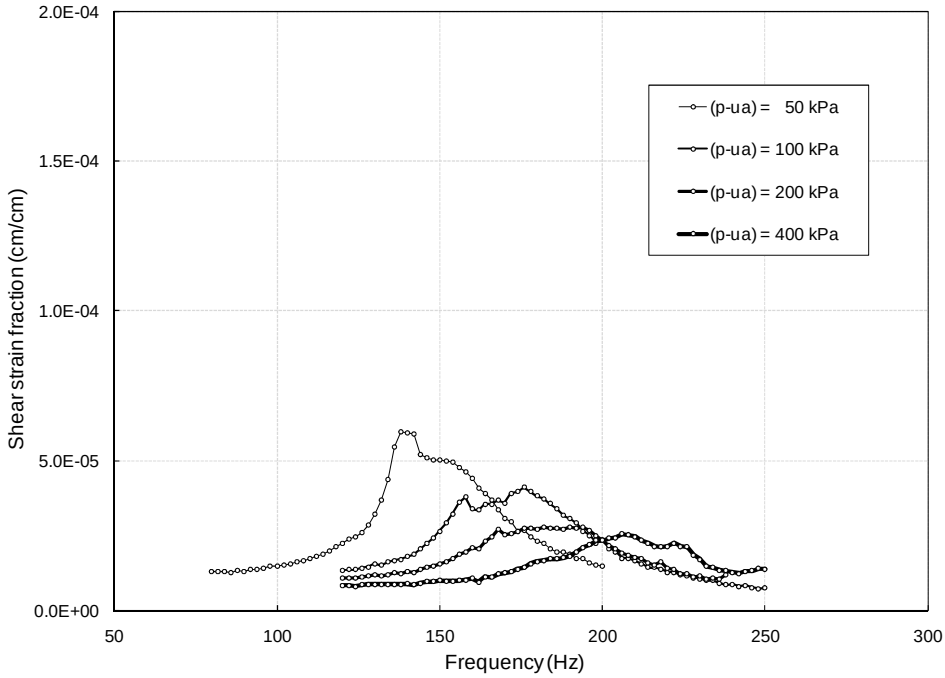


Figure 6-4 Frequency response curves from suction-controlled RC tests at s = 400 kPa

*6.2.2 Influence of matric suction ($u_a$-$u_w$) under constant net mean stress*

A family of frequency response curves from suction-controlled RC tests conducted on four identically prepared SM soil samples at matric suction ($u_a$-$u_w$) = 50, 100, 200, and 400 kPa, respectively, and under four constant net mean stresses (p-$u_a$) = 50, 100, 200 and 400 are shown in Figures 6-5, 6-6, 6-7, and 6-8.

As it was previously mentioned, the induced shear strain amplitudes vary from 0.017% to 0.0025%. However, the differences with the prior analysis lie in the resonant frequency response changes. For each individual figure, it is noted that although matric suction controls the frequency increments, this variable does not have as significant influence as the confining pressure.

The following four figures show that resonant frequencies oscillate between 110 and 145 Hz for (p-$u_a$) = 50 kPa (figure 6-5), 135 and 175 Hz for (p-$u_a$) = 100 kPa (figure 6-6), 155 and 185 Hz for (p-$u_a$) = 200 kPa (figure 6-7), and 190 and 225 Hz for (p-$u_a$) = 400 kPa (figure 6-8).

In addition, confining pressure levels have an even more pronounced effect on resonant frequency response. As net mean stress varies from 50 to 400kPa, the frequency response curves progressively move toward the right side of the chart. This can be directly attributed to an in-crease in effective stress and, hence, an increase in the rigidity of the SM soil skeleton at higher suction states. It can also be noted that the maximum shear strain induced by a 0.1 kN-m torque (peak response in the frequency response curve) decreases at higher suction states.

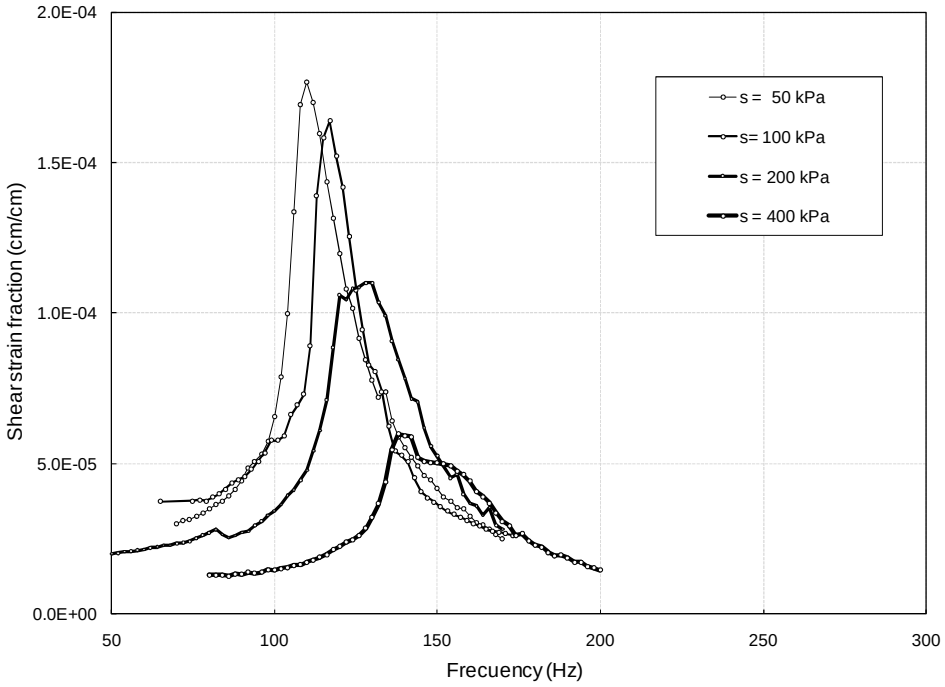


Figure 6-5 Frequency response curves from suction-controlled RC tests at ($p-u_a$) = 50 kPa

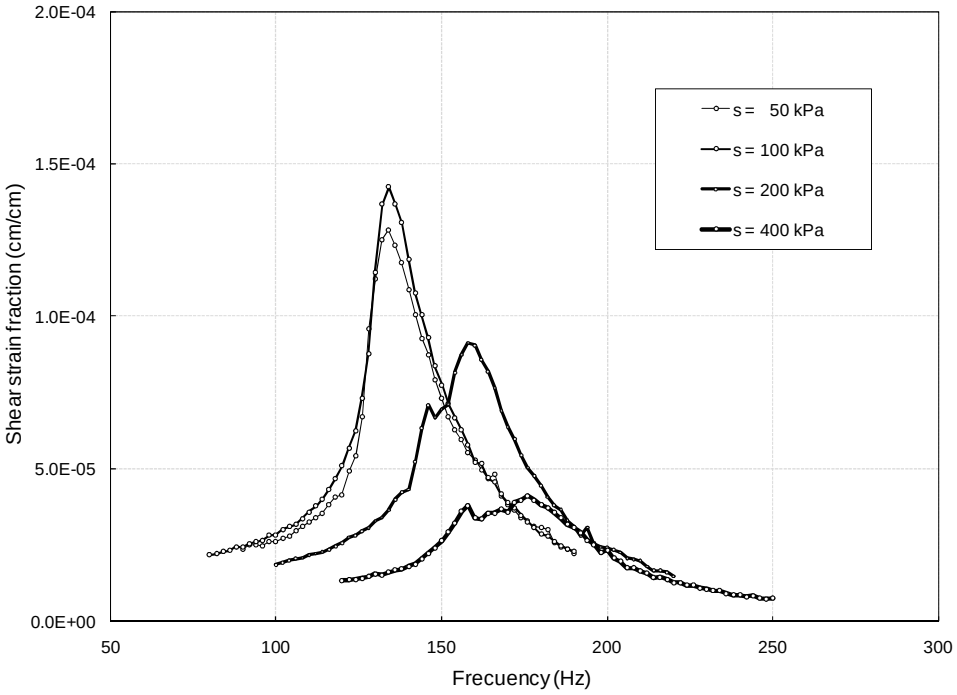


Figure 6-6 Frequency response curves from suction-controlled RC tests at $(p\text{-}u_a)$ = 100 kPa

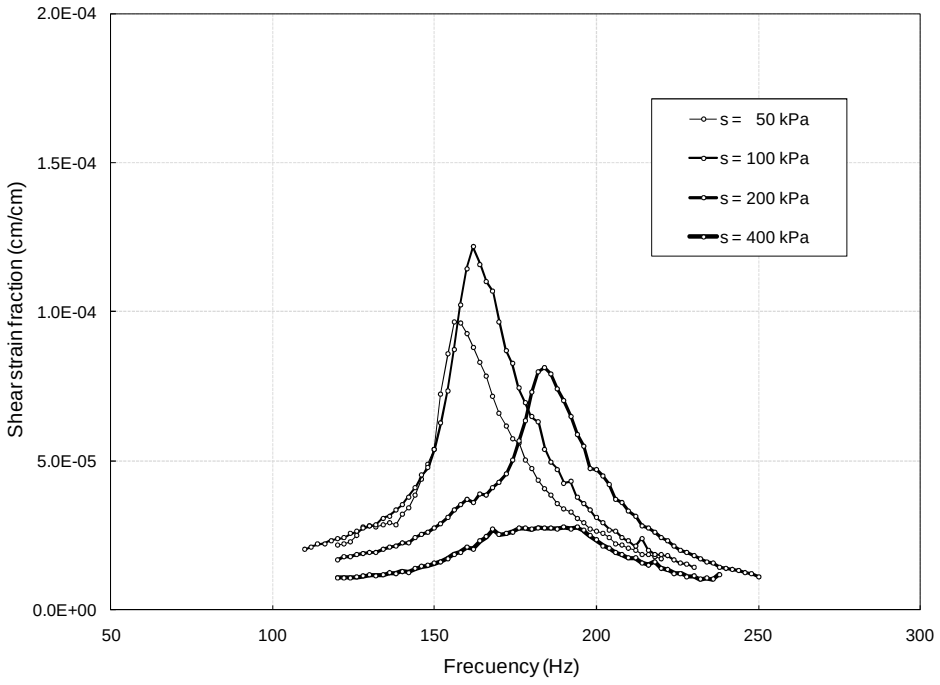


Figure 6-7 Frequency response curves from suction-controlled RC tests at $(p\text{-}u_a)$ = 200 kPa

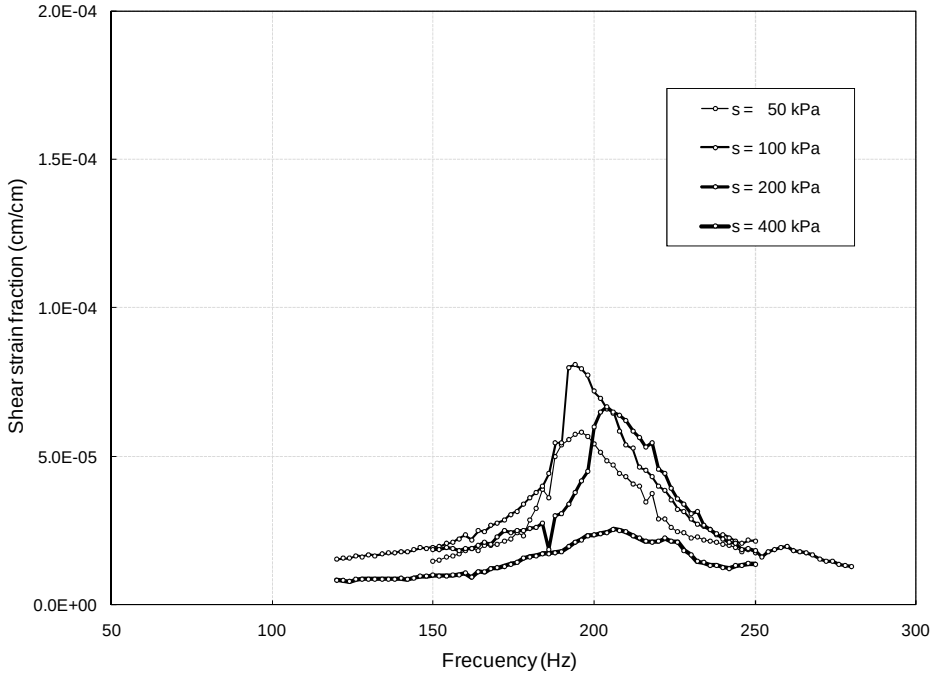


Figure 6-8 Frequency response curves from suction-controlled RC tests at $(p\text{-}u_a)$ = 400 kPa

## 6.3 Free-vibration response

### *6.3.1 Effect of net confinement pressure*

The following figures show the behavior of SM soil sample subjected to free-vibration motion once the input torque is cut off. For all four net confining pressures and matric suction states, a comparative analysis is reported. The following four figures (figures 6-9 to 6-12) show logarithmic decay curves from four SM soil specimens at matric suction states, s = 50, 100, 200, and 400 kPa, and net confining pressure, $(p - u_a)$ = 50, 100, 200, and 400 kPa. For instance, figure 6-9 presents free-vibration decay curves for same soil sample at constant matric suction of 50 kPa and different net confining pressures. It is observed that the level of net confinement has an even more pronounced effect on the decay response. The initial peak shear-strain amplitude at time, t = 0, is considerably lower at higher net confining pressures.

It can also be noted from first curve in Figure 6-9, which belongs to $(p\text{-}u_a)$ = 50 kPa, appears to be fully attenuated after 0.08 seconds of free vibration, while for the last curve, which

corresponds to ($p-u_a$) = 400 kPa, this time is reduced to 0.04 seconds. In addition, since the initial peak amplitude is higher at confining pressure, ($p-u_a$) = 50 kPa, and lower at 400 kPa, this is indicative of lower material damping at higher pressures, which further confirms the increase in rigidity of the soil skeleton with an increase in confinement, as it may be seen in the subsequent figures (6-10 to 6-12).

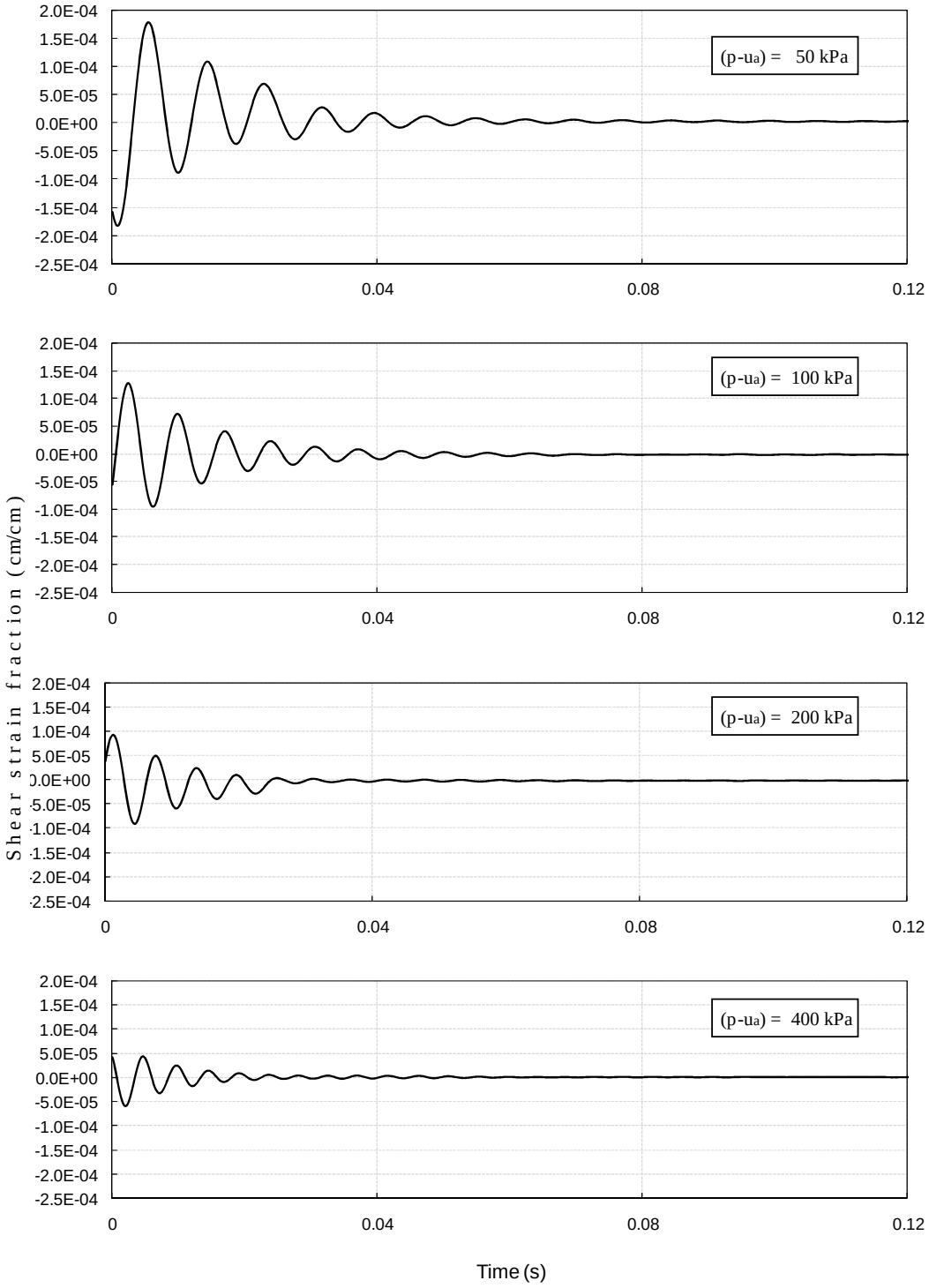


Figure 6-9 Logaritmic decay curves at different net confining pressures under constant suction, s = 50 kPa

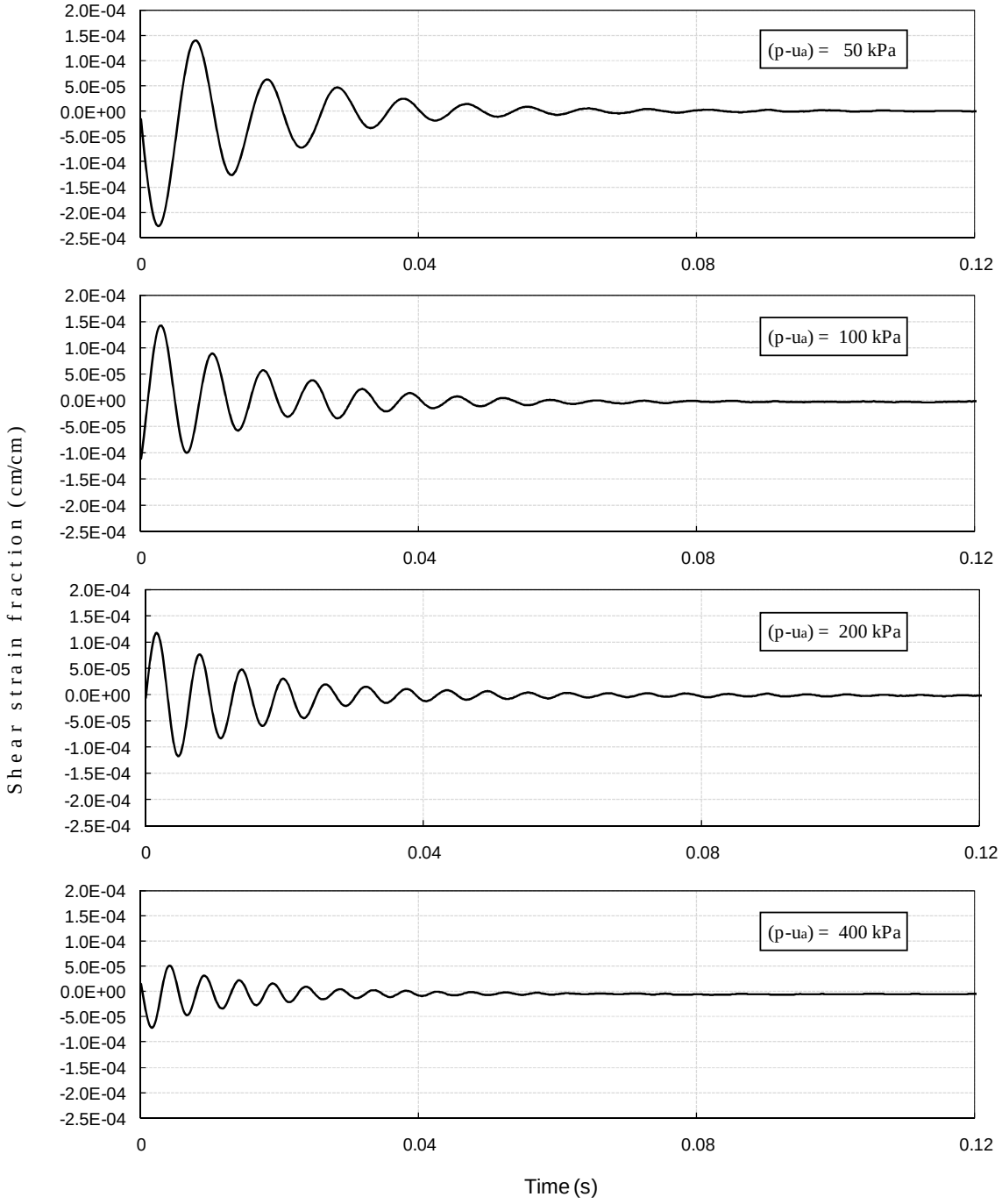


Figure 6-10 Logaritmic decay curves at different net confining pressures under constant suction, s = 100 kPa

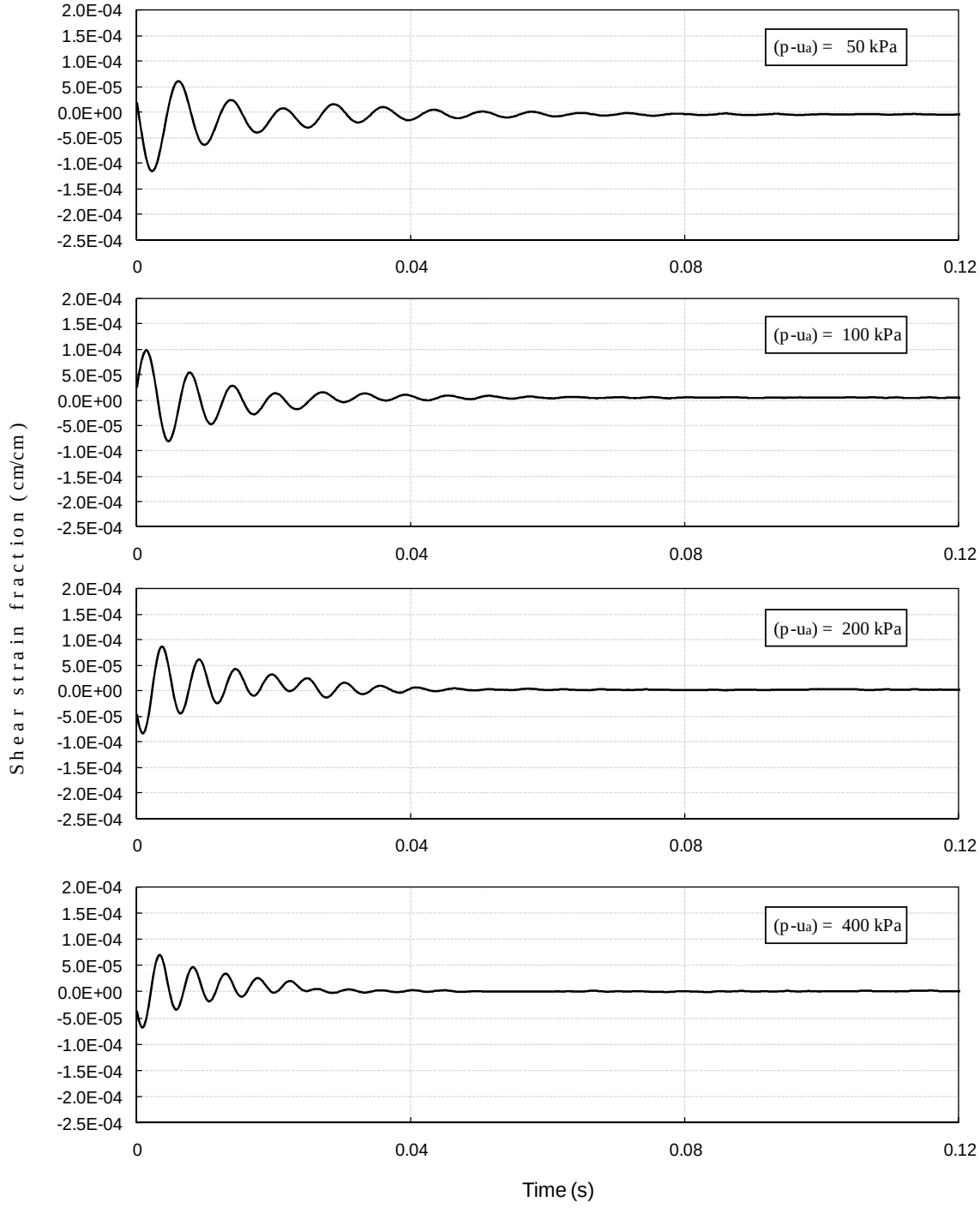


Figure 6-11 Logaritmic decay curves at different net confining pressures under constant suction, s = 200 kPa

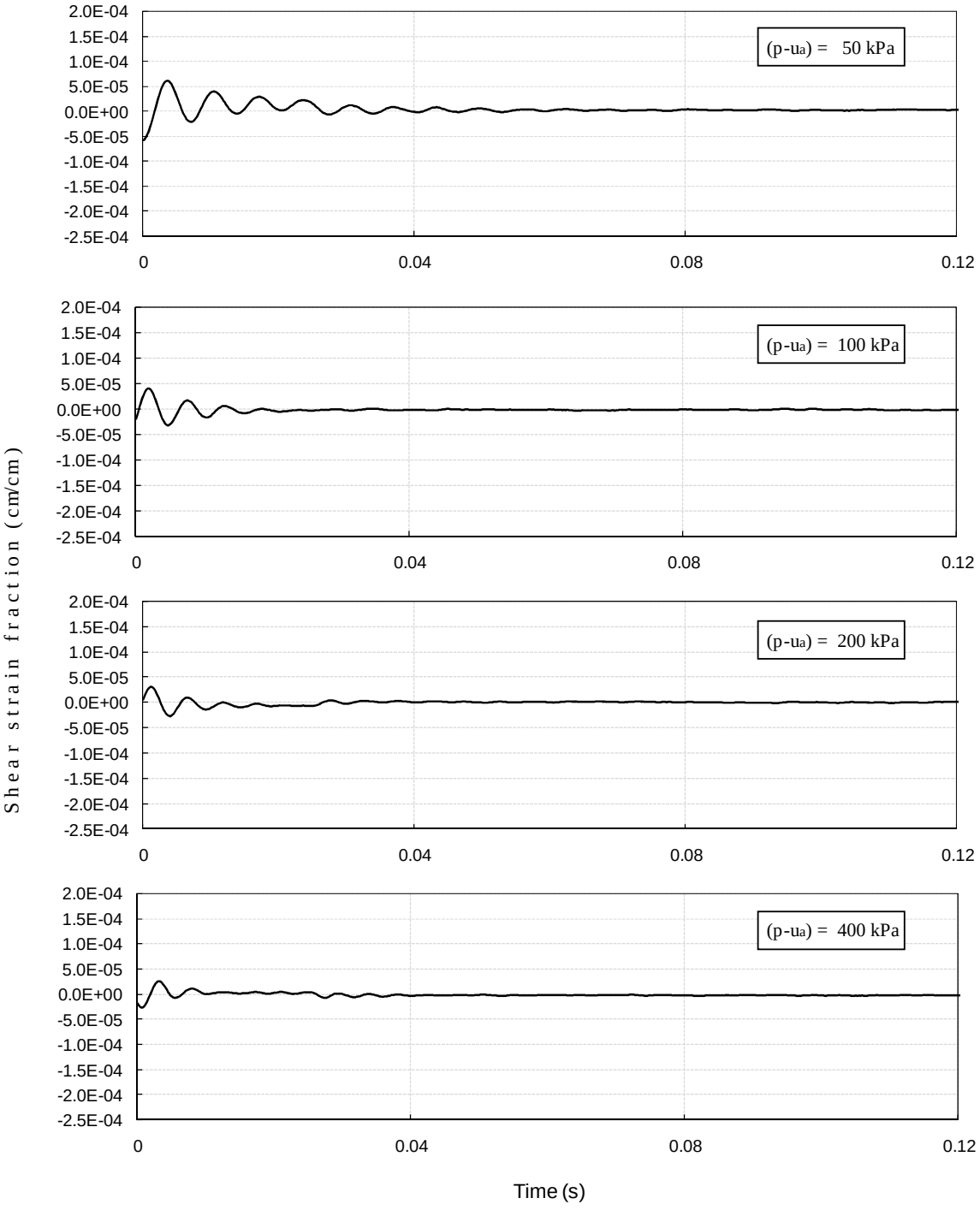


Figure 6-12 Logaritmic decay curves at different net confining pressures under constant suction, s = 400 kPa

*6.3.2 Effect of matric suction state*

The following four figures illustrate the influence of matric suction on free decay behavior of the SM soil specimens, subjected to constant confining pressure (50, 100, 200, and 400 kPa). Figure 6-13, for instance, show the variation on shape and initial amplitude values of the decay curves for a same sample with 50 kPa of confining pressure subjected to changes in suction.

It is observed that the level of matric suction has an even more pronounced effect on the decay response, and the initial peak shear-strain amplitude at time, t = 0, is considerably lower at higher suction states.

It can also be noticed that, contrary to the analysis of net mean stress effects, curves of all suction states appear to be fully attenuated after 0.08 seconds of free vibration. In addition, since the initial peak amplitude is higher at suction, s = 50 kPa, and lower at 400 kPa, this is indicative of lower material damping at higher suctions, which further confirms the increase in rigidity of the soil skeleton as the soil is subjected to a drier state. Additional figures (from 6-13 to 6-16) show similar trends that confirming the previously discussed.

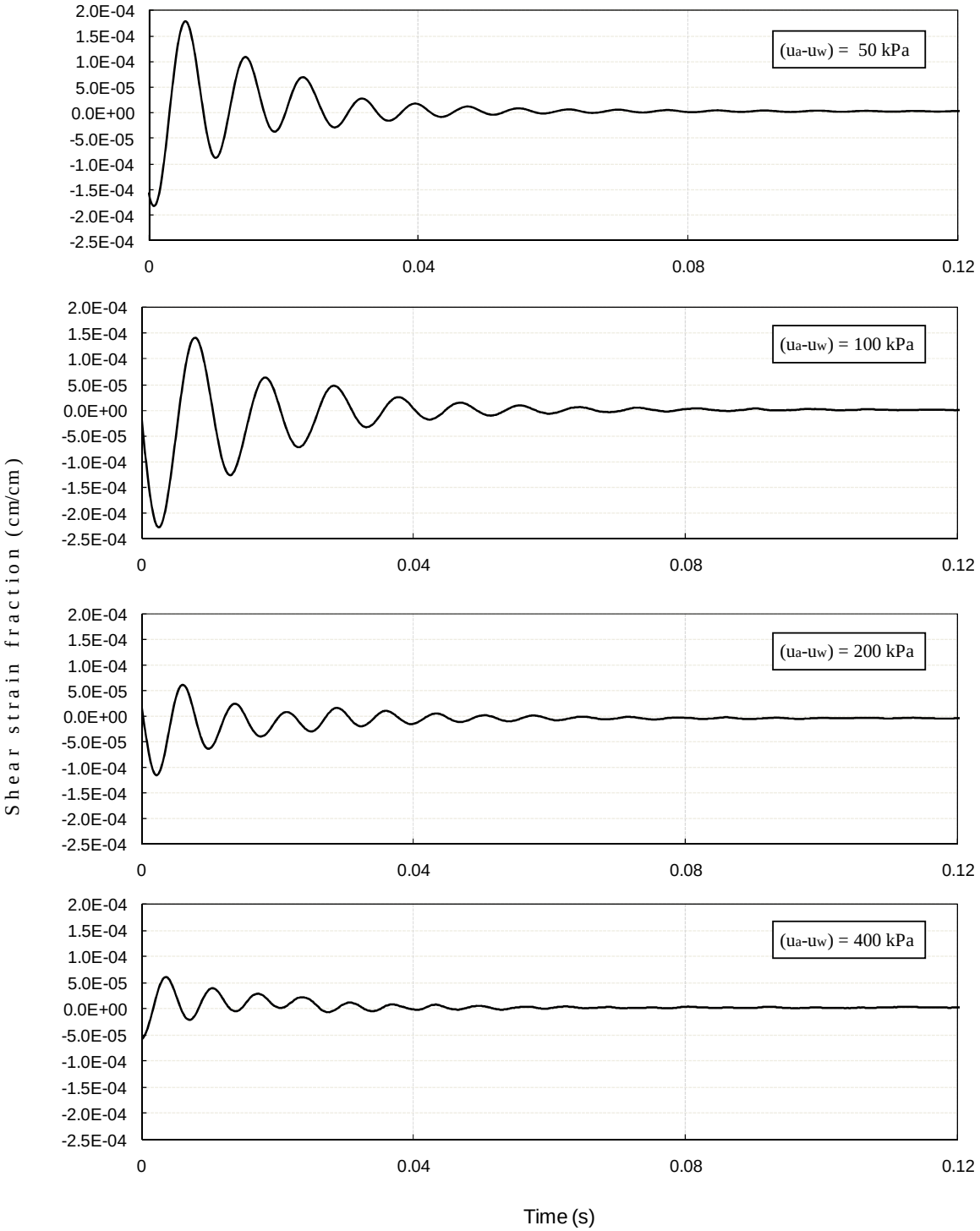


Figure 6-13 Logaritmic decay curves at different matric suction states under net mean stress ($p-u_a$) = 50 kPa

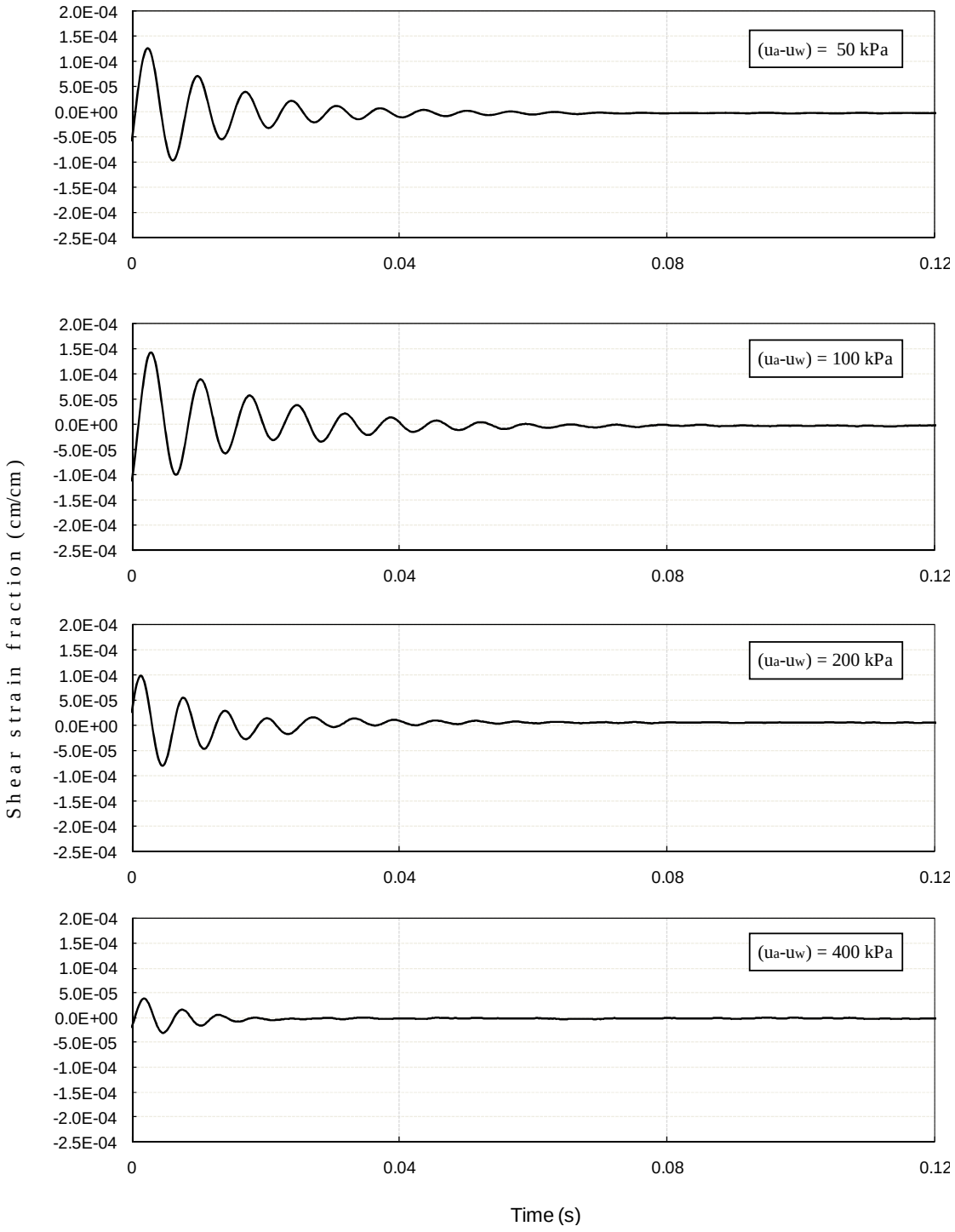


Figure 6-14 Logaritmic decay curves at different matric suction states under net mean stress ($p-u_a$) = 100 kPa

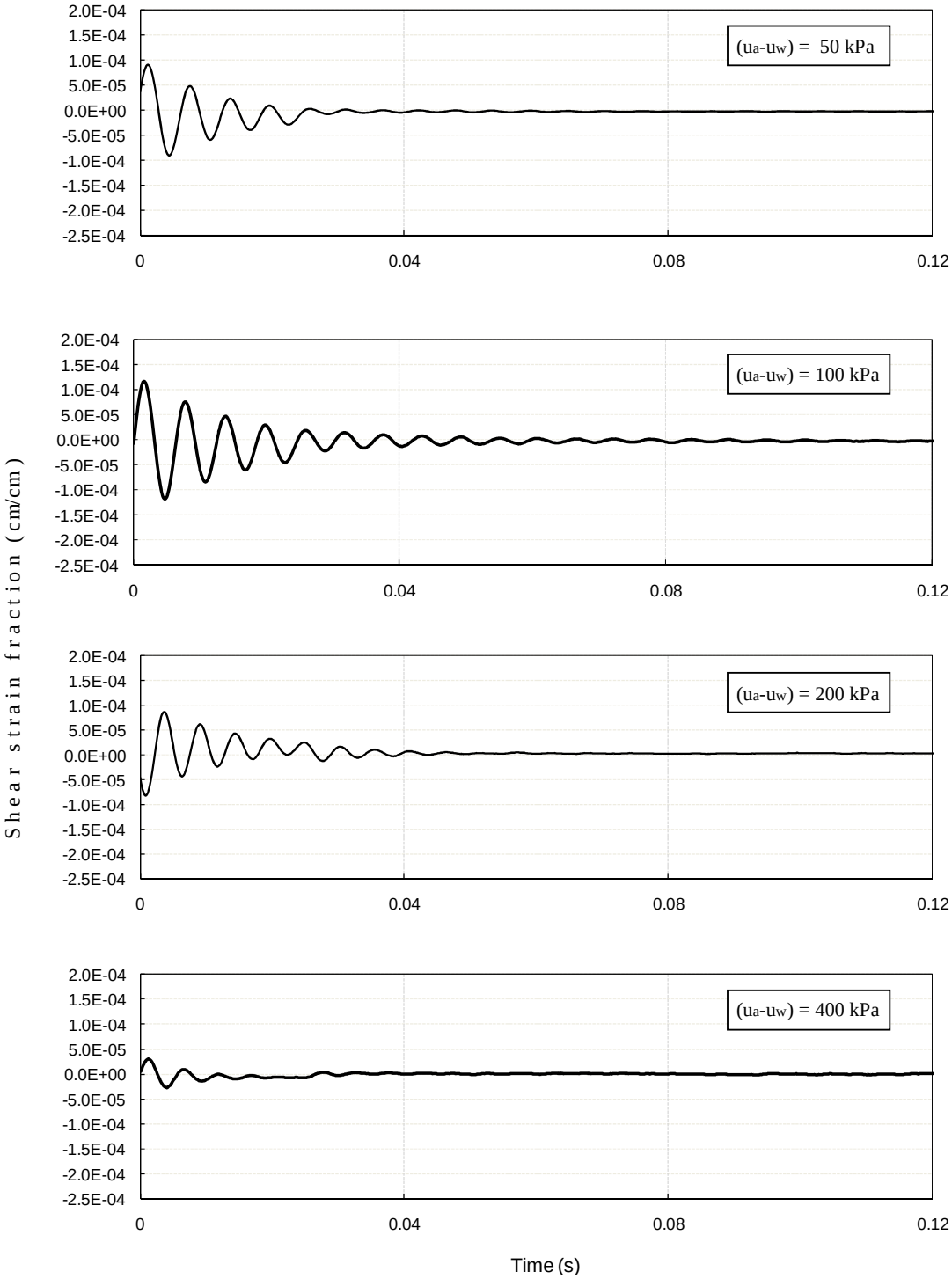


Figure 6-15 Logaritmic decay curves at different matric suction states under net mean stress ($p-u_a$) = 200 kPa

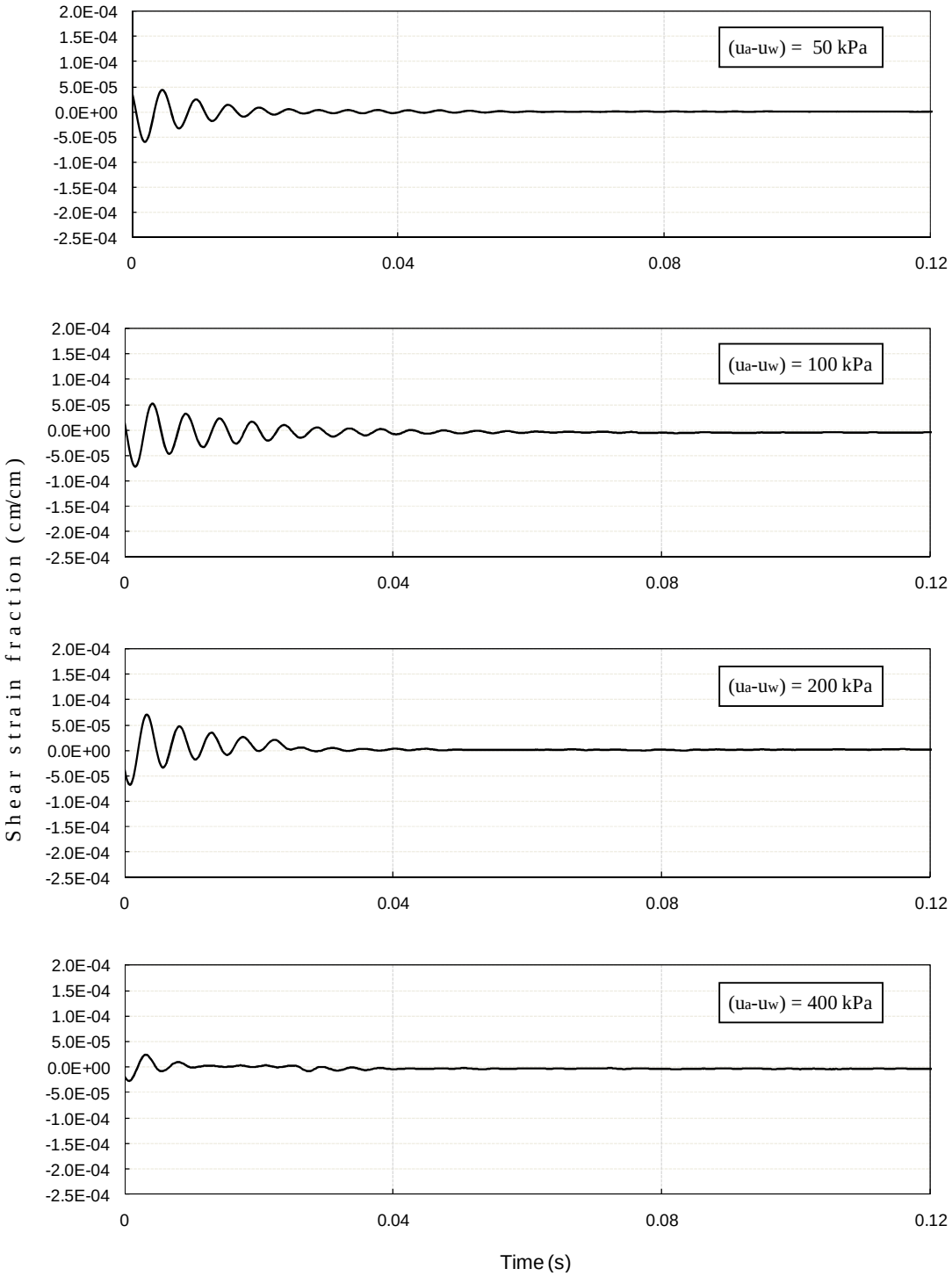


Figure 6-16 Logaritmic decay curves at different matric suction states under net mean stress ($p-u_a$) = 400 kPa

## 6.4 Empirical models for small-strain stiffness

### *6.4.1 Shear modulus*

#### 6.4.1.1 Bi-dimensional analysis

Figure 6-17 shows the variation of small-strain shear moduli $G_{max}$ with net confining pressure, $(p - u_a)$, on the basis of matric suction state, $s = (u_a - u_w)$ = 50, 100, 200, and 400 kPa. The trends further substantiate those shown in Figures 6.1 through 6.4. It is worth noting that at higher net confinement levels, the effect of suction state appears to become less critical.

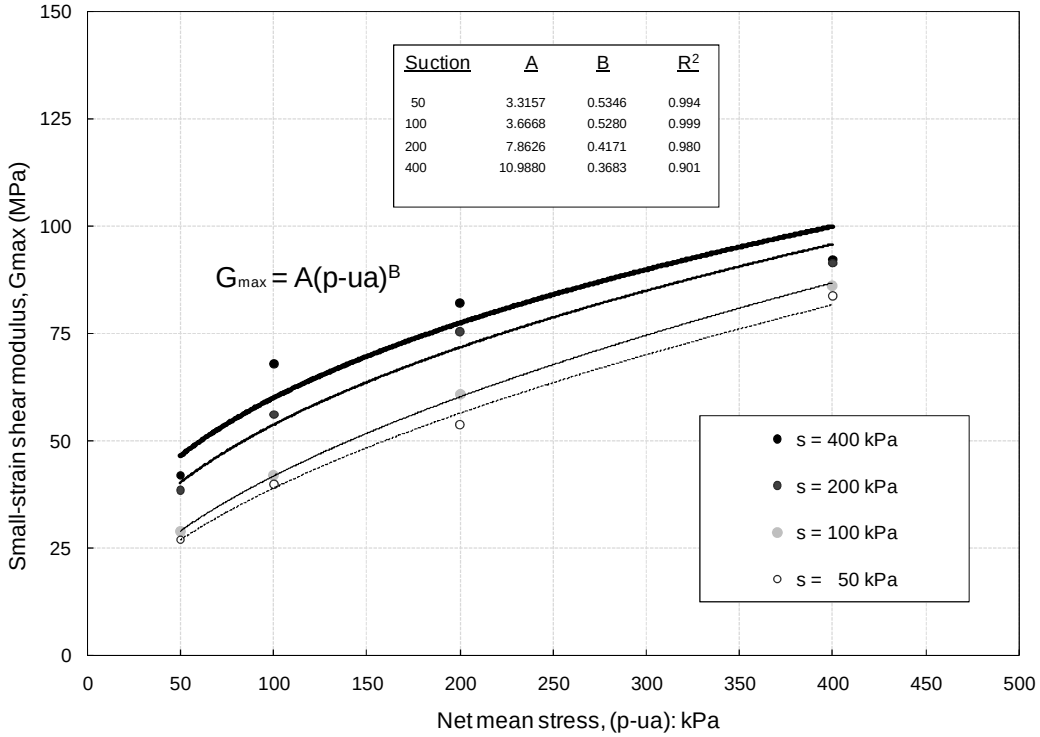


Figure 6-17 Variation of small-strain shear moduli $G_{max}$ with net confining pressure, $(p - u_a)$, on the basis of matric suction state, $s = (u_a - u_w)$.

On the other hand, figure 6-18 shows the variation of shear moduli $G_{max}$ with matric suction $s= (u_a-u_w)$, on the basis of net mean stress state $(p - u_a) = 50, 100, 00, 400$ kPa. The trends also corroborate those shown in Figures 6.5 through 6.8. However, under this specific case, the effect of the suction seems to be less considerable than that of confining states. That is, for higher suction values such as 200 kPa and beyond, the shear modulus does not vary significantly under the same confining pressure state.

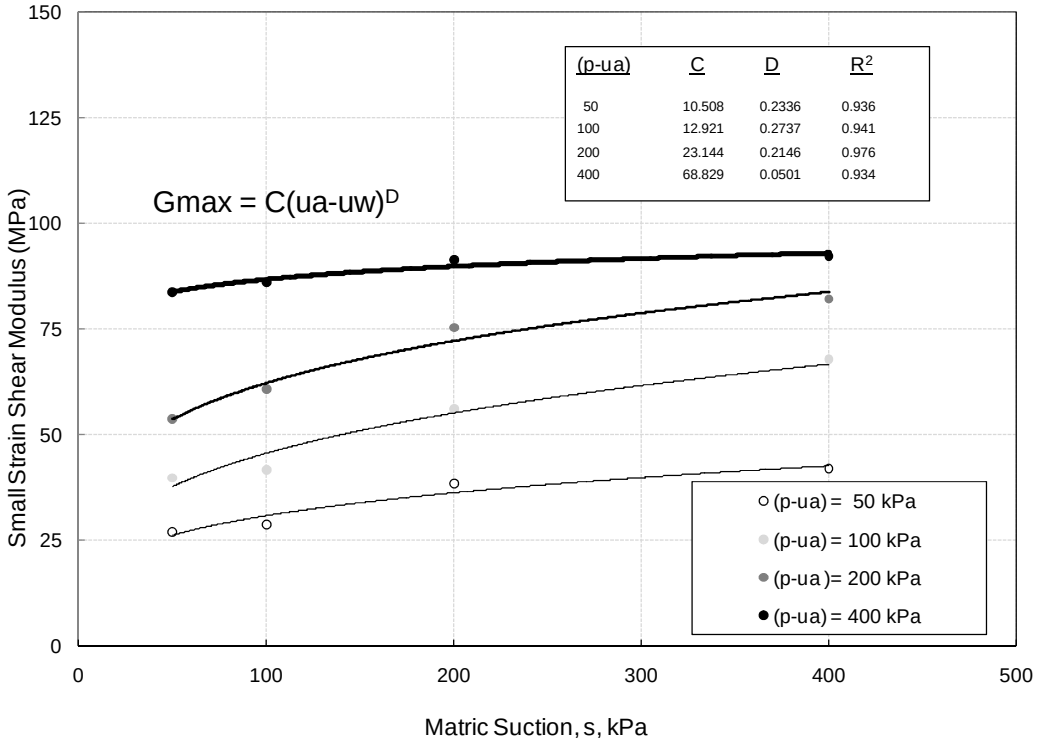


Figure 6-18 Variation of small-strain shear moduli $G_{max}$ with matric suction, $s = (u_a - u_w)$ on the basis of net confining pressure, $(p - u_a)$.

Nonetheless, there is still an appreciable increment due to suction, which leads to an enhancement of the stiffness of statically compacted silty sand. As previously mentioned, this can be attributed to the fact that matric suction produces an additional effective confining pressure effect on the soil skeleton.

As a result of the experimental data shown in figures 6-17 and 6-18, an empirical model for shear modulus as a function of two stress state variables can be assessed. The prediction of G with respect to ($p-u_a$) and ($u_a-u_w$) is presented in equations 6.1 and 6.2, respectively. Likewise, table 6-1 shows the best-fit model parameters obtained from the experimental data:

$$G_{max} = A(p - ua)^B \qquad (6.1)$$

and

$$G_{max} = C(ua - uw)^D \qquad (6.2)$$

where,

A, B, C, and D are constants shown in table 6.1.

A general solution for estimating the small-strain shear modulus, $G_{max}$, can then be given as:

$$G_{max} = A'(p - ua)^B + C'(ua - uw)^D \qquad (6.3)$$

However, additional experimental evidence is needed for a thorough assessment of constants A' and C' in equation 6.3, which is beyond the scope of the present work.

Table 6-1 Best-fit model parameters for Prediction Model of Shear Modulus

| $G_{max} = A\ (p-u_a)^B$ | | | | $G_{max} = C\ (u_a-u_w)^D$ | | | |
|---|---|---|---|---|---|---|---|
| $(u_a-u_w)$ | A | B | $R^2$ | $(p-u_a)$ | C | D | $R^2$ |
| 50 | 3.3157 | 0.5346 | 0.9949 | 50 | 10.508 | 0.2336 | 0.9362 |
| 100 | 3.6668 | 0.5280 | 0.9997 | 100 | 12.921 | 0.2737 | 0.9418 |
| 200 | 7.8626 | 0.4171 | 0.9800 | 200 | 23.144 | 0.2146 | 0.9762 |
| 400 | 10.9880 | 0.3683 | 0.9013 | 400 | 68.829 | 0.0501 | 0.9348 |

Several attempts to link Gmax with matric suction and net mean stress have been proposed in the last three decades by other researches. Hardin and Black (1968) suggested the following empirical relation for sands:

$$G_{max} = f(e) * {\sigma_3}^n \qquad (6.4)$$

where f(e) is function of void ratio and n is an empirical constant. The exponent, n, was found to be 0.5. Mendoza et al. (2005) investigated the small strain stiffness of an unsaturated clayey soil and suggested that Gmax is related to matric suction y the following empirical relation:

$$G_{max} = f'(e)[\ln(u_a - u_w)]^m \qquad (6.5)$$

where f'(e) is a function of void ratio and m is an empirical constant. The exponent, m, was found to be 1.35. Similarly, Leong et al. (2006) suggested that the effects of confining pressure and matric suction on Gmax can be accounted for in a single equation as following:

$$Gmax = (G_{max})_0 \left[1 + \left(\frac{\sigma_3}{Pa}\right)^n\right]\left[1 + \left[\ln\left(1 + \frac{u_a - u_w}{Pa}\right)\right]^m\right] \qquad (6.6)$$

where $(G_{max})_0$ is the $G_{max}$ of the soil at a confining pressure of 0 kPa and a matric suction of 0 kPa, Pa is the atmospheric pressure (= 100 kPa), and n and m are empirical constants.

Although results from this research work are similar to those presented by these authors, the empirical equations 6.1, 6.2, and 6.3 from this work include stress variables that affect the stiffness response independently. In other words, the response of $G_{max}$ could be represented in a 3-D space, where the two horizontal axes are defined as matric suction $(u_a-u_w)$ and net mean stress $(p-u_a)$, as shown in the next section.

Constants A and C in equation 6.1 and 6.2 vary significantly as function of suction; hence, arithmetic average cannot truly capture the stiffness response of SM soil tested for all pressures and suctions states. Contrary to this, the exponents B and D in table 6.1 can be averaged into reasonably constant values, which is similar to the concept of $\phi$' and $\phi^b$ angles proposed in the unified Mohr-Coulomb shear strength framework for unsaturated soils (Fredlund and Rahardjo 1993).

#### 6.4.1.2 Three-dimensional representation of shear modulus experimental data

The following figure (6-19) attempts to closely represent the initial shear modulus G, from controlled-suction states, $(u_a-u_w)$, versus net mean stresses, $(p-u_a)$. Based on the equation 6.7, which is derived from the arithmetic average of the exponents B and D with coefficient of determination close to 1.0, the 3-D illustration was accomplished.

As shown in this figure, most of the suction effects are observed in the range from 0 to 200 kPa. For higher suctions, $G_{max}$ seems to tend toward a threshold value that depends on the net mean stress level. This affirmation is in agreement with the model proposed by Mancuso et al. (2006), which used a suction-controlling technique applying air and water pressures at the specimen boundaries.

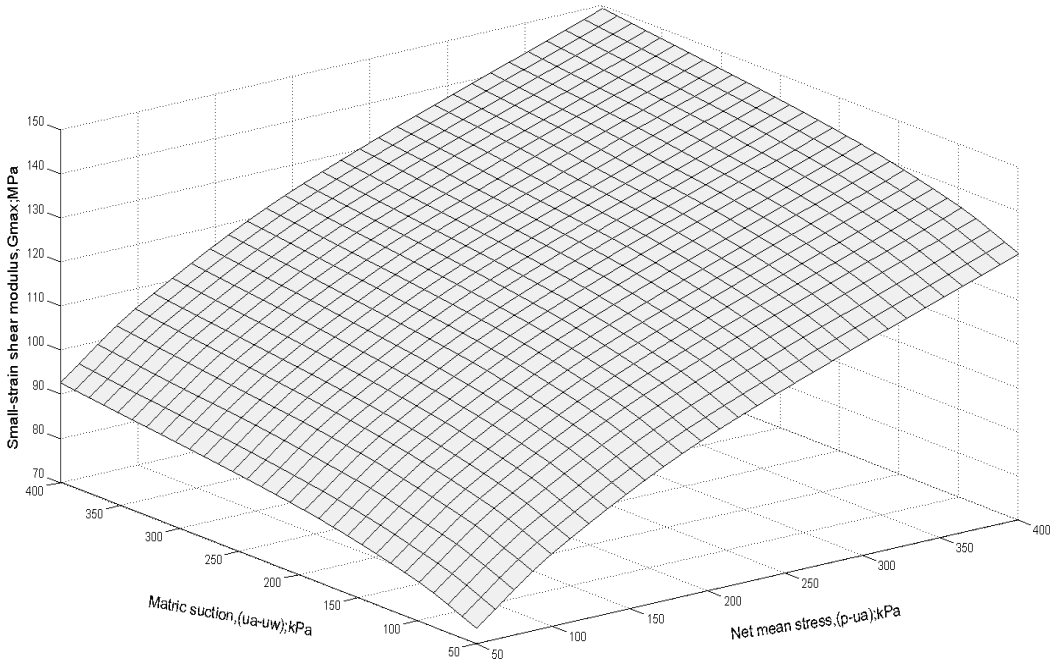


Figure 6-19 3-D Representation of experimental small-strain shear modulus data.

It can also be seen that the effect of suction on the initial shear stiffness is significant, causing an increase in G, ranging from 70 to 80 MPa at the first part of the curve, and from 80 to 95 MPa, for suctions beyond 200 KPa. This mechanical behavior response is explained to be on the basis of the different ways in which menisci water affects soil behavior. It is then justified by identifying two major zones on the G as function of $(u_a-u_w)$. The zone 1, which varies from 0 to 200 kPa, refers suction values surrounding air-entry value, and a progressive shift of soil behavior from bulk-water to a menisci-water regulated response, and zone 2 where the menisci-water effects predominate.

*6.4.2 Material damping*

Contrary to shear modulus behavior, material damping ratio value is inversely proportional to the confinement pressures and matric suction. The higher the confinement and suction, the stiffness increases, and therefore damping values are decreased. This affirmation is

corroborated analyzing all initial amplitudes from the decay curves in figures 6.9 through 6.16, and well as, from variation of material damping with confining pressure and suction which are shown in the following figures.

Figures 6-20 and 6-21 show the variation of small-strain damping ratio, $D_{min}$, with net confining pressure, $(p - u_a)$ on the basis of suction states, $s = (u_a - u_w)$, = 50, 100, 200, and 400 kPa. Damping ratio can be readily obtained from either a logarithmic decay curve or half-power bandwidth method. Since results from those methods are captured from the logarithmic decay curve and frequency response respectively, damping values results may vary. A graphic analysis by using both techniques was assessed.

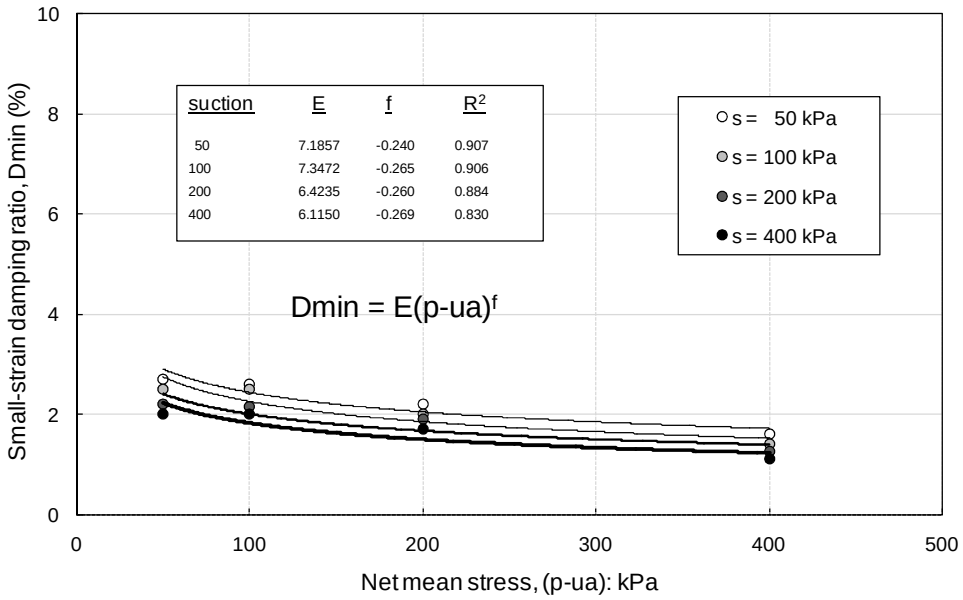


Figure 6-20 Variation of small-strain damping ratio with net confining pressure, $(p - u_a)$, on the basis of matric suction state, $s = (u_a - u_w)$ using free vibration decay curve method.

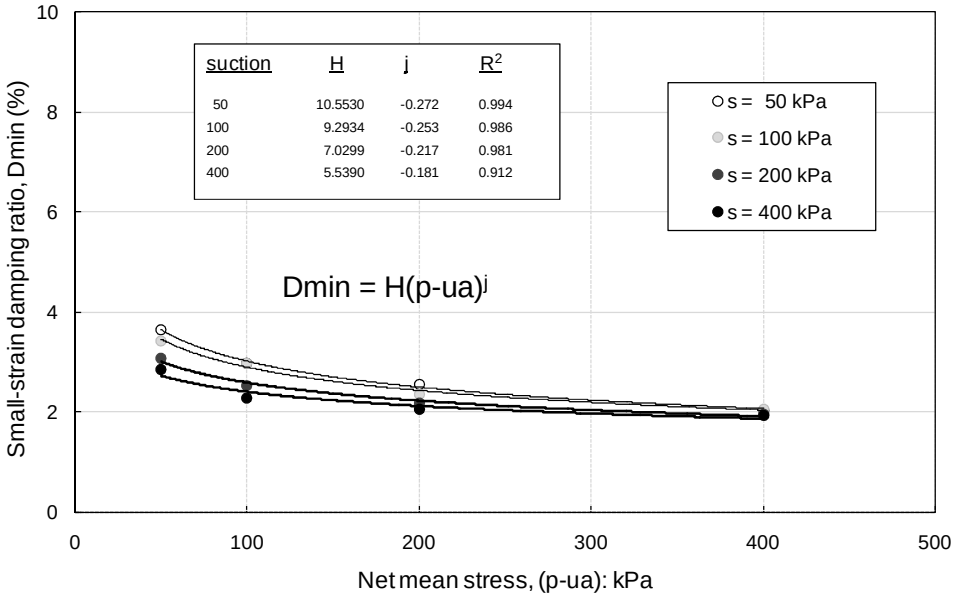


Figure 6-21 Variation of small-strain damping ratio with net confining pressure, ($p - u_a$), on the basis of matric suction state, $s = (u_a - u_w)$ using half-power bandwidh method.

On the other hand, figures 6-22 and 6-23 show the variation of small-strain damping ratio $D_{min}$, with suction, $s = (u_a - u_w)$, on the basis of net confining pressure, ($p - u_a$) = 50, 100, 200, and 400 kPa, through free vibration decay curve and half-power bandwidth techniques respectively. The effect of the suction seems to be less considerable than that of confining states. That is, for higher suction values as 200 kPa and beyond, the damping ratio does not vary significantly under the same confining pressure state.

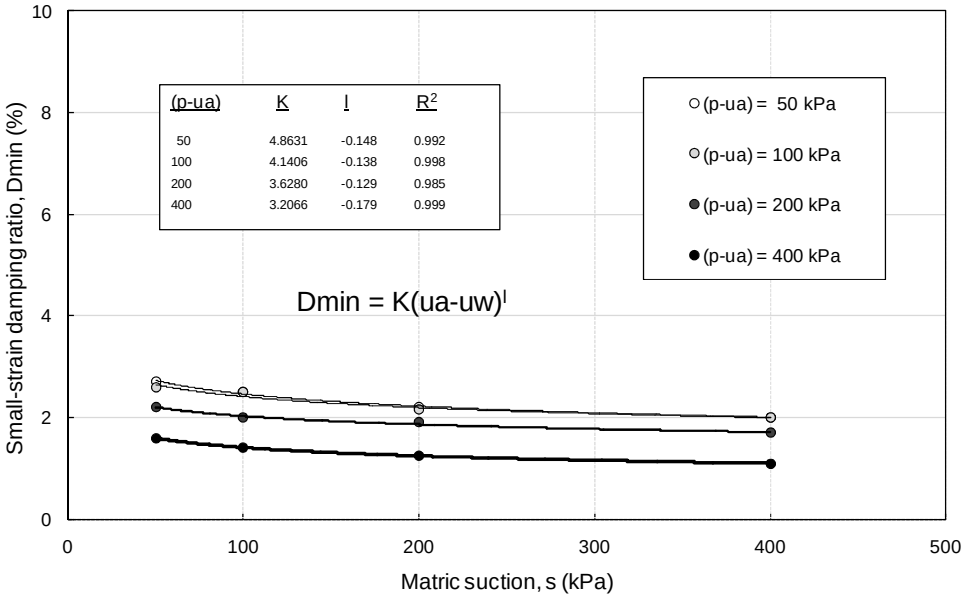


Figure 6-22 Variation of small-strain damping ratio, Dmin with matric suction, s = ($u_a$ – $u_w$) on the basis of.net confining pressure, (p – $u_a$) by using free vibration decay method

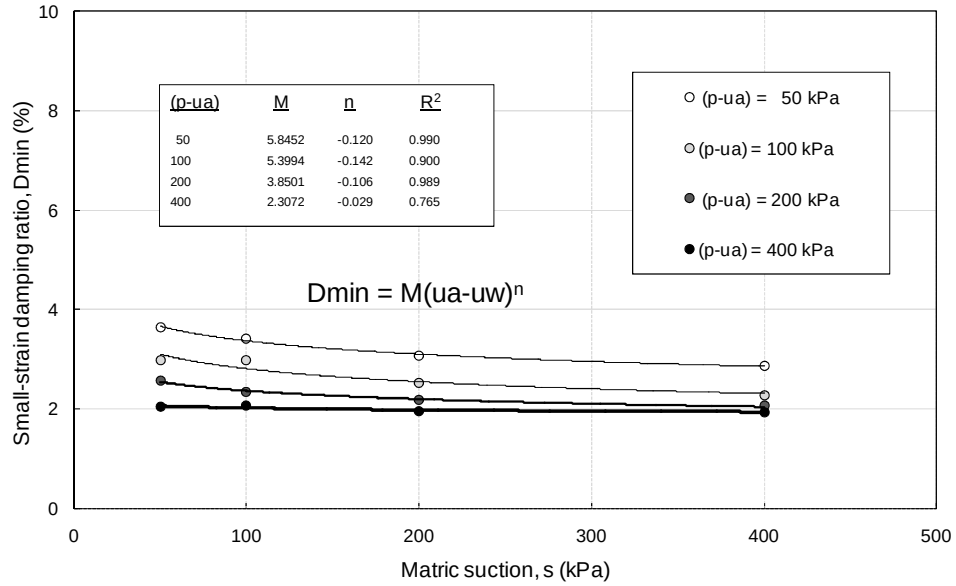


Figure 6-23 Variation of small-strain damping ratio, Dmin with matric suction, s = ($u_a$ – $u_w$) on the basis of.net confining pressure, (p – $u_a$) by using half-power bandwidth method

Nonetheless, there is still and appreciable decrement due to suction, which leads an enhancement of the stiffness of statically compacted silty sand. As a result of the experimental data shown in figures 6-20, 6-21, 6-22, and 6-23, an empirical model for material damping ratio as a function of two stress state variables can be assessed. The prediction of $D_{min}$ respect to ($p-u_a$) and ($u_a-u_w$) is presented in equations 6.7 and 6.8, respectively. Likewise, tables 6-2 and 6-3 show the best-fit model parameters obtained from the experimental data:

$$D_{min} = E(p - ua)^f \qquad (6.7)$$

and

$$D_{min} = K(ua - uw)^n \qquad (6.8)$$

where,

E, K, f, and n are constants shown in tables 6.2 and 6.3.

A general solution for estimating the small-strain damping ratio, $D_{min}$, can then be given as:

$$Dmin = E'(P - ua)^f + K(ua - uw)^n \qquad (6.9)$$

However, additional experimental evidence is needed for a thorough assessment of constants E' and K' in equation 6.9, which is beyond the scope of the present work.

Table 6-2 Constant Values for Damping Prediction Model with confining pressure as input variable

| $D_{min} = E\,(p\text{-}u_a)^f$ Free decay curve | | | | $D_{min} = H\,(P\text{-}u_a)^j$ Half-power Bandwidth | | | |
|---|---|---|---|---|---|---|---|
| $(u_a\text{-}u_w)$ | E | f | $R^2$ | $(u_a\text{-}u_w)$ | H | j | $R^2$ |
| 50 | 7.1857 | -0.240 | 0.9077 | 50 | 10.5530 | 0.272 | 0.9945 |
| 100 | 7.3472 | -0.265 | 0.9063 | 100 | 9.2934 | 0.253 | 0.9861 |
| 200 | 6.4235 | -0.260 | 0.8842 | 200 | 7.0299 | 0.217 | 0.9817 |
| 400 | 6.1150 | -0.269 | 0.8298 | 400 | 5.5390 | 0.181 | 0.9125 |

Table 6-3 Constant Values for Damping Prediction Model with matric suction as input variable

| $D_{min} = K\,(u_a\text{-}u_w)^l$ Free decay curve | | | | $D_{min} = M\,(u_a\text{-}u_w)^n$ Half-power Bandwidth | | | |
|---|---|---|---|---|---|---|---|
| $(P\text{-}u_a)$ | K | l | $R^2$ | $(P\text{-}u_a)$ | M | n | $R^2$ |
| 50 | 4.8631 | -0.148 | 0.9928 | 50 | 5.8452 | -0.120 | 0.9908 |
| 100 | 4.1406 | -0.138 | 0.9982 | 100 | 5.3994 | -0.142 | 0.9000 |
| 200 | 3.6280 | -0.129 | 0.9852 | 200 | 3.8501 | -0.106 | 0.9893 |
| 400 | 3.2066 | -0.179 | 0.9991 | 400 | 2.3072 | -0.029 | 0.7653 |

Although results from this research work are similar to those presented by these authors, the empirical equations 6.7, 6.8, and 6.9 from this work include stress variables that affect the stiffness response independently. In other words, the response of $D_{min}$ could be represented in a 3-D space, where the two horizontal axes are defined as matric suction ($u_a$-$u_w$) and net mean stress ($p$-$u_a$), as shown in the next section.

Constants E and K in equation 6.7 and 6.8 vary significantly as function of suction; hence, arithmetic average cannot truly capture the stiffness response of SM soil tested for all

pressures and suctions states. Contrary to this, the exponents f and n in table 6.2 and 6.3 can be averaged into reasonably constant values, which is similar to the concept of $\phi$' and $\phi^b$ angles proposed in the unified Mohr-Coulomb shear strength framework for unsaturated soils.

#### 6.4.2.1 Three-dimensional representation of material damping experimental data

Likewise as shear modulus, the 3-D analysis, shown in figure 6-24, is devoted to closely characterize the variation of material damping ratio, D, from controlled-suction states, ($u_a$-$u_w$), versus net mean stresses, (p-$u_a$) simultaneously. Based on the equation 6.6, which is obtained using arithmetic averages for exponents with $R^2$ close to one, the 3-Dimensional illustration for damping values determination was plotted.

As shown in figure 6-24, most of the suction effects are observed in the range from 0 to 200 kPa. For higher suctions, the decrement of Damping seems to tend toward a threshold value that depends on the net mean stress level. Even though the confining stresses have a more influence in damping variation than matric suction, it is worth to highlight the considerable role of the suction plays on this parameter.

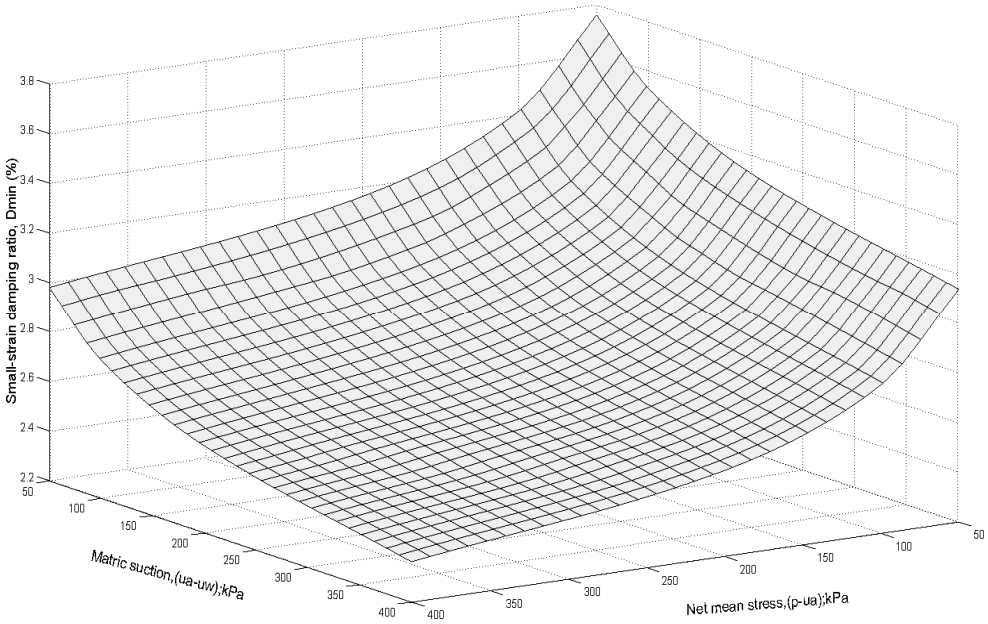


Figure 6-24 3-D Representation of experimental small-strain damping ratio data.

# CHAPTER 7

# BENDER ELEMENT TEST RESULTS AND ANALYSIS

## 7.1 Introduction

In this chapter, results from simultaneous resonant column and bender element tests on compacted SM soil are presented. Typical transmitting and arriving BE wave signals are also reported. Shear modulus values from BE tests are compared with those from RC tests. Bender element tests were performed as soon as the resonant frequency from resonant column test was achieved.

In order to compare the shear modulus response of the same SM soil sample at different stress states, two suction levels, 50 and 200 kPa, were selected for a range of net confinements from 50 to 400 kPa.

## 7.2 Typical bender element signal outputs

Typical sinusoidal output signals from suction-controlled BE tests conducted on one SM soil samples at matric suction ($u_a$-$u_w$) = 50 kPa, and five different net mean stresses ($p$=$u_a$) = 0, 50, 100, 200 and 400 kPa, are shown in Figure 7-1.

It can be observed that the shear wave arrival time decreases as the net mean stress increases, which can be directly attributed to an increase in soil stiffness.

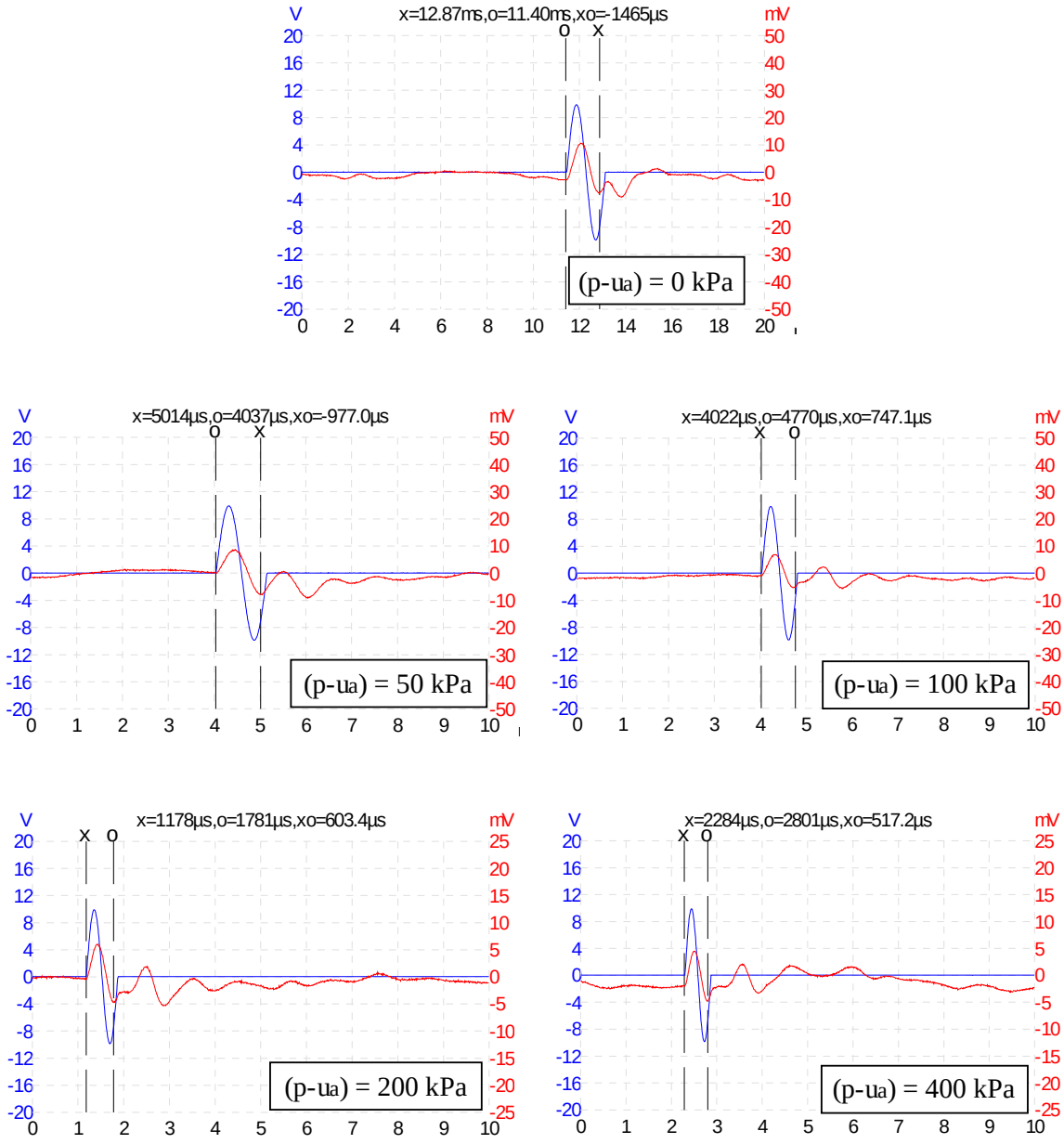


Horizontal axes units: ms

Figure 7-1 BE response for silty sand SM at constant matric suction ($u_a$-$u_w$) = 50 kPa, for different net mean stresses

## 7.3 Comparison of shear modulus from BE and RC testing techniques

Results from suction-controlled bender element and resonant column tests on silty sand (SM) are shown in figure 7-2. BE and RC tests were carried out at different net mean stresses ($p-u_a$) = 50, 100, 200, and 400 kPa, for 50 and 200 kPa matric suction states. It is observed that the shear modulus obtained from both techniques follow a reasonably similar pattern. However, it is worth noting that the bender element results tend to be slightly higher than those from the resonant column.

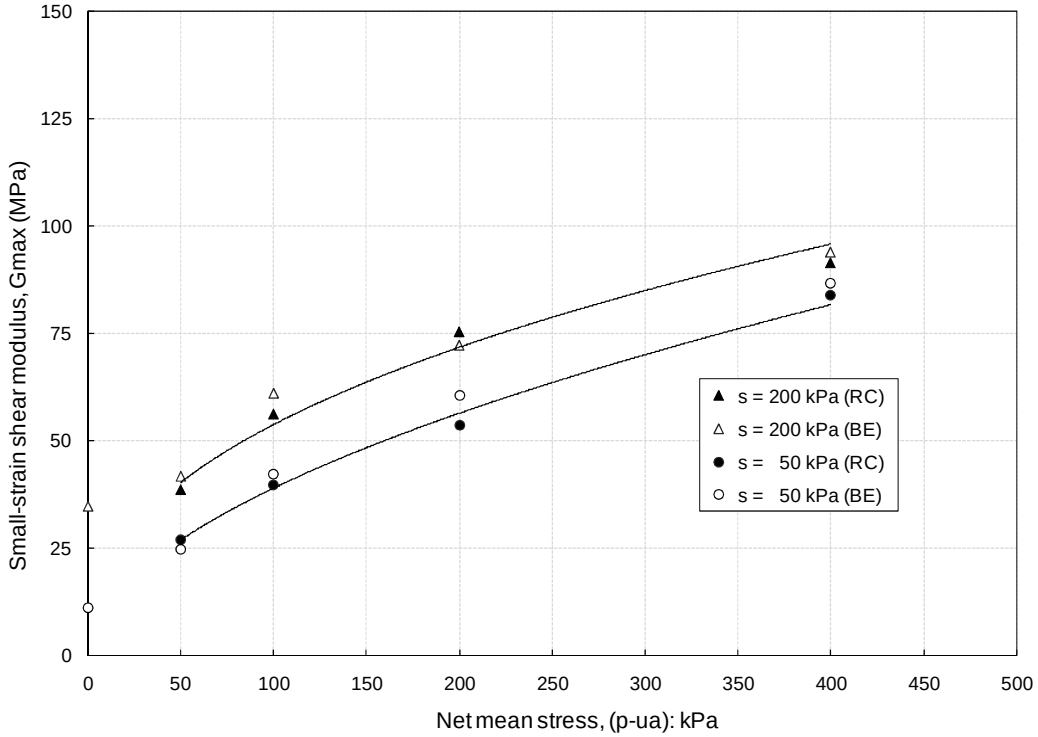


Figure 7-2 Shear modulus response from BE and RC tests on compacted silty sand on the basis of matric suction, s = (u-uw)

Figure 7-3 shows that most of the bender element data fall slightly below a 45 degree line when compared to RC data, which indicates that BE values are slightly higher than those from the newly developed proximitor-based resonant column. It can be assumed that data which lie

on the 45 degree line would have a perfect correlation between both devices. In other words, those values that fall exactly on the 45 degree line are supposed to be equal. Although shear modulus from both resonant column and bender element testing are not fully identical, results from this experimental analysis show very close trends, which allows concluding that both techniques, when assembled and used simultaneously, yield similar small-strain stiffness results.

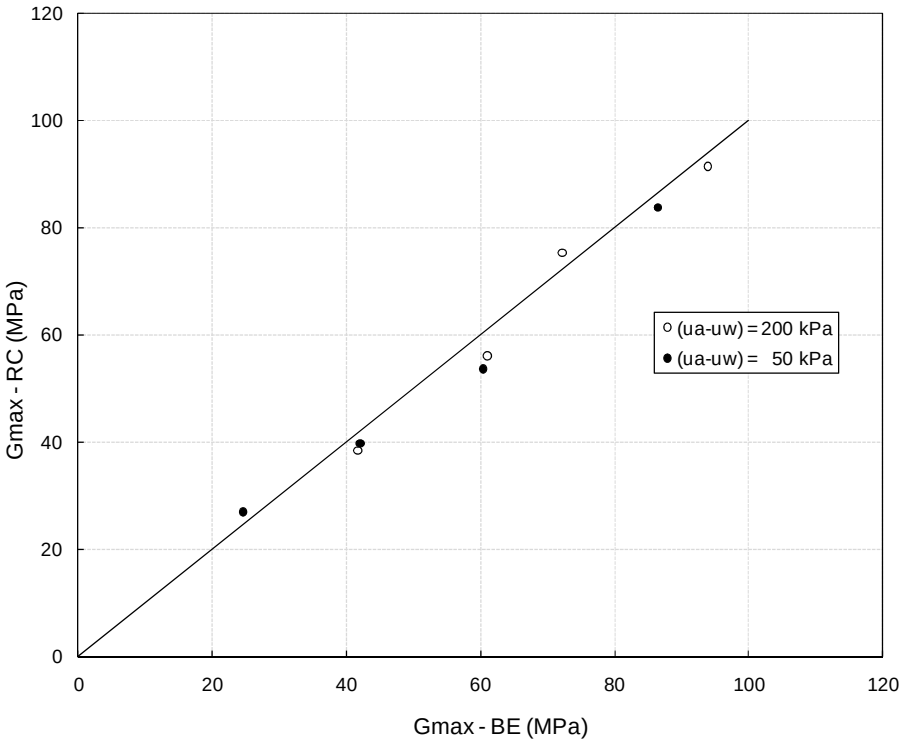


Figure 7-3 Comparison of shear modulus response from BE and RC for silty sand SM.

# CHAPTER 8

# CONCLUSIONS AND RECOMMENDATIONS

## 8.1 Summary

Small-strain soil stiffness properties such as shear modulus, shear wave velocity, and material damping, are key subsoil parameters for an adequate analysis and design of unsaturated earth structures subject to static and non-static loading. Most conventional geotechnical testing techniques, however, are not able to capture this small-strain behavior and, hence, enormously underestimate the true soil stiffness, primarily due to inaccuracies in small-strain measurements. Around the world, a great deal of research efforts has been dedicated to field and laboratory based measurements of soil suction, assessments of soil-water retention properties, and analyses of swell-collapse behavior. However, very few efforts have been focused on small-strain response of unsaturated soils and their dynamic characterization at small strains.

The overall purpose of this research was to study the dynamic properties of soils at very small shear strain amplitudes under different controlled matric suction states via resonant column and bender elements testing. This research work introduced a suction-controlled, proximitor-based resonant column device featuring a PCP-15U pressure control panel that allows the implementation of the axis-translation technique via the independent control of pore-air and pore-water pressures in the specimen. The apparatus also features a full set of self-contained bender elements for simultaneous testing of small-strain dynamic properties under both techniques.

A comprehensive series of suction-controlled resonant column and bender element tests were conducted on statically compacted samples of silty sand for a range of constant suction states between 50 kPa and 400 kPa, at different net confining pressures. Results showed the critical role of matric suction on the small-strain response of the of the test soil, also highlighted the potential and reliability of the developed apparatus.

## 8.2 Conclusions

Based on all the experimental findings and analyses of the test results, the following conclusions can be drawn from the present thesis work:

### *8.2.1 Calibration of Proximitor-based RC device*

1. A new proximitor-based resonant column with suction-controlled and bender element testing capabilities was introduced. RC tests were performed through a torsional actuator system, in which the magnitude of the input torque is given in pfs units (percent of full scale). The appropriate input torque was found to be 1 pfs, which corresponds to a 0.25 V input signal in the conventional accelerometer-based resonant column apparatus.
2. The calibration process of the poximitor-based resonant column device was accomplished in two major steps: the first step involves the use of a calibration kit provided with the core system of the new proximitor-based RC device: a second step involves comparison of results from both proximitor-based and accelerometer-based RC device on identically prepared SM soil samples.
3. Through the first step of this calibration process, the mass moment of the torsional driver system acting on a aluminum rod inertia for the device was evaluated. Then, frequency sweeps and shear modulus values for calibration rod were obtained for validating the reliability of the proximitor-based RC apparatus.

4. During the second stage of the calibration process, the shear modulus of SM soil from both devices was found to be significantly affected by shearing strains larger than a threshold value at any confining level. When the peak shearing strain was greater than the threshold strain, then, the shear modulus decreased.
5. Comparison of linear and non-linear response of SM soil from conventional accelerometer-based RC and the proximitor-based RC devices confirm the reliability and accuracy of the newly developed proximitor-based RC apparatus.

*8.2.2 Small-strain stiffness response of compacted SM soil*

1. A complete series of RC tests was conducted on compacted SM soil specimens using the new suction-controlled proximitor-based resonant column device with self-contained bender elements. Results show that the new apparatus is suitable for testing unsaturated soils under suction-controlled states via axis-translation technique.
2. As expected, the small-strain shear modulus, $G_{max}$, tends to increase with an increase in the matric suction state. This can be readily attributed to the fact that suction increases the effective stress, enhancing the soil stiffness properties.
3. Likewise, the small-strain shear modulus, $G_{max}$, tends to considerably increase when the net mean stress is increased.
4. Results also show a reasonable matching between $G_{max}$ values from resonant column and bender elements tests, with a slight overestimation of $G_{max}$ from bender elements results for higher matric suction states.
5. As it was expected, material damping ratio, $D_{min}$, decreased as either matric suction or net mean stress increased. The increase in stiffness when the suction is increased makes the soil column system experience lower damping under free-decay vibration mode.

6. In general, the experimental results highlight the critical influence that soil suction states have on small-strain soil stiffness properties.

## 8.3 Recommendations for Future Work

The following recommendations can be made to further study the dynamic properties of soils at very small strain levels using the proximitor-based resonant column with suction control and bender element capabilities developed in this work:

1. A broader series of tests under partially saturated conditions in different type of soils should be performed in order to validate the results achieved in this current project.
2. A detailed analysis of the non-linear increase in $G_{max}$ with respect to matric suction ($u_a$-$u_w$) and its relationship with the air entry value obtained from the soil water characteristic curve (SWCC) is subjected to further studies.
3. Since the developed RC device is also capable to apply axial and radial confining pressures independently, the independent effect of anisotropic stress paths and matric suction levels can be studied in future research projects.
4. Empirical models for small-strain shear modulus and material damping of unsaturated soils can be thoroughly devised once additional data become available.

REFERENCES

[1] Alonso, E.E., A. Gens & Josa (1990). “A constitutive model for partially saturated soils.” Geotechnique 40(3), 405-430.

[2] ASTM (1993) “Test methods for modulus and damping of soils by the resonant column method,” Standard D 4015-92, ASTM, Philadelphia, PA, pp. 581-593.

[3] Atkinson, J.H. (2000). “Nonlinear soil stiffness in routine design”. Géotechnique, 50(5): 487-588.

[4] Borden, R.H., Shao, L. and Gupta, A. (1996).”Dynamic properties of piedemont residual soils”. J. of Geotechnical Engineering, ASCE, 122(10): 813-821.

[5]

[6] Brull, A. (1980). Caracteristiques mécaniques des sols de fondation de chaussées en fonction de leur état d’humidité et de compacité. Proc., International Conf. on Soil Compaction, Paris, vol. 1: 113-118.

[7] Cabarkapa, Z., Cuccovillo, T., and Gunn, M. (1998). A new triaxial apparatus for testing unsaturated soils. Proc., 2nd International Conf. on Unsaturated Soils, Beijing, China, vol. 2: 194-195.

[8] Cabarkapa, Z., T. Cuccovillo & M Gunn (1999). “Some aspects of the pre-failure behaviour of unsaturated soil.” II International Conference on pre-failure behaviour of geomaterials, Turin 1, 159-165.

[9] Cho, G., and Santamarina, J.C. (2001). Unsaturated particulate materials: Particle-level studies. J. of Geotechnical and Geoenvironmental Engineering, ASCE, 127(1): 84-96.

[10] Chowdhury, M. (2004). “Dynamic properties of low and high plasticity clays using resonant column and bender element testing technique”. Ms. Thesis, The University of Texas at Arlington, Arlington, Texas.

[11] Craig, Roy. Jr (1981). Structural Dynamics: An introduction to computer methods. Jhon Wiley and Sons, New York, NY.

[12] Fredlund, D. G. and Rahardjo, H. (1993). "Soil mechanics for unsaturated soils," John Wiley and Sons, Inc., New York.

[13] Fredlund, D. G., and Xing, A. (1994). “Equation for the soil-water characteristic curve.” Can. Geotech. J., 31(4), 521-532.

[14] Fredlund, D. G., Xing, A., Huang, S., (1994). “Predicting the permeability functions for unsaturated soils using the soil-water characteristic curve.” Can. Geotech. J. 31, 533-546.

[15] Fredlund, M. D., Wilson, G. W., and Fredlund, D. G., (1997). “Prediction of the soil-water characteristic curve from the grain-size distribution curve.” Proceedings of the 3rd Symposium on Unsaturated Soil, Rio de Janeiro, Brazil, 13-23.

[16] Fredlund D. G. (1998). “Bringing unsaturated soil mechanics into engineering practice.” II International Conference on Unsaturated Soils, UNSAT ’98, Beijing 2, 1-36.

[17] Fredlund, M. D., Fredlund, D. G., and Wilson, G. W. (2000). “An equation to represent grain-size distribution.” Can. Geotech. J., 37(4), 817-827.

[18] Geotechnical Consulting and Testing System (2009). CATS Resonant column and torsional shear test mode 1.8: User guide and reference. GCTS, Tempe, AZ.

[19] Greening, P.D. and Nash, D.F. (2004). “Frequency domain determination of Go using bender elements.” Geotechnical Testing Journal, 27(3), 1-7.

[20] Hoyos, L. R. (1993). “Dynamic properties of puertorican residual soils using The resonant column device,” M.S. Thesis, The University. of Puerto Rico, Mayaguez, P.R., pp. 85-87.

[21] Hoyos, L. R., Takkabutr, P., Puppala, A. J., (2005). “A pressure plate extractor device for assessment of SWCC under net radial confinement.” Proceeding of International Conference on Problematic Soils, Eastern Mediterranean University, Famagusta, N. Cyprus.

[22] Hoyos, L. R., Suescun, E.A., Pineda, J. and Puppala A. (2010). “Small-strain stiffness of compacted silty sand using a proximitor-based suction-controlled resonant column device.” Fifth International Conference Unsaturated Soils, Barcelona, Spain.

[23] Huoo-Ni, S. (1987). Dynamic properties of sand under true triaxial stress states from resonant column/torsional shear tests. Ph.D. Dissertation, Univ. of Texas, Austin, TX.

[24] Kramer, Steven L. (1996), “Geotechnical earthquake engineering,” Prentice Hall, First Edition.

[25] Lee, J., and Santamarina, C. (2005). “Bender elements: performance and signal interpretation”. *Journal of Geotechnical and Geoenviromental Engineering*, 131(9), 1063-1070.

[26] Leong, E.C., Yeo, S.H. and Rahardjo, H. (2005). “Measuring shear wave velocity using bender elements”. *Geotechnical Testing Journal,* 28(5), 488-498.

[27] Leong, E.C., Cahyadi, J. and Rahardjo, H. (2006). “Stiffness of a compacted residual soil”. *Unsaturated Soils 2006*, 1169-1180.

[28] Mancuso, C., Simonelli, A. L., and Vinale, F. (1998), “Numerical analysis of in situ S-wave measurements,” proceedings, Twelfth International Conference on Soil Mechanics and Foundation Engineering, Rio de Janeiro, Vol. 3, pp 277-280.

[29] Mancuso, C., Vassallo R., and d’Onofrio A. (2002). Small strain behavior of a silty sand in controlled-suction resonant column–torsional shear tests. Canadian Geotechnical Journal, 39: 22-31.

[30] Marinho, E.A., Chandler, R.J., and Crilly, M.S. (1995). Stiffness measurements on high plasticity clay using bender elements. Proc., 1st International Conf. on Unsaturated Soils, Paris, vol. 1: 535-539.

[31] Mitchell, J. K. (1993). “Fundamental of soil behavior,” John Wiley & Sons, New York.

[32] Mohammad, R. (2008). “Dynamic properties of compacted soils using resonant column with self-contained bender elements”. Ms. Thesis, The University of Texas at Arlington, Arlington, Texas.

[33] Picornell, M., and Nazarian, S. (1998). Effects of soil suction on low-strain shear modulus of soils. Proc., 2nd International Conf. on Unsaturated Soils, Beijing, vol. 2: 102-107.

[34] Qian, X., Gray, D.H., and Woods, R.D. (1991). Resonant column tests on partially saturated sands. Geotechnical Testing Journal, ASTM, 14(3): 266-275.

[35] Ramakant, K.R. (2003). “Evaluation of low strain shear moduli of stabilized sulfate-bearing soils using bender elements”. Ms. Thesis, The University of Texas at Arlington, Arlington, Texas.

[36] Santamarina, J. C., and Fam, M. A. (1997). “Interpretation of bender element tests-discussion.” Geotechnique, 47(4), 873–875.

[37] Stokoe, K. H. II, Anderson, A. M., Hoar, R. J., and Isenhower, W. M. (1978). “Insitu and laboratory shear velocity and modulus,” Proceedings from Earthquake Engineering and Soil Dynamics Conference, ASCE, III, The University of Texas, Austin, TX, pp. 1498-1502.

[38] Stoke, K. H. and Huoo-Ni, S. (1985). “Effects of stress state and strain amplitude on shear modulus of dry sand,” Proceedings of the Second Symposium on the Interaction of Non-Nuclear Munitions with Structures, Panama City, FL, pp. 407- 412.

[39] Vanapalli, S. K., Pufahl, D. E., Fredlund, D. G., (1998). “The effect of stress on the soil-water characteristic behaviour of a compacted sandy-clay till. 51st Canadian Geotechnical Conference, Edmonton, 81-86.

[40] Vanapalli, S., Fredlund, D., Pufahl, D. (1999). “The influence of soil structure and stress history on the soil-water characteristics of a compacted till. Geotechnique, 49(2), 143-159.

[41] Vassallo, R., Mancuso, C., and Vinale, F. (2006). Effects of net stress and suction history on small strain stiffness of a compacted clayey silt. Canadian Geotechnical Journal, 44(4): 447-462.

[42] Venkatarama, R.B., and Jagadish, K.S. (1993). The static compaction of soils. Géotechnique, 43(2): 337-341.

[43] Viggiani, G., and Atkinson, J. H. (1995a). “Interpretation of bender element tests.” Geotechnique, 45(1), 149-154.

[44] Vinale, F., A. d’Onofrio, C. Mancuso, F. Santucci De Magistris & F. Tatsuoka (1999). “The prefailure behaviour of soils as construction materials.” II International Conference on pre-failure behaviour of geomaterials, Turin.

[45] Takkabutr, P. (2006). “Experimental investigations on small-strain stiffness properties of partially saturated soils via resonant column and bender element testing”. Ph. D. Dissertation, The University of Texas at Arlington, Arlington, Texas.

[46] Wu, S., Gray, D.H., and Richart, Jr., F.E. (1984). Capillary effects on dynamic modulus of sands and silts. Journal of Geotechnical Engineering, ASCE, 110(9): 1188-1203.

[47] Zhang, J., Andrus, R. and Juang H. (2005). “Normalized shear modulus and material damping ratio relationships”. Journal of Geotechnical and Environmental Engineering, ASCE, 131(4): 453-464

## BIOGRAPHICAL INFORMATION

Eduardo Suescun-Florez was born on May 16, 1976 in the City of Bucaramanga, Colombia. He received his bachelor degree in Civil Engineering from Universidad De La Salle, Bogota, Colombia in February 2000. After graduating, he worked in several geotechnical consulting companies as a civil engineer, and obtained the degree of specialist on geotechnical engineering from the Universidad Nacional de Colombia in 2004. Thereafter, he founded and managed *Geotecnia de Colombia Ltd* in Bogota, Colombia. After three years of consulting services for public and private sectors, he became a consultant engineer for The World Bank on infrastructure projects in Latin American countries. Two years later, he decided to pursue graduate studies majoring in geotechnical engineering at The University of Texas at Arlington, Arlington, Texas, USA in 2009. During his studies, he had the opportunity to work as a graduate research assistant under the supervision of Dr. Laureano Hoyos. Mr. Eduardo Suescun-Florez received his Master of Science degree in Civil Engineering from The University of Texas at Arlington in May 2010.